Journal of Physics G:
Nuclear and Particle
Physics

PURPOSE-LED
PUBLISHING™

PAPER • OPEN ACCESS

Combination of searches for nonresonant Higgs boson pair production in proton–proton collisions at $\sqrt{s} = 13\,\text{TeV}$

To cite this article: The CMS Collaboration 2026 *J. Phys. G: Nucl. Part. Phys.* **53** 095001

View the article online for updates and enhancements.

You may also like

- ATLAS searches for di-Higgs production at 13 TeV and prospects for HL-LHC
Y Sano and on behalf of the ATLAS Collaboration
- Search for Higgs decaying to WW at CMS
Leonardo Di Matteo and (on behalf ofthe CMS Collaboration)
- Search for additional Higgs bosons in fermionic final states with the CMS experiment
Punnawich Chokeprasert and Chayanit Asawatangtrakuldee

This content was downloaded from IP address 129.13.194.163 on 04/11/2026 at 13:28

Journal of Physics G: Nuclear and Particle Physics

Check for updates

PAPER

OPEN ACCESS

RECEIVED
27 October 2025

REVISED
3 July 2026

ACCEPTED FOR PUBLICATION
24 July 2026

PUBLISHED
3 September 2026

Original content from this work may be used under the terms of the Creative Commons Attribution 4.0 licence.

Any further distribution of this work must maintain attribution to the author(s) and the title of the work, journal citation and DOI.

Combination of searches for nonresonant Higgs boson pair production in proton–proton collisions at $\sqrt{s} = 13\,\text{TeV}$

The CMS Collaboration*

CERN, Geneva, Switzerland

* Author to whom any correspondence should be addressed.

E-mail: cms-publication-committee-chair@cern.ch

Keywords: CMS, Higgs, HH, BSM

Supplementary material for this article is available online

Abstract

This paper presents a combination of searches for the nonresonant production of Higgs boson pairs (HH) in proton–proton collisions at a centre-of-mass energy of 13 TeV. The dataset was collected by the CMS experiment at the LHC from 2016 to 2018 and corresponds to a total integrated luminosity of 138 fb^{-1}. The observed (expected) upper limit on the inclusive HH production cross-section relative to the standard model (SM) prediction is found to be 3.5 (2.5). Assuming all other Higgs boson couplings are equal to their SM values, the Higgs boson trilinear self-coupling modifier $\kappa_\lambda = \lambda_3/\lambda_3^{\text{SM}}$ is constrained in the range $-1.35 \leqslant \kappa_\lambda \leqslant 6.37$ at 95% confidence level (CL). Similarly, for the coupling modifier $\kappa_{2\text{V}}$, which governs the interactions between two vector bosons and two Higgs bosons, we have excluded $\kappa_{2\text{V}} = 0$ at more than five standard deviations for all values of κ_λ. At 95% CL, assuming that the other couplings are equal to their SM values, $\kappa_{2\text{V}}$ is constrained in the range $0.64 \leqslant \kappa_{2\text{V}} \leqslant 1.40$. This work also investigates HH production in several new physics scenarios, using the Higgs effective field theory (HEFT) framework. The HEFT framework is further exploited to study various ultraviolet complete models with an extended Higgs sector and set constraints on specific parameters. An extrapolation of the results in the expected integrated luminosity following the high-luminosity upgrade of the LHC is also reported.

1. Introduction

In 2012, the ATLAS and CMS Collaborations at the CERN and LHC discovered a new particle with a mass of approximately 125 GeV [1–3]. Extensive measurements of its properties, including mass, spin, parity, couplings to other standard model (SM) particles, and decay width, have revealed that this particle is compatible with the SM Higgs boson (H) [4, 5]. However, the question of the Higgs boson self-interaction remains unresolved. Measurements of the Higgs boson trilinear (λ_3) and quartic self-couplings (λ_4) provide valuable information about the Brout–Englert–Higgs mechanism, the process by which a complex scalar doublet field—the Higgs doublet—generates the masses of the W and Z bosons via spontaneous electroweak (EW) symmetry breaking. These findings will confirm the SM or point to new physics scenarios, such as extended Higgs sectors [6–15]. Beyond particle physics, the true nature of the electroweak phase transition will highlight cosmological questions related to inflation, gravitational waves, and baryogenesis [16–22]. Although the quartic coupling is challenging to measure at the LHC and requires future colliders [23–26], the trilinear coupling can be directly accessed by studying Higgs boson pair production.

At the LHC, pairs of SM Higgs bosons (HH) are primarily produced via gluon–gluon fusion (ggF), with a cross-section of $31.05^{+0.06}_{-0.23}$ fb [27, 28] at next-to-next-to-leading order (NNLO) in quantum chromodynamics (QCD) for a centre-of-mass energy of 13 TeV and a Higgs boson mass of 125 GeV, which is assumed in this paper. At leading order (LO), the two amplitudes contribute to the ggF HH production cross-section, namely the Higgs boson self-interaction ('triangle diagram') and the top quark loop ('box diagram'), represented by the Feynman diagrams in figure 1. The triangle diagram amplitude is

© 2026 The Author(s). Published by IOP Publishing Ltd

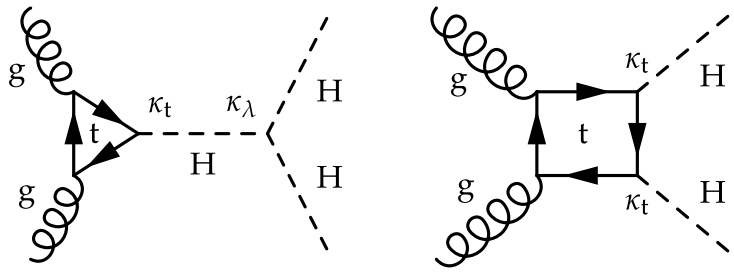


Figure 1. Feynman diagrams for the leading order of nonresonant Higgs boson pair production via gluon–gluon fusion in the SM. The modifiers of the Higgs boson coupling with the top quark and the Higgs boson trilinear self-coupling are shown as κ_t and κ_λ, respectively.

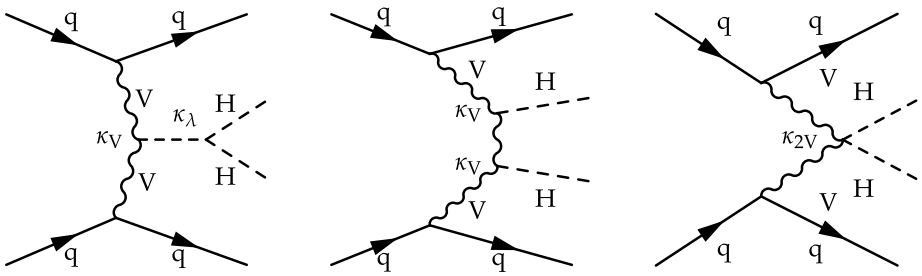


Figure 2. Feynman diagrams for the leading order of nonresonant Higgs boson pair production via vector boson fusion in the SM. The modifiers of the Higgs boson coupling with a vector boson, the Higgs boson trilinear self-coupling, and the coupling between two Higgs bosons and two vector bosons are shown as κ_V, κ_λ, and κ_{2V}, respectively.

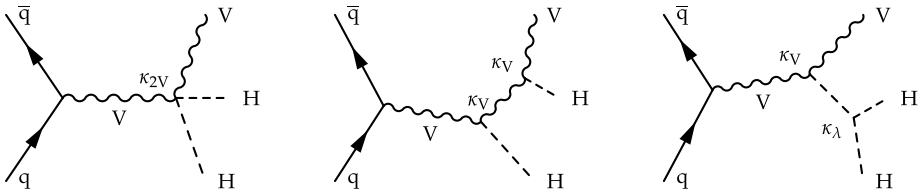


Figure 3. Feynman diagrams for the leading order of nonresonant Higgs boson pair production associated with a vector boson in the SM. The modifiers of the Higgs boson coupling with a vector boson, the Higgs boson trilinear self-coupling, and the coupling between two Higgs bosons and two vector bosons are shown as κ_V, κ_λ, and κ_{2V}, respectively.

proportional to the Higgs boson trilinear self-coupling, or in the theoretical framework described in section 3, to the coupling modifier $\kappa_\lambda = \lambda_3/\lambda_3^{\mathrm{SM}}$, where λ_3^{SM} is the Higgs boson trilinear self-coupling in the SM. The triangle and box diagram amplitudes interfere destructively, leading to a significant reduction in the ggF cross-section for certain values of κ_λ.

The second largest production mechanism for HH events is vector boson fusion (VBF) with a cross-section of 1.726 ± 0.036 fb [29] in the SM at $\sqrt{s} = 13$ TeV and next-to-NNLO ($\mathrm{N^3LO}$) in QCD. The VBF production mode, shown in figure 2, provides access to the coupling modifier of the interactions between two vector bosons and two Higgs bosons (κ_{2V}) and the interactions between a Higgs boson and two vector bosons (κ_V). The characteristic signature of VBF, two jets in the forward direction, with a large pseudorapidity (η) separation, allows us to identify the process despite the small cross-section. Higgs boson pairs can also be produced in association with a vector boson $V = W$ or Z (VHH) with a cross-section of approximately half that of the VBF mode, $0.36^{+0.04}_{-0.03}$ fb for ZHH and $0.33^{+0.03}_{-0.05}$ fb [30] for WHH, as shown in figure 3. The VHH production is affected differently by the destructive interference compared to the ggF and VBF due to the presence of additional diagrams at next-to-LO (NLO), offering complementary constraints on κ_λ, especially for $\kappa_\lambda > 0$ [31].

In novel physics models, additional diagrams that include couplings not present in the SM may contribute to HH production. These can be examined in the context of the Higgs effective field theory (HEFT) [32]. The HEFT Lagrangian extends the SM Lagrangian with additional operators of dimension five or greater that are invariant under $\mathrm{SU}(3)_C \times \mathrm{U}(1)_{\mathrm{EM}}$ and their corresponding couplings. Figure 4 displays the anomalous couplings c investigated in this paper. In particular, c_2 is the coupling between

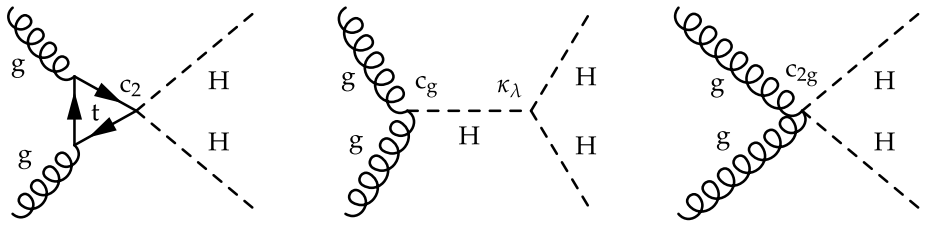


Figure 4. Feynman diagrams for the leading order of nonresonant Higgs boson pair production via gluon–gluon fusion with anomalous Higgs boson couplings c_2, c_g, and c_{2g}. The Higgs boson trilinear self-coupling modifier is shown as κ_λ.

two top quarks and two Higgs bosons, c_g is the coupling between two gluons and one Higgs boson, and c_{2g} is the coupling between two gluons and two Higgs bosons. The total HH HEFT Lagrangian as a function of the anomalous coupling modifiers is described as:

$$\begin{aligned}\Delta\mathcal{L}_{\text{HEFT}} = &-m_t\left(\kappa_t\frac{h}{v}+c_2\frac{h^2}{v^2}\right)\bar{t}t-\kappa_\lambda\frac{m_{\text{H}}^2}{2v}h^3+\frac{\alpha_S}{8\pi}\left(c_g\frac{h}{v}+c_{2g}\frac{h^2}{v^2}\right)G^a_{\mu\nu}G^{a,\mu\nu}\\&+\left(2\kappa_V\frac{h}{v}+\kappa_{2V}\frac{h^2}{v^2}\right)\left(m_W^2W^+_\mu W^{-\mu}+\frac{1}{2}m_Z^2Z_\mu Z^\mu\right).\end{aligned} \tag{1}$$

The ATLAS and CMS Collaborations have performed previous HH searches at $\sqrt{s}=8$ and 13 TeV. The ATLAS Collaboration has combined HH searches in the $b\bar{b}\gamma\gamma$, $b\bar{b}\tau\tau$, and $b\bar{b}b\bar{b}$ final states at 13 TeV and set an upper limit on the inclusive production cross-section of 2.9 times the SM expectation at 95% CL, with 2.4 expected under the background-only hypothesis [33]. A combined search in the $b\bar{b}\gamma\gamma$, $b\bar{b}\tau\tau$, $b\bar{b}b\bar{b}$, $b\bar{b}ZZ$, and multilepton final states by CMS at 13 TeV constrained (expected to constrain) the inclusive HH production cross-section to be less than 3.4 (2.5) times the SM expectation at 95% CL [4]. This paper supersedes previous results by introducing additional channels, including the $b\bar{b}WW$, $WW\gamma\gamma$, and $\tau\tau\gamma\gamma$ final states and the VHH production mode in the $b\bar{b}b\bar{b}$ final state, to perform a variety of parameter scans, as well as searches for anomalous Higgs boson couplings in the HEFT approach. The HEFT parametrization is further exploited to constrain parameters in specific ultraviolet (UV) complete models. The results presented in this paper and provided in the corresponding HEPData records [34] are based on a dataset of proton–proton (pp) collisions at 13 TeV collected by the CMS experiment from 2016 to 2018 (Run 2), corresponding to an integrated luminosity of 138 fb^{-1}.

2. The CMS detector and event reconstruction

The CMS apparatus [35, 36] is a multipurpose, nearly hermetic detector, designed to trigger on [37–39] and identify electrons, muons, photons, and (charged and neutral) hadrons [40–42]. Its central feature is a superconducting solenoid of 6 m internal diameter, providing a magnetic field of 3.8 T. Within the solenoid volume are a silicon pixel and strip tracker, a lead tungstate crystal electromagnetic calorimeter (ECAL), and a brass and scintillator hadron calorimeter (HCAL), each comprising a barrel and two endcap sections. Forward calorimeters extend the pseudorapidity coverage provided by the barrel and endcap detectors. Muons are reconstructed using gas-ionization detectors embedded in a steel flux-return yoke outside the solenoid. A more detailed description of the CMS detector together with a definition of the coordinate system used and the relevant kinematic variables can be found in [35, 36].

Events of interest are selected using a two-tiered trigger system. The first level, consisting of custom hardware processors, uses information from the calorimeters and muon detectors to select events at a rate of around 100 kHz within a fixed latency of 4 μs [37]. The second level, known as the high-level trigger, comprises a farm of processors running a version of the full event reconstruction software optimized for fast processing, and reduces the event rate to a few kHz before data storage [38, 39].

The particle-flow (PF) algorithm [43] aims to reconstruct and identify each particle in an event (PF candidate), with an optimized combination of information from the various elements of the CMS detector. The primary vertex (PV) is taken to be the vertex corresponding to the hardest scattering in the event, evaluated using tracking information alone, as described in section 9.4.1 of [44]. The energy of photons is obtained from the ECAL measurement. The energy of electrons is determined from a combination of the track momentum at the PV, the corresponding ECAL cluster energy, and the energy sum of all bremsstrahlung photons attached to the track. The momentum of muons is obtained from the

curvature of the corresponding track. The energy of charged hadrons is determined from a combination of the track momentum and the corresponding ECAL and HCAL energies, corrected for the response function of the calorimeters to hadronic showers. Finally, the energy of neutral hadrons is obtained from the corresponding corrected ECAL and HCAL energies.

Small-radius jets are reconstructed from PF candidates, using the anti-k_T clustering algorithm [45, 46] with a distance parameter $R = 0.4$ (AK4 jets). Charged particles not originating from the PV are excluded from the jet clustering, and an offset correction is applied to correct for the remaining contributions. Higgs boson decays into a pair of b quarks with high transverse momentum (p_T) result in final states with large Lorentz boost. As a result, the b jets are overlapping, forming one large merged jet ('large-radius jet') and substructure, that is, the two overlapping jets are 'subjets' of the large-radius jet. The jets are reconstructed using the anti-k_T algorithm with a distance parameter $R = 0.8$ (AK8 jets).

The missing transverse momentum vector $\vec{p}_T^{\,\text{miss}}$ is computed as the negative vector p_T sum of all the PF candidates in an event, and its magnitude is denoted as p_T^{miss} [47]. The $\vec{p}_T^{\,\text{miss}}$ is modified to account for corrections to the energy scale of the reconstructed jets in the event.

The searches presented in this paper use a variety of object identification (ID) techniques and algorithms, tailored to their specific characteristics.

3. Signal modelling

The ggF HH cross-section as a function of κ_λ and κ_t is expressed as follows:

$$\sigma(\kappa_\lambda, \kappa_t) = {\kappa_\lambda}^2 {\kappa_t}^2 t + {\kappa_t}^4 b + \kappa_\lambda {\kappa_t}^3 i, \tag{2}$$

where $t = |T|^2$, $b = |B|^2$, and $i = |TB^* + B^*T|$ are the three amplitudes that correspond to the triangle and box diagrams shown in figure 1 and their interference, respectively [48].

The same formula holds for all differential cross-section $\mathrm{d}\sigma/\mathrm{d}x$ for ggF HH production. At higher orders in the QCD perturbative expansion, T and B correspond to the sum of all diagrams of the same order in κ_λ and κ_t, and the polynomial relation in equation (2) remains valid. Since the ggF cross-section can be expressed as a polynomial in κ_λ and κ_t with three independent terms, we can model the ggF signal over a wide range of κ_λ and κ_t by evaluating the cross-section at three different combinations of values for (κ_λ, κ_t) and performing a linear combination. In our case, we use the information from three simulated data samples as a linear combination that allows us to perform scans in the κ_λ and κ_t parameters.

An event-level reweighting method is used to study modified SM couplings and couplings not present in the SM. The reweighting parametrises the differential cross-section as a function of the invariant mass of the HH pair and their angular separation in the azimuthal plane, which fully characterizes the system. This enables modelling different combinations of (κ_λ, κ_t, c_2, c_g, c_{2g}) present in $\Delta\mathcal{L}_{\text{HEFT}}$ of equation (1), including combinations without a corresponding generated sample. The method used to derive the reweighting factors is described in [49, 50]. The procedure is similar to the recommendation by the LHC Higgs Working Group 4 [32]. In our derivation, we use finer bins for high values of the invariant mass of the HH system. The results are validated using simulated samples at the generator level with custom combinations of the coupling parameters. The method is used for all HH decay channels except the $\mathrm{b\bar{b}b\bar{b}}$ channel with high Lorentz boost, where the reweighting factors are not precise enough due to the limited number of simulated events in the high m_{HH} bins. Therefore, all necessary Monte Carlo (MC) simulated samples for each benchmark are produced.

Two sets of benchmarks are produced using the reweighting method. The first set defines 13 benchmark scenarios [51] spanning a broad range of the coupling values in the HEFT parametrization at LO precision, noted as JHEP04(2016)126. The second set [52], noted as JHEP03(2020)091, is derived with NLO precision and considers direct and indirect constraints on the allowed range for the coupling values. The aim of both sets of benchmarks is to sample the parameter space describing the signal according to kinematic features of the final state. The values of the coupling modifiers corresponding to each benchmark are shown in tables 1 and 2.

We further study the c_2 modifier and perform scans with c_2 as the parameter of interest. In contrast, c_2, κ_t, and κ_λ are free parameters in the HEFT Lagrangian; hence, it is of interest to check for correlations.

Finally, constraints are set on specific UV complete models. The parameters of each model can be written in terms of κ_λ, κ_t, and c_2 based on a mapping described in [50]. Three types of models

Table 1. Values of the effective Lagrangian couplings for the Higgs effective field theory benchmarks proposed in [51] and referred to in this paper as JHEP04(2016)126.

	1	2	3	4	5	6	7	8	9	10	11	12	8a
κ_λ	7.5	1.0	1.0	−3.5	1.0	2.4	5.0	15.0	1.0	10.0	2.4	15.0	1.0
κ_t	1.0	1.0	1.0	1.5	1.0	1.0	1.0	1.0	1.0	1.5	1.0	1.0	1.0
c_2	−1.0	0.5	−1.5	−3.0	0.0	0.0	0.0	0.0	1.0	−1.0	0.0	1.0	0.5
c_g	0.0	−0.8	0.0	0.0	0.8	0.2	0.2	−1.0	−0.6	0.0	1.0	0.0	0.27
c_{2g}	0.0	0.6	−0.8	0.0	−1.0	−0.2	−0.2	1.0	0.6	0.0	−1.0	0.0	0.0

Table 2. Values of the effective Lagrangian couplings for the Higgs effective field theory benchmarks proposed in [52] and referred to in this paper as JHEP03(2020)091.

	1	2	3	4	5	6	7
κ_λ	3.94	6.84	2.21	2.79	3.95	5.68	−0.10
κ_t	0.94	0.61	1.05	0.61	1.17	0.83	0.94
c_2	−0.33	0.33	−0.33	0.33	−0.33	0.33	1.0
c_g	0.75	0.0	0.75	−0.75	0.25	−0.75	0.25
c_{2g}	−1	1	−1.5	−0.5	1.5	−1	1

are studied in this paper: models with one additional scalar [6, 7], models with two Higgs doublets (2HDM) [8–11], and composite Higgs models [12–15].

The scans on the parameters of interest κ_λ, κ_t, κ_V, and κ_{2V} are performed using a linear combination of a set of VBF and VHH samples, similar to what is done for ggF. Modifications of the Higgs boson couplings to other particles that affect HH and single Higgs boson production are considered in all the cases [53].

The simulated events for ggF production are produced using NLO matrix elements with the model described in [48], implemented in the POWHEG v2 [54–56]. The cross-section is corrected to the NNLO value as a function of κ_λ according to [31, 57]. Four ggF samples are produced with different values of the trilinear coupling modifier ($\kappa_\lambda = 0$, 2.45, 5.0, and 1.0). The simulated signal samples for VBF and VHH production modes are generated at LO using MADGRAPH5_aMC@NLO 2.6.5 [58–60]. A total of seven VBF samples are generated with different values of the coupling modifiers $(\kappa_V, \kappa_{2V}, \kappa_\lambda) = (1,1,1)$, (1, 1, 0), (1, 1, 2), (1, 0, 1), (1, 2, 1), (0.5, 1, 1), and (1.5, 1, 1), and eight VBF samples are generated with the same coupling modifier values plus $(\kappa_V, \kappa_{2V}, \kappa_\lambda) = (1,1,20)$. This last benchmark is used in the VHH case where κ_λ is less constrained; therefore, we need to model large values of κ_λ. The total cross-section is corrected to the corresponding NNLO cross-section [30, 61]. The parton shower and hadronization are simulated with PYTHIA 8.230 [62] using the CUETP8M1 [63] set of tuned parameters for 2016 simulations and the CP5 [64] tune set for 2017 and 2018 simulations. The simulated samples produced with PYTHIA and the CUETP8M1 (CP5) tune use the NNPDF3.0 (NNPDF3.1) parton distribution functions (PDFs) [65–67], whereas samples produced with MADGRAPH5_aMC@NLO or POWHEG v2 use the NNPDF3.1 set. The CMS detector response is modelled using GEANT4 [68].

4. Analysis strategy

The list of HH analyses considered in this combination, along with a summary of results, is listed in table 3. A brief description of each analysis is given later in this section. More details can be found in the respective publications. For the purposes of this combination, extensive studies are performed to avoid double counting of events among the different analyses. Specific actions taken by the various analyses are described in each section. Two channels, $b\bar{b}WW$, $WW \to 4q$ and $WW\gamma\gamma$, have not been previously published; therefore, more details are provided in the corresponding sections. The $b\bar{b}WW$ analysis is the first search for $HH \to b\bar{b}WW$ in the all-hadronic final state.

Where required, the event selection for each analysis was modified for the combination to prevent double counting of events. The strategy for this overlap removal is based upon work done for the combinations in [4].

Table 3. Summary of results for the HH analyses included in this combination. The second column is the observed (expected) 95% CL upper limit on the inclusive signal strength $\mu = \sigma_{\mathrm{HH}}/\sigma_{\mathrm{HH}}^{\mathrm{SM}}$, with one exception where $\mu_{\mathrm{VHH}} = \sigma_{\mathrm{VHH}}/\sigma_{\mathrm{VHH}}^{\mathrm{SM}}$ is shown. The third (fourth) column is the allowed 68% CL interval for the coupling modifier κ_λ ($\kappa_{2\mathrm{V}}$). The last column indicates whether the analysis is included in the results using the HEFT parametrization.

Analysis	μ	κ_λ	$\kappa_{2\mathrm{V}}$	HEFT
$\mathrm{b\bar{b}b\bar{b}}$, resolved jets [69]	3.9 (7.8)	$[-2.3, 9.4]$	$[-0.1, 2.2]$	✓
$\mathrm{b\bar{b}b\bar{b}}$, merged jets [70]	9.9 (5.1)	$[-9.9, 16.9]$	$[0.62, 1.41]$	✓
VHH, HH $\to \mathrm{b\bar{b}b\bar{b}}$ [71]	$\mu_{\mathrm{VHH}} < 294$ (124)	$[-37.7, 37.2]$	$[-12.2, 8.9]$	—
$\mathrm{b\bar{b}}\tau\tau$ [72]	3.3 (5.2)	$[-1.7, 8.7]$	$[-0.4, 2.6]$	✓
$\mathrm{b\bar{b}}\gamma\gamma$ [73]	7.7 (5.2)	$[-3.3, 8.5]$	$[-1.3, 3.5]$	✓
$\mathrm{b\bar{b}WW}$, WW $\to \ell\nu\mathrm{qq}/2\ell2\nu$ [74]	14 (18)	$[-7.2, 13.8]$	$[-8.7, 15.2]$	✓
$\mathrm{b\bar{b}WW}$, WW $\to$ 4q	141 (69)	—	$[-0.04, 2.05]$	—
HH multilepton [75]	21.3 (19.4)	$[-6.9, 11.1]$	—	✓
$\tau\tau\gamma\gamma$ [76]	33 (26)	$[-13, 18]$	—	—
$\mathrm{b\bar{b}ZZ}$ [77]	32.4 (39.6)	$[-8.8, 13.4]$	—	—
$\mathrm{WW}\gamma\gamma$	97 (53)	$[-25.8, 14.4]$	—	✓

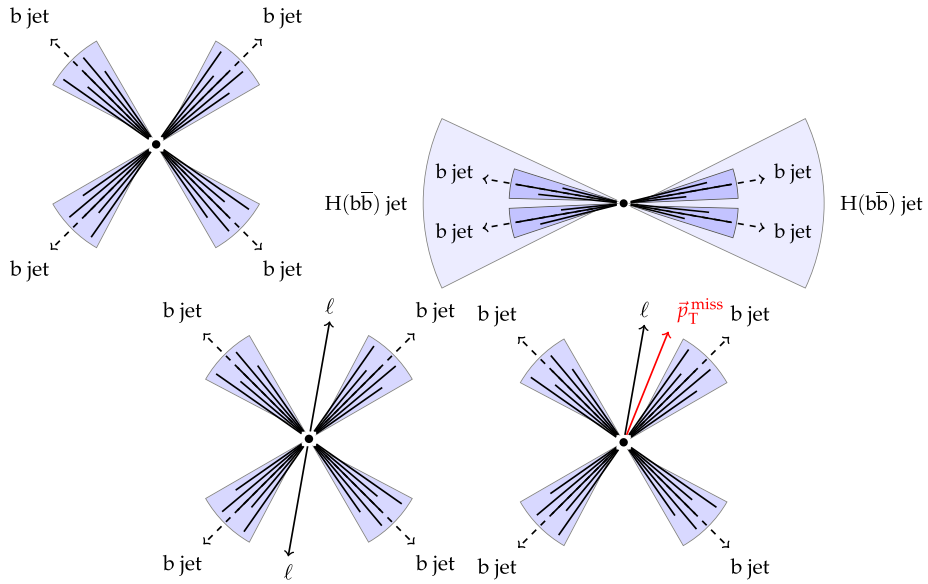


Figure 5. Illustrations of the resolved (upper left) and boosted (upper right) topologies of the $\mathrm{b\bar{b}b\bar{b}}$ decay channel. The topology of VHH production when all Higgs bosons decay to b jets and the vector boson is either a Z boson that decays into two leptons (lower left) or a W boson decaying into a lepton and a neutrino, giving missing transverse momentum (lower right).

4.1. HH $\to \mathrm{b\bar{b}b\bar{b}}$

The $\mathrm{b\bar{b}b\bar{b}}$ decay channel has the largest HH branching fraction (33.6%) among the HH decays to SM particles. Three analyses target the $\mathrm{b\bar{b}b\bar{b}}$ decay channel. The first two searches for HH pairs produced via ggF or VBF. In one case, the topology of the b jets is resolved, whereas in the other case, the b jets are produced with a high Lorentz boost resulting in a merged signature, where pairs of jets are reconstructed as single large radius jets. The third analysis is dedicated to the search for VHH production. In this case, the final state is characterized by the decay mode of the vector boson. Figure 5 illustrates the topology of each analysis.

4.1.1. HH $\to$ $\mathrm{b\bar{b}b\bar{b}}$ resolved

The resolved search [69] focuses on the kinematic phase space where each Higgs boson is reconstructed from two small-radius b-tagged jets. It explores both the ggF and VBF HH production modes. The VBF topology is characterized by two additional jets with high invariant mass and large pseudorapidity separation $\Delta\eta$. Online trigger selection requires the presence of at least four jets, satisfying thresholds on jet p_{T} and H_{T}, defined as the scalar p_{T} sum of all jets. These thresholds vary depending on the data-taking year between 30 and 90 GeV for p_{T} and 300 to 330 GeV for H_{T}. Consequently, data collected in 2016 are analysed separately from those collected in 2017 and 2018.

Events selected offline contain at least four jets. Jets originating from b quark decays have been identified using the DeepJet [78] algorithm. The four jets with the highest DeepJet score are selected as b jet

candidates. The p_T of the four b jets is corrected using a multivariate regression method based on a deep neural network (DNN) [79]. At least three b jets must satisfy the DeepJet medium working point (WP) DeepJet [78], which corresponds to a b jet ID efficiency of about 75% and a misidentification rate for light-flavour quark and gluon jets of about 1%. The VBF jet candidates are the two highest p_T non-b jets located in opposite η hemispheres. Events that contain any isolated electrons or muons are rejected.

There are three possible ways to pair the four b jets to reconstruct two Higgs boson candidates. For each pairing, a distance parameter $d = |m_{H_1} - k m_{H_2}|/\sqrt{1+k^2}$ is calculated, where m_{H_1} is the mass of the Higgs boson candidate with the highest p_T, m_{H_2} is the mass of the other Higgs boson, and $k = 1.04$. For correctly paired events in MC simulation, k is the expected ratio of the peak positions of the reconstructed Higgs boson masses. Its value is greater than one because the energy regression depends on jet p_T, which has a larger effect on the less energetic H candidate. If the difference between the two smallest distance parameters is larger than 30 GeV, then the pairing with the smallest distance parameter is selected. Otherwise, between the two pairings with the smallest distance, the one maximising the p_T of the two H candidates in the four-jet centre-of-mass frame is selected. This procedure results in a correct jet pairing of about 82–96 (91–98)% of the selected events for the different couplings studied in ggF (VBF) simulated signal events.

Events that do not have a VBF jet pair are assigned to the ggF event category. A $\mathrm{BDT}_{\mathrm{ggF/VBF}}$ discriminant is trained to separate ggF and VBF HH signals in events that contain the VBF jet pair. The $\mathrm{BDT}_{\mathrm{ggF/VBF}}$ is trained using SM ggF signal and VBF signal with $\kappa_{2V} = 2$. A threshold on the $\mathrm{BDT}_{\mathrm{ggF/VBF}}$ score is used to classify these events into either ggF or VBF event categories. The ggF and VBF categories are further divided into subcategories to optimize the search sensitivity to anomalous coupling hypotheses. In the ggF category, events are separated into low-mass and high-mass categories using a 450 GeV threshold on the Higgs boson pair invariant mass m_{HH}. In the VBF category, events are divided into 'SM-like' and anomalous-κ_{2V} categories using a threshold on $\mathrm{BDT}_{\mathrm{ggF/VBF}}$.

The dominant background source is from SM events composed uniquely of jets produced through the strong interaction, referred to as QCD multijet events. The analysis signal region (SR) contains at least four b jet candidates satisfying the DeepJet medium WP. The background of this '4b' region is estimated using events from an orthogonal region, in which the fourth-highest b-tagged jet fails in the medium WP (or '3b' region). The transfer function used to model the 4b background from the 3b data comprises a BDT reweighting and a transfer factor (TF) for reshaping and normalization corrections.

To remove overlapping events between this analysis and the analysis of $\mathrm{b\bar{b}b\bar{b}}$ events in the boosted topology described in section 4.1.2, an event veto is applied for the combination described in this paper. Events containing two massive large-radius jets with $p_T > 300\,\mathrm{GeV}$ and at least two subjets are removed from this analysis. The p_T threshold was optimized based on the expected HH signal strength.

4.1.2. $HH \to b\bar{b}b\bar{b}$ boosted

In the $\mathrm{b\bar{b}b\bar{b}}$ boosted final state [70], both Higgs bosons are highly Lorentz boosted, decay to $\mathrm{b\bar{b}}$ pairs, and are reconstructed as large-radius jets. The search is sensitive to modified coupling scenarios that enhance the production of highly boosted Higgs boson pairs, including through VBF production.

Several trigger algorithms with requirements on H_T or large-radius jet p_T are used to select events online. This search uses the soft-drop (SD) algorithm [80] to reconstruct the Higgs boson candidate masses (m_{SD}).

The graph neural network (NN) algorithm [81–84] known as ParticleNet [82, 85] is used to discriminate between $\mathrm{H} \to \mathrm{b\bar{b}}$ and QCD jets. A regression algorithm based on ParticleNet is also used to improve the jet mass estimation (m_{reg}) [86].

Events with two or more large-radius jets are selected and grouped into mutually exclusive ggF and VBF categories. Events with two additional small-radius jets in the opposing forward regions of the detector, consistent with the characteristic VBF signature, are sorted into the VBF categories. Three VBF event categories (high, medium, and low purity) are defined using the ParticleNet discriminant ($D_{\mathrm{b}}\bar{\mathrm{b}}$) scores of the Higgs boson candidate jets.

The ggF categories comprise events that fail the criteria for the VBF categories. The BDT is trained to discriminate the HH signal from QCD multijet or $\mathrm{t\bar{t}}$ backgrounds based on the m_{SD}, η, and $D_{\mathrm{b}}\bar{\mathrm{b}}$ of the $D_{\mathrm{b}}\bar{\mathrm{b}}$-leading jet, and additional kinematic and substructure properties of both Higgs boson candidate jets. Three SRs targeting the ggF production are constructed depending on the BDT discriminant and the $D_{\mathrm{b}}\bar{\mathrm{b}}$-subleading large-radius jet $D_{\mathrm{b}}\bar{\mathrm{b}}$ score. The m_{reg} distribution of the $D_{\mathrm{b}}\bar{\mathrm{b}}$-subleading jet in each ggF category is fit simultaneously to extract the signal.

Dominant SM backgrounds are $\mathrm{t\bar{t}}$ and QCD multijet production. Control regions (CRs) for QCD multijet processes are defined by inverting or loosening the requirements on the $D_{\mathrm{b}}\bar{\mathrm{b}}$ score. The QCD multijet background in the SRs is estimated using the data from the CRs and fitted TFs [87–89].

Corrections for the $t\bar{t}$ background estimate are derived from a data sample enriched in $t\bar{t}$ events with one W boson decaying leptonically [90].

4.1.3. $VHH, VHH \to b\bar{b}b\bar{b}$

This analysis [71] focuses on the final state with both Higgs bosons decaying into a b quark-antiquark pair. All decay modes of vector bosons Z and W are considered. Experimentally, the events are divided into four categories based on the presence of a light lepton $\ell(=\boldsymbol{\mu}, \mathrm{e})$ and jets: two leptons, one lepton, $p_{\mathrm{T}}^{\mathrm{miss}}$ and fully hadronic channel, corresponding to the $\mathrm{Z} \to \ell\ell, \mathrm{W} \to \ell\nu, \mathrm{Z} \to \nu\nu$, and $\mathrm{Z/W} \to \mathrm{qq}$ processes, respectively. Due to the large overlap with the ggF and VBF $\mathrm{b\bar{b}b\bar{b}}$ channels, the VHH fully hadronic channel is removed from this combination. Two event topologies are explored in this analysis: one involving four small-radius b jets and the other with two large-radius jets, each from a $\mathrm{H} \to \mathrm{b\bar{b}}$ decay.

In the leptonic channels, events are selected using triggers requiring isolated leptons or large $p_{\mathrm{T}}^{\mathrm{miss}}$. In the resolved topology, at least three AK4 jets are required to pass the medium WP of the DeepJet b tagging algorithm. If there are more than four b-tagged jets, the ones with the highest b tagging scores are selected. An energy-regression method [79] is applied to the b jets to improve the resolution of the dijet mass. The two Higgs boson candidates are reconstructed by pairing the four jets with the same method used in the resolved $\mathrm{b\bar{b}b\bar{b}}$ analysis. In the boosted topology, two AK8 jets are required to have ParticleNet $D_{\mathrm{b}}\bar{\mathrm{b}}$ scores greater than 0.8. Given the high sensitivity of the boosted topology, it is prioritized if an event can be assigned to both topologies.

A categorization BDT is trained to divide events into regions sensitive to κ_λ and $\kappa_{2\mathrm{V}}$. In each region, another BDT is trained using all the signal processes to optimize the signal versus background discrimination. The final signal strength is extracted by fitting the BDT score distribution in the signal and CRs.

4.2. $\mathrm{HH} \to \mathrm{b\bar{b}}\tau\tau$

In the $\mathrm{b\bar{b}}\tau\tau$ channel [72], the events are characterized by the decay mode of the two τ leptons. With a branching fraction of 7.3%, this channel combines a relatively large branching fraction with easy to reconstruct final states. This analysis delves into final states where at least one of the τ leptons decays hadronically, that is, $\tau_\mu\tau_{\mathrm{h}}$, $\tau_{\mathrm{e}}\tau_{\mathrm{h}}$, and $\tau_{\mathrm{h}}\tau_{\mathrm{h}}$. The light leptons and τ_{h} candidates must have opposite electric charges. The τ_{h} candidates are reconstructed using the DeepTau algorithm [91], an NN method discriminating τ_{h} candidates from jets, electrons, and muons. Events are required to have at least two b jets identified using the DeepJet algorithm.

The events are selected by triggers requiring a single light lepton or a lepton to be accompanied by a τ_{h} candidate or two τ_{h} candidates. A trigger dedicated to the VBF topology was introduced in late 2017, requiring two τ_{h} candidates and two additional jets.

For each event, all b jet candidates are assigned a score by an NN trained to recognise the $\mathrm{H} \to \mathrm{b\bar{b}}$ topology. The two jets with the highest score are selected as the b jets from the Higgs boson decays. Events with two additional small-radius jets are identified as originating from the VBF process.

After the event selection, the events are divided into categories. The first set of categories splits the events according to the number and topology of the jets. Events with two overlapping small-radius jets are classified in the boosted category. All remaining events are classified in the resolved categories. The resolved category is further split according to whether one or both jets pass the medium WP of the DeepJet b tagging algorithm. Finally, an additional VBF category selects events with at least two VBF jet candidates. The contamination of this category from ggF events with an extra jet is significant; therefore, a multiclassifier DNN is trained. The DNN splits the events in the VBF category into signal-like VBF events, ggF contamination, $\mathrm{t\bar{t}H}$, $t\bar{t}$, and Drell–Yan (DY) background events.

All selected events are subject to a selection in the two-dimensional plane of the invariant mass of the dijet ($m_{\mathrm{b\bar{b}}}$) and ditau ($m_{\tau\tau}$) systems, where the $m_{\tau\tau}$ is reconstructed using the SVFIT algorithm [92]. This selection is optimized separately for the resolved and the boosted categories and does not apply to the VBF categories.

The eight event categories defined earlier are used for signal extraction using a DNN developed to identify $\mathrm{HH} \to \mathrm{b\bar{b}}\tau\tau$ events. The DNN is trained to classify the events from each event category as signal or background-like by assigning a single prediction per event. A maximum likelihood fit for signal extraction is performed using the DNN distribution simultaneously for all categories and channels.

The primary background processes for this search, $t\bar{t}$, DY, and QCD multijet, are estimated using control samples from data. The shapes of the $t\bar{t}$ and DY processes are taken from the simulation and then scaled using background-enriched regions. The scaling is extracted with a simultaneous fit over all the CRs and applied to the simulated events in the SR.

The QCD multijet process is entirely determined from data in jet-enriched regions where two selection requirements for the τ pair are inverted. The event yield and shape are obtained in a region where the τ_h is not required to be isolated from other tracks. In τ_h events, only the τ_h with the lowest p_T is allowed to not be isolated. Next, the yield is scaled by the ratio of event yield in a region where the opposite charge requirement is inverted and a region where both the charge and the isolation are inverted. The contributions from other backgrounds are subtracted. The QCD multijet background is estimated after the $t\bar{t}$ background has been scaled.

4.3. HH $\to$ b$\bar{\text{b}}\gamma\gamma$

The b$\bar{\text{b}}\gamma\gamma$ final state [73] despite the small branching fraction (0.26%), profits from the good mass resolution of the diphoton system. The parameters of interest of the model are extracted from a two-dimensional fit to the invariant mass distributions of the photon pair ($m_{\gamma\gamma}$) and b jet pair ($m_{\text{b}\bar{\text{b}}}$). The HH signal can be identified as a peak in the ($m_{\gamma\gamma}$, $m_{\text{b}\bar{\text{b}}}$) distribution at the value of the Higgs boson mass. Jets originating from the b quark decay are identified using the DeepJet algorithm. The background is dominated by the $\gamma\gamma$+jets and γ+jets continuum and is modelled from the data sidebands of the $m_{\gamma\gamma}$ and $m_{\text{b}\bar{\text{b}}}$ distributions. Other important background sources are the single Higgs boson production processes, wherein the Higgs boson decays into a photon pair (H $\to \gamma\gamma$). The largest H $\to \gamma\gamma$ background is the $t\bar{t}$H($\gamma\gamma$) process due to the sizable cross-section with the b jets in the final state from the t$\bar{\text{t}}$ decay. The H $\to \gamma\gamma$ processes are modelled using MC simulations.

Exclusive categories targeting specific HH production modes are defined to maximize the sensitivity to the signal. The SR targeting the VBF mechanism has requirements on the two additional jets. The VBF event candidates are classified into two exclusive categories depending on the value of the reduced four-body mass M_X, defined as $M_X = m_{\text{bb}\gamma\gamma} - m_{\gamma\gamma} - m_{\text{b}\bar{\text{b}}} + 250\,\text{GeV}$, where $m_{\text{bb}\gamma\gamma}$ is the four-body invariant mass of the pairs of photons and b jets. A BDT classifier is defined to isolate the VBF signal from the ggF signal and the continuum background. For the ggF-enriched categories, a BDT classifier is used to reject the continuum background. The values of the BDT score and M_X are used to classify the events in 12 ggF-enriched categories. The number and boundaries of the categories is optimized to maximize the expected significance of the SM HH signal.

Furthermore, a DNN is trained to separate the HH signal from the $t\bar{t}$H($\gamma\gamma$) process. The selection of the DNN output score reduces the $t\bar{t}$H background by between 80% and 85% and provides an efficiency between 90% and 95% for the HH signal, depending on the analysis category.

4.4. HH $\to$ b$\bar{\text{b}}$WW

The b$\bar{\text{b}}$WW decay mode has the second largest branching fraction (24.8%) among all HH decay modes. Two different analyses target the b$\bar{\text{b}}$WW decay channel. The analysis addresses distinct final states and experimental signatures. The first is a search for the WW $\to \ell\nu$qq/2ℓ2ν final state. Higgs boson candidates decaying to b quarks can lead to either resolved or boosted topologies, that is forming two narrow-radius b jets or one large-radius b jet. The second analysis is a search for WW $\to$ 4q, which is studied only in boosted topologies. All four jets from the W decays are expected to be overlapped and form one large-radius jet. The accompanying pair of b jets is also merged into one large-radius jet. Figure 6 illustrates the final states of the two analyses.

4.4.1. HH $\to b\bar{b}WW, WW \to \ell\nu qq/2\ell 2\nu$

Although b$\bar{\text{b}}$WW is the dominant channel in this final state, b$\bar{\text{b}}$ZZ and b$\bar{\text{b}}\tau\tau$ decays of the HH system that result in a pair of b quarks and one or two light leptons are also included in the signal. The analysis [74] considers two final states: single-lepton (1ℓ) bb$\ell\nu$qq and dilepton (2ℓ) bb$2\ell 2\nu$. The most significant background contribution is the t$\bar{\text{t}}$ process, whereas other backgrounds include events with misidentified leptons and the DY process and W+jets process for the 2ℓ and 1ℓ channels, respectively.

The data are collected using single- and double-lepton triggers. The event selection criteria require the presence of one isolated lepton in the 1ℓ channel or two isolated leptons of opposite charge in the 2ℓ channel, originating from the W leptonic decays. The H $\to$ b$\bar{\text{b}}$ system is characterized by two jets. In the resolved category, these are small-radius jets, and for the signal they are both originating from b quarks. In event selection, at least one must be classified as a b jet by the DeepJet algorithm. If the H $\to$ b$\bar{\text{b}}$ system is produced with high momentum, the two b jets are Lorentz boosted and can be reconstructed as a single large-radius jet with substructure. In the 1ℓ case, the events must have at least one additional small-radius jet present, corresponding to the hadronic W decay.

To avoid event overlap with the b$\bar{\text{b}}\tau\tau$ analysis, this analysis vetoes events containing at least one τ_h candidate, as defined in [72]. The events are classified using multiclass DNNs, trained separately for the 1ℓ and 2ℓ cases. DNNs are trained using high-level features, such as invariant masses, hadronic activity,

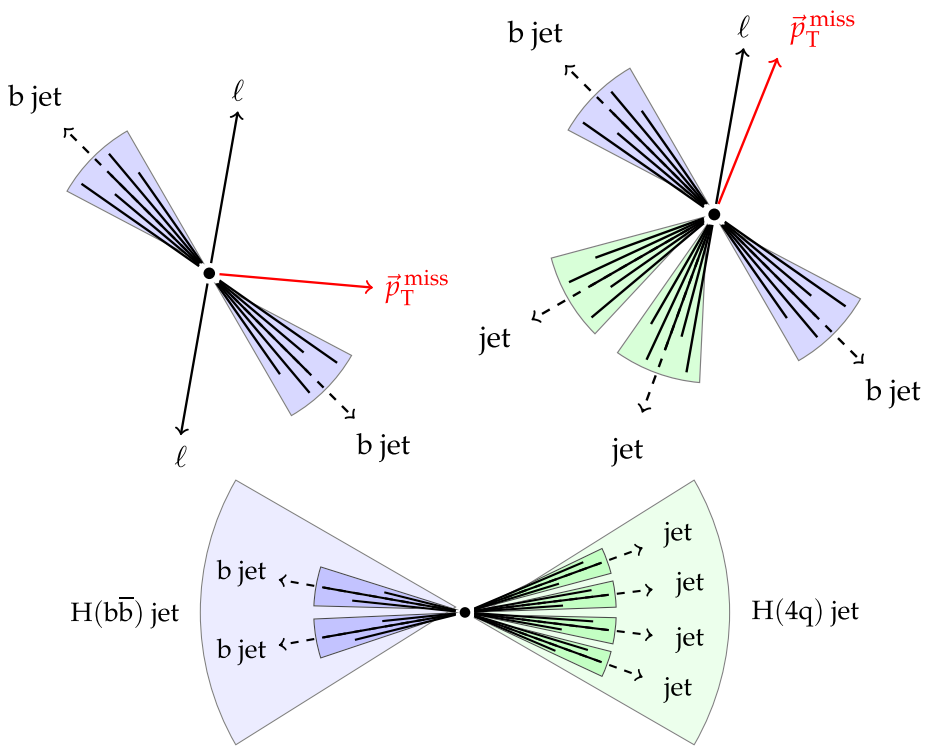


Figure 6. Illustrations of the resolved topology of the bb̄WW decay channel in the final state with two leptons (upper left) and one lepton (upper right). The boosted topology of the fully hadronic bb̄WW decay channel (lower).

and the output of a Lorentz-boosted network that performs automated feature engineering using the four-momenta of selected leptons and jets. The DNN training dataset includes signal samples with SM and anomalous κ_λ values to ensure good performance on the full model spectrum.

The multiclass DNNs have different output nodes corresponding to several background processes and two signal processes: ggF and VBF HH production. DNNs provide a score for each node that can be interpreted as the probability of each event to belong to that class. The events are categorised according to the node with the highest score. The resulting background categories are defined as follows: DY or W+jets for the 2ℓ or 1ℓ channel, respectively, and $\mathrm{t\bar{t}}$ for both channels. The two signal categories are further divided into subcategories according to the b jet multiplicity and topology into resolved-1b, resolved-2b, and boosted.

The background contribution from the misidentified leptons is estimated using the misidentification factor method [93]. In the 2ℓ channel, the DY background is estimated using data. Events with zero b-tagged jets are weighted by TFs extracted from events with dilepton invariant mass inside the Z boson mass window. All other backgrounds are estimated using simulated events. The signal extraction is performed using a simultaneous maximum likelihood fit to the distributions of the DNN outputs in the signal and background event categories.

4.4.2. $HH \to b\bar{b}WW, WW \to 4q$

The all-hadronic bb̄WW search targets highly Lorentz-boosted pairs of Higgs bosons produced via ggF and VBF. The $\mathrm{b\bar{b}}$ quark pair is reconstructed as a large-radius jet and all four quarks from the W decays form another large-radius jet. This analysis focuses primarily on the bb̄WW decays; however, HH decaying into bb̄ZZ in the fully hadronic final state are also included in the signal. The MC samples used for the modelling of the backgrounds are the same as in [74].

Each Higgs boson can be reconstructed as an AK8 jet. Additional AK4 jets are used to identify the VBF HH topology, whereas events containing isolated muons or electrons are vetoed. Events have been selected online using triggers that require high hadronic activity and the presence of AK8 jets.

Offline, two AK8 jets with $p_{\mathrm{T}} > 300\,\mathrm{GeV}$ and $|\eta| < 2.4$ are required, representing the $\mathrm{H} \to \mathrm{b\bar{b}}$ and $\mathrm{H} \to \mathrm{WW}$ decays. The ParticleNet algorithm [82] is used to isolate the signal. The $\mathrm{H} \to \mathrm{b\bar{b}}$ jets are separated from the QCD jets using the ParticleNet [82] discriminant $D_{\mathrm{b\bar{b}}}$, whereas the $\mathrm{H} \to \mathrm{WW} \to 4\mathrm{q}$

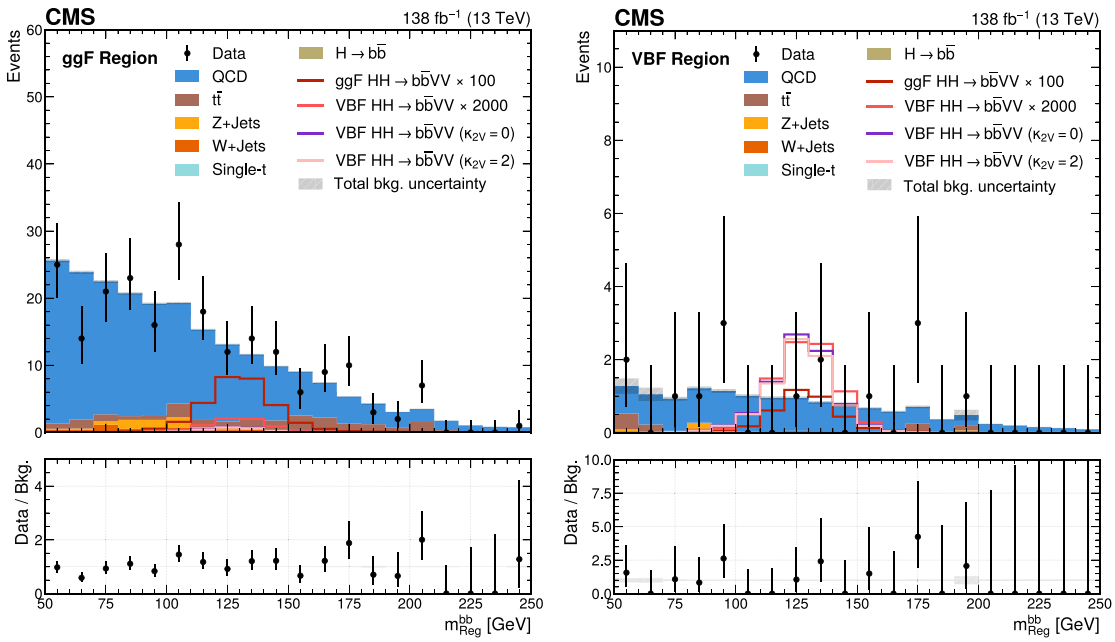


Figure 7. Distributions of the $m^{b\bar{b}}_{reg}$ observable in the ggF (left) and VBF (right) signal regions of the all-hadronic $b\bar{b}WW$ search, after a maximum likelihood fit of the background and SM HH signal to the data.

jets are identified using an attention-based NN, based on the 'particle transformer' (PART) architecture [94, 95]. To enable the background estimation and their calibration, both discriminants are decorrelated from the mass of their respective AK8 jets by training the NNs with jets sampled from a nearly uniform distribution in mass and p_T [85]. Furthermore, the PARTICLENET mass regression m_{reg} [86] is used to enhance the AK8 jet mass resolution. The $b\bar{b}$- (WW-) candidate jets are defined as the AK8 jet with a higher (lower) $D_b\bar{b}$ score.

The VBF topology comprises two jets in the opposite forward regions of the detector, with large invariant mass and $\Delta\eta$. To identify events consistent with this topology, AK4 jets with $p_T > 25\,\text{GeV}$ and $|\eta| < 4.7$, which are well separated from the $b\bar{b}$- (WW-) candidate AK8 jet, are selected. Out of the selected jets, the two highest p_T AK4 jets are considered. The VBF jet candidates, and their invariant mass and $\Delta\eta$ are used as inputs to a BDT trained to discriminate signals from the QCD multijet and $t\bar{t}$ backgrounds. Other BDT inputs include the $b\bar{b}$- and WW-candidate jet kinematics and PART tagger outputs. The inputs are selected to optimize the BDT performance without inducing correlations with the $b\bar{b}$-candidate jet mass.

The BDT is trained to classify both SM ggF and $\kappa_{2V} = 0$ VBF signal events as well as QCD multijet and $t\bar{t}$ background events. The 'ggF' and 'VBF' SRs are defined using discriminants, BDT_{ggF} and BDT_{VBF}, built from the output probabilities for the corresponding signal and background classes. Separate BDTs for the two processes were also tested, and the difference in performance was negligible.

The VBF SR selection comprises thresholds on the $D_b\bar{b}$ score of the $b\bar{b}$-candidate jet ($D^b\bar{b}_b\bar{b}$) and the BDT_{VBF} discriminant. These thresholds correspond to $\kappa_{2V} = 0$ VBF signal (background) efficiencies of 40% (≈0.1%) and 20% (≈0.003%), respectively, and are selected to minimize the expected upper limit on the $\kappa_{2V} = 0$ VBF signal. Likewise, the ggF SR selection vetoes events in VBF SR and comprises thresholds on $D^b\bar{b}_b\bar{b}$ and BDT_{ggF}, corresponding to ggF signal (background) efficiencies of 60% (≈0.3%) and 7% (≈0.01%), respectively. The dominant uncertainty in the BDT signal efficiency is related to the PART tagger calibration [96], which applies data/MC scale factors to the primary Lund jet plane [97] densities of each quark subjet.

The search is performed on the two SRs using a one-dimensional likelihood model binned in the m_{reg} of the $b\bar{b}$-candidate jet ($m^b\bar{b}_{reg}$). The background in these regions is dominated by QCD multijet events. It is estimated through data in a QCD multijet CR defined by inverting the $D_b\bar{b}$ selection. The QCD multijet yield in the SRs is estimated to be the product of data in the fail region and polynomial TFs [87–89]. The $t\bar{t}$, V+jets, and other minor backgrounds are estimated using MC simulations and their systematic and statistical uncertainties are incorporated in the final statistical analysis. The resulting $m^b\bar{b}_{reg}$ in the SRs, after a maximum likelihood fit to the data of the background model and SM HH signal, are shown in figure 7.

4.5. HH → multilepton

The HH multilepton analysis [75] focuses on HH decays into the 4W, 2W2τ, and 4τ channels. Events are selected using a set of single, double, and triple lepton triggers, as well as lepton and τ_h triggers and double τ_h triggers. The leptons and τ_h candidates are reconstructed using a set of special ID criteria originally developed for the CMS $t\bar{t}H$ multilepton analysis [98]. These IDs are customised for the use of the misidentification factor method [93] applied for the estimation of the background with misidentified lepton or τ_h candidates from control samples in data. For electrons and muons, these two IDs also use a specialised multivariate analysis specifically trained to recognise genuine leptons that originate from vector boson and τ lepton decays. All categories veto events containing at least one b jet are identified with the medium WP of the DeepJet algorithm. Next, events containing at least two b jets are identified with the loose WP, corresponding to a b jet selection efficiency of about 84% and a misidentification rate for light-flavour quark and gluon jets of about 11%. This reduces contributions from top quark–related backgrounds, such as $t\bar{t}$, making this analysis orthogonal to the HH analyses requiring b jets.

The events are split into seven mutually exclusive event categories, with final states containing multiple leptons $\ell(\mu, e)$ or hadronically decaying τ leptons (τ_h): 2ℓ with the same electric charge (SS), 3ℓ, 4ℓ, $3\ell + 1\tau_h$, $2\ell + 2\tau_h$, $1\ell + 3\tau_h$, and $4\tau_h$. All categories require a specified number of final-state light leptons and τ_h. The 2ℓ SS and 3ℓ categories additionally require the presence of jets originating from hadronic W boson decays. The primary background in most categories is provided by events containing misidentified ℓ or τ_h candidates. All categories also contain sizable contributions from genuine multiboson backgrounds from ZZ and WZ decays. As a result, two kinematic distributions in WZ and ZZ CRs are included in the fit. The categories are constructed by inverting the Z boson veto into the 3ℓ and 4ℓ categories, respectively. The inclusion of these two CRs helps to constrain the two primary diboson backgrounds, as well as the corresponding systematic uncertainties.

The analysis uses a parameterized BDT tuning the sensitivity to the SM and to the EFT benchmark set JHEP04(2016)126 described in section 3. The maximum likelihood fit for the signal extraction is performed simultaneously on the seven event categories. The results for each benchmark point are extracted from the corresponding BDT output. For the benchmarks not included in the BDT training, the most similar one based on the shape of the parton-level m_{HH} spectrum is used during inference.

4.6. HH → ττγγ

The search for HH production in the $\tau\tau\gamma\gamma$ final state aims to cover both the hadronic and leptonic decay modes of the τ lepton. Despite the small HH → $\tau\tau\gamma\gamma$ branching fraction in the SM (2.85×10^{-4}), the diphoton pair offers a clean experimental signature to trigger on with a good mass resolution, whereas the additional tau leptons in the event help to further isolate signals from the background. The goal of the search is the nonresonant HH production via ggF. The VBF production is not considered in this analysis.

Events are selected online using a diphoton trigger with asymmetric photon p_T thresholds of 30 and 18 GeV. All events are required to have at least one diphoton candidate. In the case where more than one candidate exists, the candidate with the highest scalar p_T sum of photons is selected.

Events are required to have at least one τ lepton candidate. Both hadronic and leptonic decay modes of the τ lepton are considered. A $\tau\tau$ candidate can be identified from any of the following pairs of reconstructed objects: $\tau_h\tau_h$, $\tau_h\mu$, $\tau_h e$, μe, $\mu\mu$, ee, τ_h+isolated track. The DeepTau discriminant is used to select τ_h candidates. Events consistent with an Z → $\ell\ell$ or Z → $\ell\ell\gamma$ decay are rejected.

A BDT classifier is used to further isolate events with signal-like characteristics from the background. Hadronic jets in the event are only used in the BDT to reject backgrounds like $t\bar{t}$. To reduce the probability of creating an artificially peaking structure, $m_{\gamma\gamma}$ is not included as an input feature to the BDT. The p_T of the photon candidates are divided by $m_{\gamma\gamma}$ to reduce correlations between the photon p_T and $m_{\gamma\gamma}$. Sequential boundaries are placed on the BDT output to define event categories of different signal purity, where the boundary positions are selected to maximize the signal sensitivity.

The $m_{\gamma\gamma}$ distribution is used in the maximum likelihood fit for each event category. The smoothly falling background (continuum) is modelled directly from the data. The signal and the single Higgs boson production, which have a resonant background, are modelled using simulations.

4.7. HH → bb̄ZZ

This analysis [77] focuses on ggF HH production where one Higgs boson decays to a $b\bar{b}$ pair, while the other decays to a ZZ pair resulting in a 4ℓ final state. The 4ℓ decay channel provides a clean signature despite the small branching fraction, which is partially compensated by the high branching fraction of the $b\bar{b}$ decay channel. The final state comprises two jets and two pairs of oppositely charged isolated

electrons or muons. The 4ℓ SR is defined by requiring that the four-lepton invariant mass $m(4\ell)$ is within the Higgs boson mass window, whereas events with $m(4\ell)$ outside this range comprise the 4ℓ CR.

The dominant Z+X background is characterized by nonprompt and misidentified leptons, primarily from decays of heavy-flavour hadrons, misidentified jets, and electrons from photon conversions. The Z+X background is estimated from data CR, and the probabilities of a light lepton to be misidentified. The main contributions to the systematic uncertainty in the reducible background estimation are the limited sizes of the CR and the samples used to estimate the misidentification rates. Uncertainties related to the difference in composition between the SR and the misidentification rate estimation sample are also considered.

The BDT is trained using MC simulated events in the 4ℓ SR to further discriminate the ggF HH signal process from all background processes. The BDT output distribution is fit to constrain the parameters of interest.

4.8. HH $\rightarrow$ WW$\gamma\gamma$

This analysis examines three WW decay modes: semileptonic (1ℓ), fully hadronic, and fully leptonic (2ℓ) decays. Events are selected using double-photon triggers with thresholds on the leading (subleading) photon p_{T} of $p_{\mathrm{T}}^{\gamma} > 30$ (18) GeV for the data collected during 2016 and $p_{\mathrm{T}}^{\gamma} > 30$ (22) GeV for 2017 and 2018. The MC samples used in this analysis are the same as the ones used in the $\mathrm{b\bar{b}}\gamma\gamma$ analysis [73]. The continuum background is modelled from the data using the $m_{\gamma\gamma}$ distribution. The single Higgs boson background is modelled using simulated samples.

A BDT classifier is trained for photon-jet separation, resulting in a photon ID score. Jets from the hadronization of bottom quarks are identified using the DeepJet algorithm. The number of light leptons is used to maintain orthogonality in all three analyses. We assign an event to the fully hadronic channel if it has no leptons, to the 1ℓ channel if it has exactly one lepton, and to the 2ℓ channel if it has two leptons. Each channel requires a diphoton candidate, which is defined as a pair of two photons.

The 1ℓ channel uses a multiclassifier DNN to differentiate between signal, single Higgs boson, and background events, as shown in figure 8, upper left.

The $\mathrm{b\bar{b}}\gamma\gamma$ signal contaminates the WW$\gamma\gamma$ phase space in the fully hadronic channel. As a result, two binary classifiers are used for the fully hadronic channel, one acting as a $\mathrm{b\bar{b}}\gamma\gamma$ discriminator and the other distinguishing between signal and background events. The latter is shown in figure 8, upper right. A specific challenge in the fully hadronic channel is differentiating between the ZZ$\gamma\gamma$ and the WW$\gamma\gamma$ signal processes due to the identical experimental signatures of the hadronic Z and W decays. There are residual $\mathrm{b\bar{b}}\gamma\gamma$ events that pass the WW$\gamma\gamma$ event selection but are not favoured by the $\mathrm{b\bar{b}}\gamma\gamma$ analysis due to low $\mathrm{b\bar{b}}\gamma\gamma$ discriminator scores. Therefore, the combination of WW$\gamma\gamma$, ZZ$\gamma\gamma$, and residual $\mathrm{b\bar{b}}\gamma\gamma$ processes is considered signal in this analysis. Finally, due to the limited size of the samples available for training and validating a multivariate event classifier, a selection based on traditional variables is adopted for the 2ℓ channel. The diphoton invariant mass distribution is used for the signal extraction across all channels. The signal-plus-background and background-only fits for all channels weighted by $S/(S+B)$ are shown in figure 8, lower portion.

5. Systematic uncertainties

Hundreds of systematic uncertainties are considered, affecting HH signal and background processes' yields (i.e. normalization uncertainties) and/or shapes (i.e. shape uncertainties). Systematic uncertainties are introduced as nuisance parameters in the maximum likelihood fit used to extract the results. Common uncertainties among different analyses are fully correlated, whereas others specific to each analysis are treated as uncorrelated. The uncertainties with the biggest impact (20%–23%) are the ones affecting the background in $\mathrm{b\bar{b}b\bar{b}}$ and $\mathrm{b\bar{b}}\tau\tau$ analyses and the uncertainty in the theoretical prediction of the HH production cross-section.

5.1. Theoretical uncertainties

Theoretical uncertainties on the renormalization and factorization scale, strong coupling constant α_{S}, and PDFs affecting the cross-section of all the simulated processes are included. Other uncertainties considered concern EW corrections for the $\mathrm{t\bar{t}Z}$, $\mathrm{t\bar{t}W}$, $\mathrm{q\bar{q}ZZ}$, and ggZZ processes. Theoretical uncertainties in the Higgs boson branching fractions [99] are applied to both the HH signal and single-Higgs backgrounds. The assigned uncertainties are 1.2% for $\mathrm{H} \rightarrow \mathrm{b\bar{b}}$, 1.5% for $\mathrm{H} \rightarrow \mathrm{WW}$ and $\mathrm{H} \rightarrow \mathrm{ZZ}$, 2.1% for $\mathrm{H} \rightarrow \gamma\gamma$, and 1.6% for $\mathrm{H} \rightarrow \tau\tau$. These uncertainties are treated as correlated across all channels. The

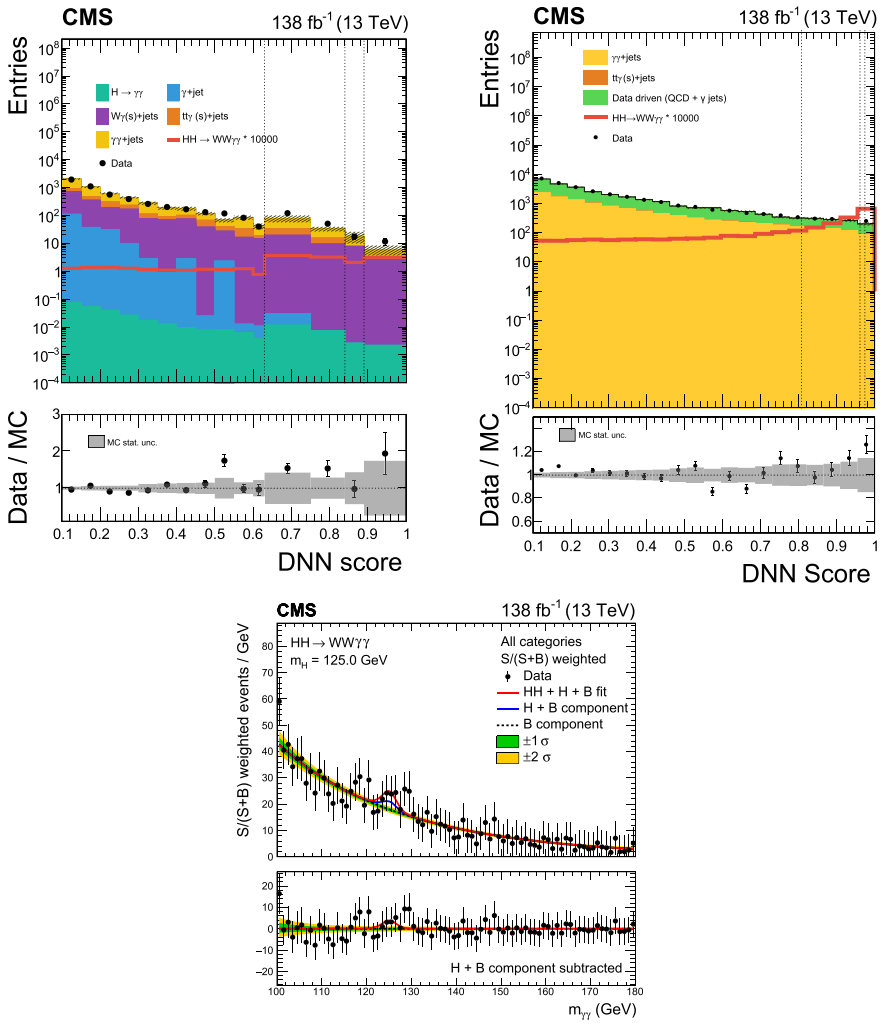


Figure 8. The distributions of DNN scores for the signal and main backgrounds in the 1ℓ (upper left) and fully hadronic (upper right) channels of the WW$\gamma\gamma$ analysis. The signal-plus-background (red), single H plus continuum background (blue), and continuum background (dashed black) fits for all channels weighted by $S/(S+B)$ (lower).

uncertainty in the rate of Higgs boson production associated with heavy-flavour jets is assumed to be 50% [100].

Theoretical uncertainties on the nonresonant HH cross-section via ggF are applied as a function of κ_λ and include a combination of uncertainties in the renormalization and factorization scales, as well as the uncertainty in the top quark mass. In the SM case when $\kappa_\lambda = 1$, this combined uncertainty corresponds to $-23\%/+6\%$. The PDF uncertainty is 3% [101]. Uncertainties for VBF production include $+0.03\%/-0.04\%$ (scales) and 2.1% (PDF+α_S) [61, 102]. An additional scale uncertainty is applied to the $b\bar{b}\tau\tau$, $b\bar{b}WW$, and multilepton analyses related to PYTHIA and the colour-correlated recoil effect. This effect was found to be negligible in other analyses.

Some analyses suffer from a significant $t\bar{t}$ background contribution ($b\bar{b}WW$, multilepton, and $b\bar{b}\tau\tau$) and a shape uncertainty that corresponds to the NNLO correction on the top quark p_T is applied to the $t\bar{t}$ simulated samples [103]. The $b\bar{b}WW$ and multilepton analyses include additional uncertainties on the parton shower initial- and final-state radiation for background processes, on the top quark mass for the $t\bar{t}$ background, as well as renormalization and factorization scale uncertainties for $t\bar{t}$ and single top quark production.

5.2. Experimental uncertainties

The integrated luminosities for 2016, 2017, and 2018 data-taking years have demonstrated 1.2%–2.5% uncertainty per year [104–106], whereas the overall uncertainty for the 2016–2018 period is 1.6%. The number of pppp interactions is calculated from the instantaneous luminosity and an estimated inelastic pppp collision cross-section with 4.6% uncertainty [107]. An uncertainty in the shape of the distribution of the mean number of pppp interactions per bunch crossing (pileup) is also applied to all simulated

samples. The trigger selection efficiency is corrected in each analysis to account for the differences between the data and simulation, and a corresponding uncertainty is applied.

When ID criteria are applied to muons, electrons, and τ_h candidates, the ID efficiencies in the simulated samples are corrected to match those in the data. The uncertainties related to these corrections affect the shapes of the kinematic distributions. For analyses that use the same selection criteria, these uncertainties are treated as correlated. For analyses that use photons, the shape uncertainties related to the photon ID efficiency are also considered.

Similarly, the uncertainties in the efficiency of the jet selection criteria in simulations are considered as uncertainties in the shape of the kinematic distributions. Nuisance parameters that affect the shape of the jet flavour discriminant are also included. Different types of flavour contamination are treated with separate parameters. Uncertainties in the jet energy scale and resolution are used as shape uncertainties for all simulated samples. For analyses where p_T^{miss} is relevant, uncertainties related to the unclustered energy reconstruction efficiency are considered as correlated uncertainties in p_T^{miss} distribution shapes in simulated samples.

During data collection in 2016 and 2017, a gradual change in the timing of the ECAL first-level trigger inputs in the region with $|\eta| > 2.0$ caused a specific trigger inefficiency. For events containing an electron (jet) with $p_T \gtrsim 50$ (100) GeV in the region $2.5 < |\eta| < 3.0$, the efficiency loss is approximately 10%–20%, depending on p_T, η, and time. Correction factors are computed from the data and applied to the acceptance evaluated from simulations. In addition, a normalization uncertainty is included in the global maximum likelihood fit, described in section 6.

A correction factor is applied to simulated data for the 2018 era to account for two HCAL modules being switched off, and an associated shape uncertainty is introduced that is treated as correlated among most analyses. Analyses that perform data-driven background estimation methods include dedicated uncertainties, which are treated as uncorrelated.

Finally, uncertainties from the limited number of simulated events are considered using the Barlow–Beeston approach [108]. These uncertainties are not considered in the case of the HL–LHC projections, as it is assumed that we will have sufficient simulated data at the time.

6. Results

Upper limits on HH production cross-sections and constraints on coupling modifiers that contribute to SM HH production are derived based on the asymptotic formulae for the profile likelihood ratio test statistic $-2\Delta\ln(L)$ [109, 110] and the CLs [111, 112] criterion. Generally, the test statistic is defined as

$$-2\Delta\ln(L) \equiv -2\ln\left(\frac{L\left(\vec{\mu}, \hat{\vec{\nu}}(\vec{\mu})\right)}{L\left(\hat{\vec{\mu}}, \hat{\vec{\nu}}\right)}\right), \tag{3}$$

where L is the combined likelihood function, $\vec{\mu}$ are the parameters of interest, such as signal strengths or coupling modifiers, $\hat{\vec{\mu}}$ are the best fit values of $\vec{\mu}$, $\hat{\vec{\nu}}(\vec{\mu})$ is the maximum likelihood estimator of the nuisance parameters for a given set of values of $\vec{\mu}$, and $\hat{\vec{\nu}}$ is the global maximum likelihood estimator of the nuisance parameters for the best fit values of $\vec{\mu}$. In general, confidence intervals at 68% (95%) CL are derived by finding the values of the parameters of interest for which the test statistic is less than 1 (3.84), following Wilks' theorem [113]. However, due to the quadratic dependence of the expected yields on the values of the coupling modifiers, the corresponding intervals may undercover or overcover the true values [114, 115]. For comparison, constraints on the coupling modifiers are also computed by performing a scan of the 95% CL upper limit on the signal strength of HH production while varying the coupling modifier of interest, as reported in table 4. The results of the different analyses described in this paper have been statistically combined in a global maximum likelihood fit. The HEFT parametrization is used to provide constraints on a number of different BSM scenarios. In all cases, expected limits are derived under the background-only hypothesis. The results have been determined using the CMS statistical analysis tool COMBINE [116], which is based on the ROOFIT [117] and ROOSTATS [118] frameworks.

An upper limit at 95% CL on the inclusive HH production cross-section is observed (expected) to be 3.5 (2.5) times the SM prediction, whereas the equivalent upper limit for the VBF alone is 79 (91) times the SM prediction. The limits on the HH cross-section divided by the SM prediction, that is the signal strength μ, for each contributing channel and their combination are shown in figures 9 and 10 for the inclusive and VBF cases, respectively.

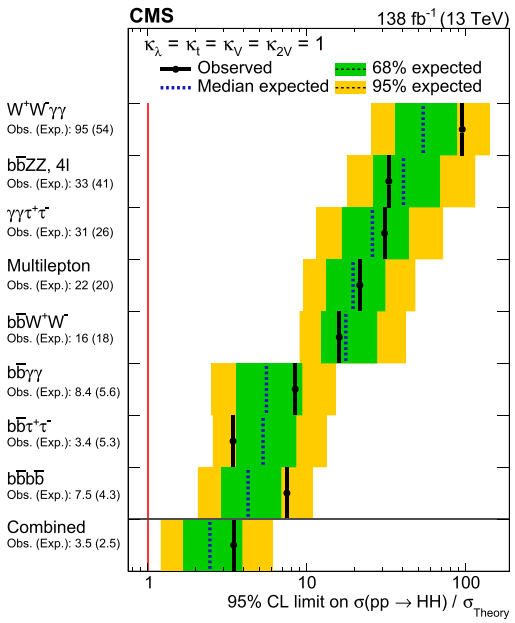


Figure 9. The upper limits at 95% CL on the inclusive signal strength $\mu = \sigma_{\mathrm{HH}}/\sigma_{\mathrm{HH}}^{\mathrm{SM}}$ for each channel and their combination. The inner (green) and outer (yellow) bands indicate the 68 and 95% CL intervals, respectively, under the background-only hypothesis. The individual contributions within the bb̄bb̄ and bb̄WW channels have been combined to simplify the presentation of results.

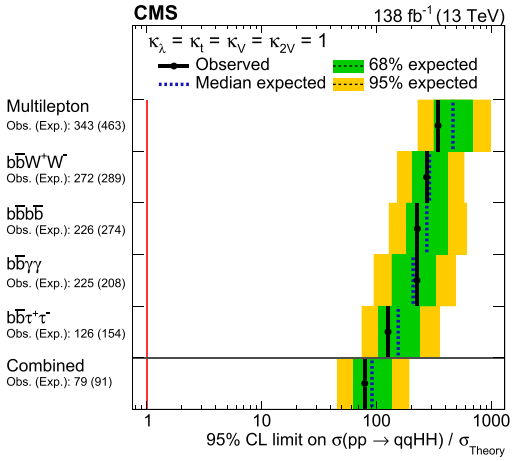


Figure 10. The upper limits at 95% CL on the VBF signal strength $\mu_{\mathrm{VBF\,HH}} = \sigma_{\mathrm{VBF\,HH}}/\sigma_{\mathrm{VBF\,HH}}^{\mathrm{SM}}$ for each channel and their combination. The inner (green) and outer (yellow) bands indicate the 68 and 95% CL intervals, respectively, under the background-only hypothesis. The five contributing channels are indicated in the figure. The individual contributions within the bb̄bb̄ and bb̄WW channels have been combined to simplify the presentation of results.

The $-2\Delta\ln(L)$ scans as a function of κ_λ and $\kappa_{2\mathrm{V}}$ is shown in figure 11. Besides the ones varied as shown, all other couplings are set to the values expected by the SM. All eight channels are included in the combination. The best fit value of κ_λ is found to be 1.51 and κ_λ is constrained at 68% CL to be within -0.07 and 4.18, whereas the expected constraint is from -0.87 to 6.31. At 95% CL, κ_λ is constrained to be within -1.35 to 6.37, with an expected constraint of -2.24 to 7.89.

For $\kappa_{2\mathrm{V}}$, the best fit value is at 1.02, the 68% CL interval is from 0.81 to 1.23 (0.77—to 1.26 expected), and the 95% CL interval is from 0.64 to 1.40 (0.62—to 1.41 expected). The value of $\kappa_{2\mathrm{V}} = 0$ is excluded with a significance of 6.6 standard deviations. This level of significance marks a decisive step in establishing the presence of quartic Higgs-vector boson interactions in nature.

In figure 12, the upper limits at 95% CL on the HH cross-section are shown to be functions of κ_λ (left) and $\kappa_{2\mathrm{V}}$ (right), respectively. We exclude HH production at 95% CL, meaning a 95% CL upper limit on the inclusive HH signal strength $\mu < 1$, for values of κ_λ outside the range from -1.39 to 7.02.

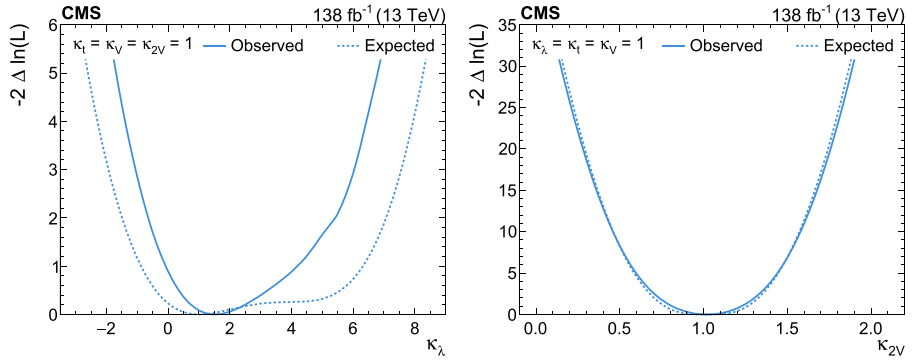


Figure 11. The $-2\Delta\ln(L)$ scan as functions of coupling modifiers κ_λ (left) and κ_{2V} (right) for the combination of all channels when all the other parameters are fixed to their SM values.

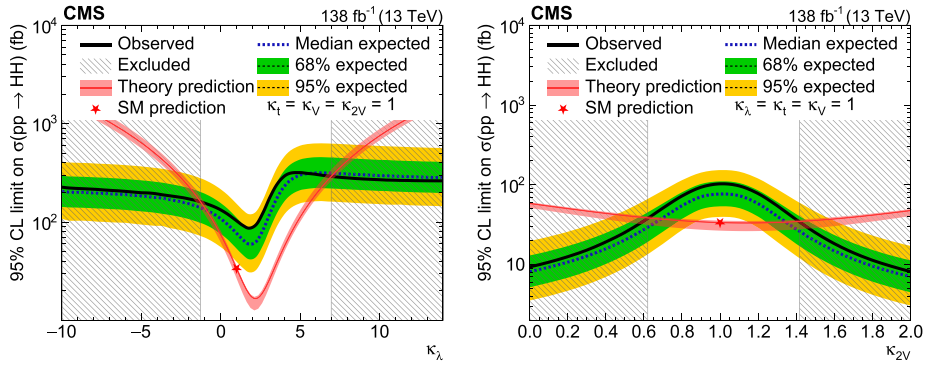


Figure 12. The 95% CL upper limits on the inclusive HH cross-section as functions of κ_λ (left) and κ_{2V} (right). All other couplings are set to the values predicted by the SM. The theoretical uncertainties in the ggF and VBF HH signal cross-sections are not considered because here we directly constrain the measured cross-section. The inner (green) band and the outer (yellow) band indicate the 68 and 95% CL intervals, respectively, under the background-only hypothesis. The star shows the limit at the SM value for κ_λ and κ_{2V}.

Table 4. Summary of results on constraints to the coupling modifiers κ_λ and κ_{2V}. The ranges are either extracted using either the $-2\Delta\ln(L)$ scan at 68% and 95% CL, or upper limits on the signal strength μ at 95% CL. The theoretical uncertainties in the ggF and VBF HH signal cross-sections are considered in all the results tabulated here.

Method	κ_λ observed (expected)	κ_{2V} observed (expected)
$-2\Delta\ln(L)$ scan, 68% CL	$[-0.07, 4.18]$ ($[-0.87, 6.31]$)	[0.81, 1.23] ([0.77, 1.26])
$-2\Delta\ln(L)$ scan, 95% CL	$[-1.35, 6.35]$ ($[-2.24, 7.89]$)	[0.64, 1.40] ([0.62, 1.41])
Limits on μ, 95% CL	$[-1.39, 7.02]$ ($[-1.02, 7.19]$)	[0.62, 1.42] ([0.69, 1.35])

Similarly, we exclude HH production at 95% CL for values of the κ_{2V} coupling modifier outside the range from 0.62 to 1.42, with the expected range from 0.69 to 1.35.

A summary of the constraints on the coupling modifiers κ_λ and κ_{2V} is provided in table 4.

Figure 13 shows 68% and 95% CL contours of $-2\Delta\ln(L)$ in the (κ_λ, κ_{2V}), (κ_V, κ_{2V}), and (κ_λ, κ_t) planes for the combination of all contributing channels. In the (κ_λ, κ_{2V}) and (κ_V, κ_{2V}) planes, the five standard deviation CL contours are also shown. All the other parameters, besides the ones scanned, are set to the values expected by the SM. The value of $\kappa_{2V} = 0$ is excluded at a CL of more than five standard deviations, for every value of κ_λ, adding to the robustness of this exclusion. No significant deviation from the SM is observed.

Beyond varying κ_λ, κ_{2V}, κ_V, and κ_t, we interpret the data in terms of couplings that are not predicted in the SM, namely c_2, c_g, and c_{2g}. All BSM interpretations studied in this paper only alter the ggF production, whereas the VBF production is assumed to be as predicted by the SM. The channels contributing to the BSM interpretations are $b\bar{b}\gamma\gamma$, $b\bar{b}b\bar{b}$ boosted and resolved, $b\bar{b}\tau\tau$, $b\bar{b}$WW, multilepton, WW$\gamma\gamma$, and $\tau\tau\gamma\gamma$.

First, we interpret the results in the context of two sets of benchmarks, JHEP04(2016)126 [51] and JHEP03(2020)091 [52], combinations of the coupling modifiers $(\kappa_\lambda, \kappa_t, c_2, c_g, c_{2g})$ as described in

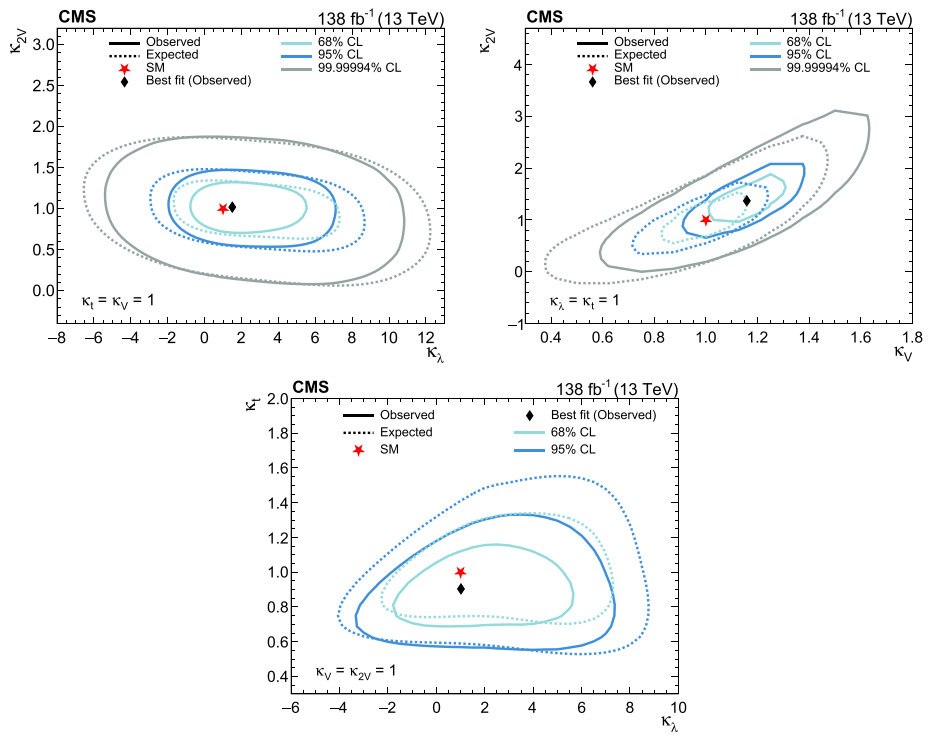


Figure 13. The 68% and 95% CL contours of $-2\Delta\ln(L)$ in the $(\kappa_\lambda, \kappa_{2V})$ (upper left), (κ_V, κ_{2V}) (upper right), and $(\kappa_\lambda, \kappa_t)$ (lower) planes for the combination of all channels when all the other parameters are fixed to their SM values. In the $(\kappa_\lambda, \kappa_{2V})$ and (κ_V, κ_{2V}) planes, the five standard deviation CL contours are also shown.

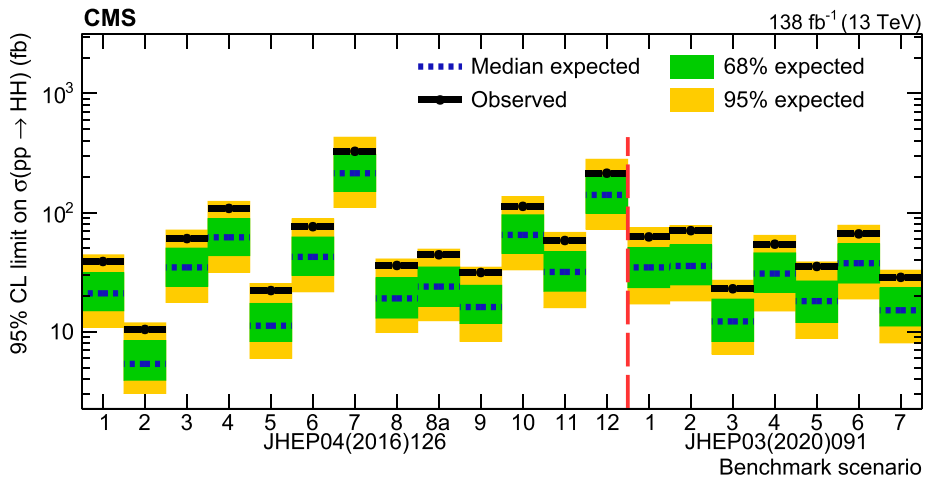


Figure 14. The upper limits at 95% CL on the HH production cross-section for the two sets of HEFT benchmarks. The theoretical uncertainties in the ggF HH signal cross-section are not considered since we directly constrain the measured cross-section.

section 3. The $\tau\tau\gamma\gamma$ channel only contributes to the results for the benchmarks JHEP04(2016)126, whereas the rest of the channels contributes towards both sets. The upper limits on the HH cross-section at 95% CL are shown in figure 14. No significant deviations from expectations are observed, but there is an overall excess in all benchmarks, between 68% and 95% CL, consistent with excesses observed in the most sensitive channels, namely $b\bar{b}\gamma\gamma$ and $b\bar{b}b\bar{b}$ especially in the boosted topology, visible in figure 9.

In the HEFT Lagrangian, the term containing κ_t is correlated with the coupling modifier c_2, which corresponds to the BSM coupling between two top quarks and two Higgs bosons. Figure 15 depicts the $-2\Delta\ln(L)$ scan for c_2 on the left and the upper limits on the HH cross-section as a function of c_2 on the right. For c_2, the best fit to the data is found to be 0.40, the 68% CL interval is from 0.20 to 0.52 (-0.15–0.42 expected), and the 95% CL interval is from -0.29 to 0.63 (-0.27–0.56 expected). Considering the theoretical uncertainties in the ggF and VBF HH signal cross-sections, we exclude HH production at 95% CL for c_2 values outside the range from -0.28 to 0.59. The corresponding expected

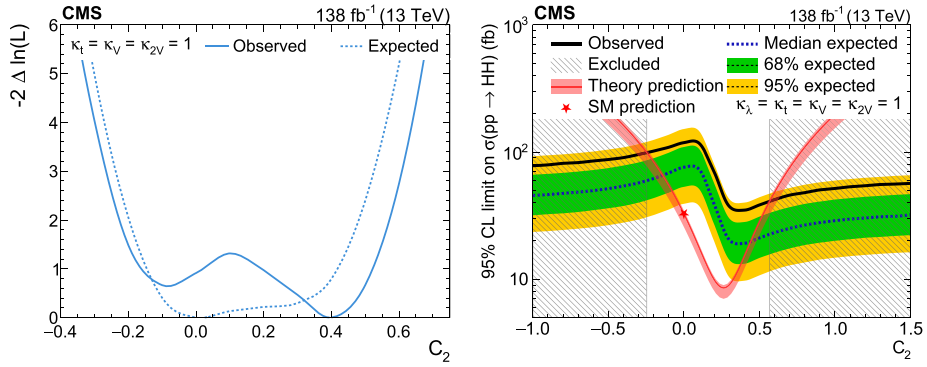


Figure 15. The upper limits at 95% CL on the HH cross-section as a function of the c_2 coupling modifier (left). The theoretical uncertainties in the ggF HH signal cross-section are not considered since we directly constrain the measured cross-section. The $-2\Delta\ln(L)$ scan as a function of the c_2 coupling modifier (right).

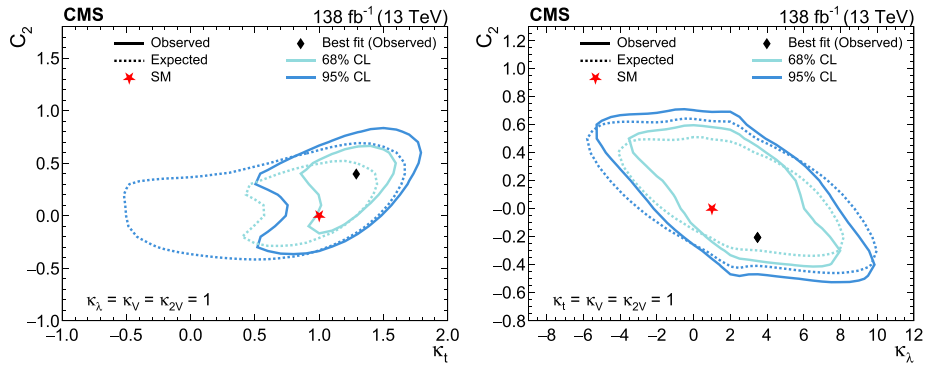


Figure 16. The 68% and 95% CL contours of $-2\Delta\ln(L)$ in the (c_2, κ_t) (left) and (c_2, κ_λ) (right) planes for the combination of all channels when all the other parameters are fixed to their SM values.

range is from −0.17 to 0.47. Figure 16 shows the two-dimensional contours of $-2\Delta\ln(L)$ in the (c_2, κ_λ) and (c_2, κ_t) planes for the combination of all contributing channels.

The data are further interpreted in the context of several UV complete models, exploiting the HEFT parametrization described in section 3. Experimental constraints on the parameters that characterize each model are extracted using a mapping between κ_λ, κ_t, and c_2 and the specific model parameters.

The simplest extensions of the SM Higgs sector, are models with the addition of a single new scalar Φ with couplings to the Higgs doublet [6, 7]. In the following, we consider the cases where the Z_2 symmetry of the resulting potential $V(\Phi, H)$ is either explicitly or spontaneously broken. In the explicit case, the modifications of the Higgs boson interactions can be written in terms of α, the mixing angle of the new scalar with the Higgs doublet, m_2, the coefficient of the triple singlet coupling, and λ_α the coefficient of the biquadratic term between the scalar and Higgs potentials. In the spontaneously broken symmetry case, the modifications depend only on α. Figure 17 shows the $-2\Delta\ln(L)$ scan as a function of $\cos\alpha$ and the 95% CL contour in the ($\cos\alpha$, λ_{eff}) plane, where $\lambda_{\text{eff}} = \lambda_\alpha - \tan(\alpha)\frac{m_2}{\nu}$, for singlet extensions of the SM with both explicit and spontaneous Z_2 symmetry breaking. For the spontaneous case, the allowed range of $\cos\alpha$ at 68% CL is from 0.92 to 1 (expected: 0.86 to 1) and at 95% CL is from 0.79 to 1 (expected: 0.82 to 1). The strongest constraints come from the $b\bar{b}\tau\tau$ and $b\bar{b}b\bar{b}$ boosted channels.

In the 2HDM, additional bosons arise from the introduction of a second complex Higgs doublet that mixes with the SM Higgs doublet [8–11]. Four cases are considered, based on which of the two doublets the SM fermions couple to. For 'Type-I,' the charged fermions only couple to the second doublet. For 'Type-II,' up- and down-type fermions couple to different doublets. In 'Type-X,' charged leptons couple to the first doublet and both up- and down- type quarks couple to the second doublet. Finally for 'Type-Y,' up-type quarks and charged leptons couple to the second doublet, whereas down-type quarks couple to the first. Based on the mixing of the two doublets, five scalar bosons arise: a CP-even scalar H, a CP-odd scalar A (both of which are usually heavy), a light SM-like Higgs boson h, and two charged Higgs bosons $H^\pm$. The model is characterized by the masses of these five bosons, the mixing angle of the

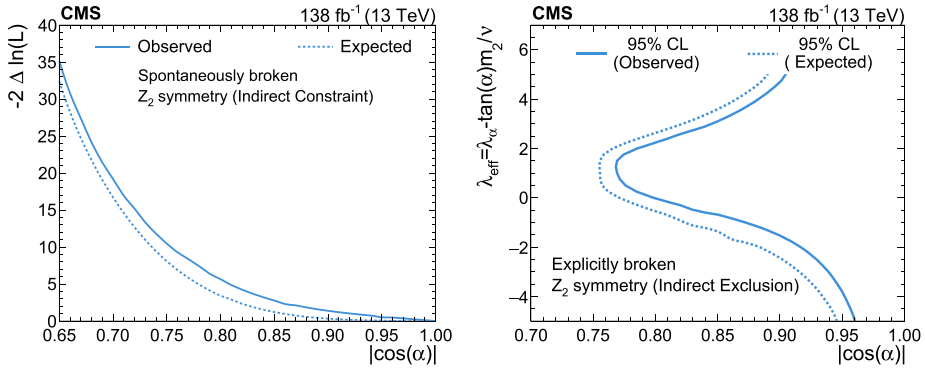


Figure 17. The $-2\Delta\ln(L)$ scan for the combination of all channels as a function of $\cos\alpha$ for singlet extensions of the SM with spontaneous Z_2 symmetry breaking (left). The $\cos\alpha$ is constrained at 95% CL from 0.79 to 1. The 95% CL contour of $-2\Delta\ln(L)$ in the ($\cos\alpha$, λ_{eff}) plane (right), where $\lambda_{\text{eff}} = \lambda_\alpha - \tan(\alpha)\frac{m_2}{v}$. The ranges of $\cos\alpha$ and λ_{eff} are selected to ensure the validity of the models. The excluded regions are below and to the left of the curves shown.

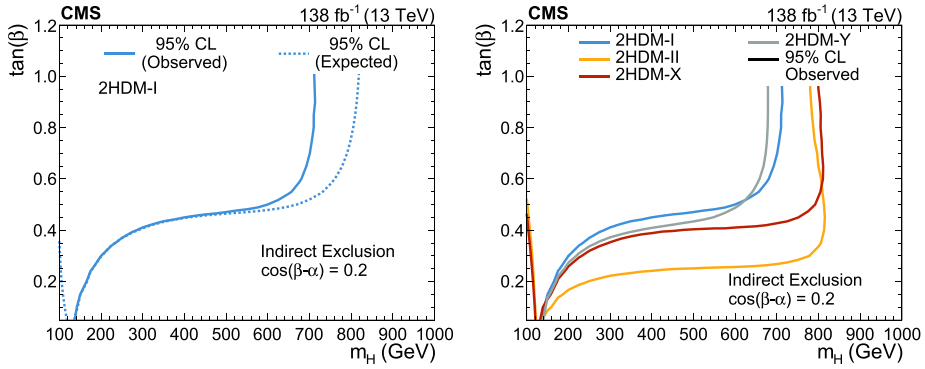


Figure 18. The 95% CL contour of $-2\Delta\ln(L)$ for the combination of all channels in the (m_{H}, $\tan\beta$) plane for a fixed value of $|\cos(\beta-\alpha)| = 0.2$ in the 2HDM-I model (left) and the four considered 2HDM models (right). In these and all other cases considered in this paper, $m_{\text{H}} = m_{\text{A}}$. The ranges of m_{H} and $\tan\beta$ are selected to ensure the validity of the models. The excluded regions are below the curves shown. The value $\tan\beta = 0.5$ is excluded for $m_{\text{H}} > 800$ GeV for all the models considered.

CP-even Higgs fields α, the ratio of the vacuum expectation values in the two associated Higgs potentials $\tan\beta = \frac{\nu_2}{\nu_1}$ and the mass mixing parameter m_{12}. The masses of the heavy scalars H and A are considered to be equal and noted as m_{A}.

Figures 18 and 19 show the results of the combination in the (m_{H}, $\tan\beta$) and ($|\cos(\beta-\alpha)|$, $\tan\beta$) planes, respectively. On the left are the observed and expected 95% CL contours for the 2HDM-I case, whereas the right shows the observed contours in all 2HDM cases. The excluded regions are below the curves shown. The results are derived under the assumption that we are not sensitive to the direct features of the resonant signal and that the interference effects between the resonant and nonresonant signals are negligible. Therefore, no interference effects are considered in this study.

Another simple extension of the SM is the minimal composite Higgs model (MCHM) [12–15]. Two cases are studied, MCHM_4 and MCHM_5, where the SM fermions either transform as spinors or as fundamental representations of the underlying SO(5) symmetry. These models are characterized by the compactness parameter $\xi = (\frac{\nu}{f})^2$ with ν being the vacuum expectation value and f the strong dynamics scale.

Figure 20 shows the observed and expected $-2\Delta\ln(L)$ scan as a function of ξ for MCHM_4 and MCHM_5. For MCHM_4, the best fit is $\xi = 0.0$, whereas the observed (expected) 68% and 95% CL ranges are found to be from 0 to 0.18 (0 to 0.35) and 0 to 0.45 (0 to 0.55), respectively. The strongest constraints come from the WW$\gamma\gamma$ and b$\bar{\text{b}}$WW channels. Likewise, for MCHM_5, the best fit is $\xi = 0.05$. In contrast, the observed (expected) 68% and 95% CL ranges are found to be from 0 to 0.15 (0 to 0.13) and 0 to 0.26 (0 to 0.21), respectively. In this case, the strongest constraints come from the multilepton and WW$\gamma\gamma$ channels.

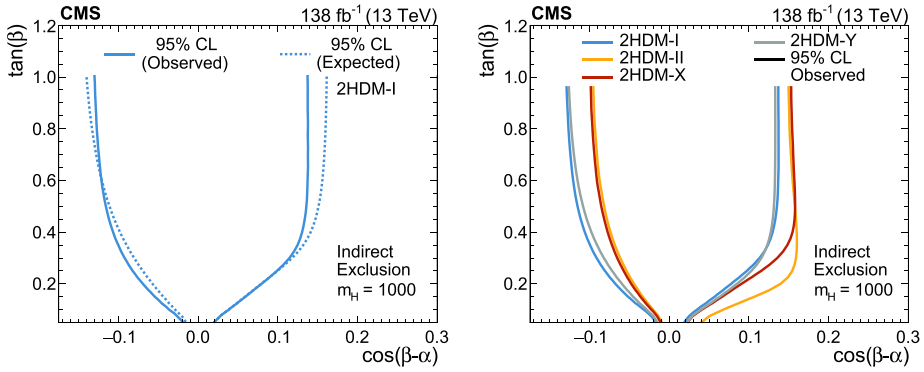


Figure 19. The 95% CL contour of $-2\Delta\ln(L)$ for the combination of all channels in the $(\cos(\beta-\alpha), \tan\beta)$ plane for a fixed value of $m_{\mathrm{H}} = 1000\,\mathrm{GeV}$ in the 2HDM-I model (left) and the four considered 2HDM models (right). In these and all other cases considered in this paper, $m_{\mathrm{H}} = m_{\mathrm{A}}$. The ranges of $\cos(\beta-\alpha)$ and $\tan\beta$ are selected to guarantee the validity of the model. The excluded regions are below the curves shown. The value $\tan\beta = 0.5$ is excluded for $\cos(\beta-\alpha) > 0.16$ and $\cos(\beta-\alpha) < -0.13$ for all models considered.

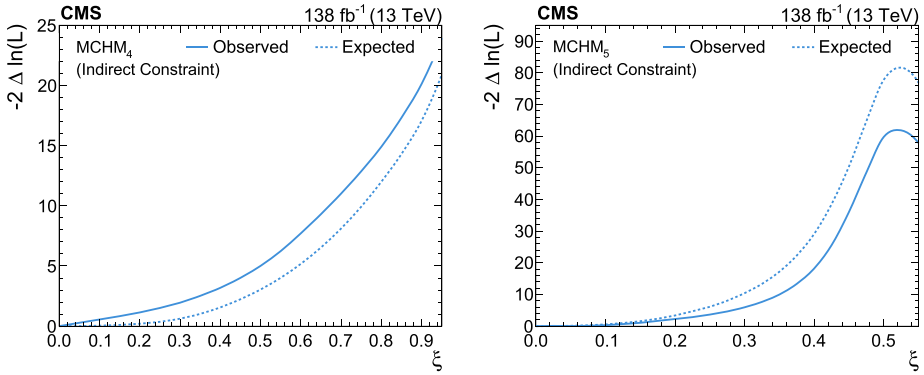


Figure 20. The $-2\Delta\ln(L)$ scan for the combination of all channels as a function of ξ for $\mathrm{MCHM_4}$ (left) and $\mathrm{MCHM_5}$ (right). The range of ξ is chosen to guarantee the validity of the model. At 95% CL, ξ is constrained to be between 0 and 0.45 in $\mathrm{MCHM_4}$ and 0 and 0.26 in $\mathrm{MCHM_5}$.

7. Projections for the High-Luminosity LHC (HL–LHC)

To further probe the SM, with particular interest in the Higgs boson self-coupling, the HL–LHC [119] operation is currently scheduled to begin in 2030. An integrated luminosity of up to 3000 fb^{-1} is expected to be collected over the anticipated 10 years of data-taking. This unparalleled dataset will open a unique window on the weak-scale nature of the Universe, and the study of the Higgs boson self-coupling represents one of the most important targets of the HL–LHC. It is therefore of interest to extrapolate the current results to predict the sensitivity that can be achieved at the HL–LHC.

The results are projected to different integrated luminosity values, that is 300, 1000, 2000, and 3000 fb^{-1} to track the evolution during data collection. In the projection studies, only the $\mathrm{b\bar{b}}\gamma\gamma$, $\mathrm{b\bar{b}}\tau\tau$, $\mathrm{b\bar{b}b\bar{b}}$, multilepton, and $\mathrm{b\bar{b}WW}$ channels are included as they are the ones with the greatest sensitivity. The procedure for the statistical combination is the same as described in sections 5 and 6.

The extrapolation of the Run-2 results in the HL–LHC follows the same strategy used in previous projections of Higgs boson searches and measurements [24]. For projections to a certain integrated luminosity L, the Run-2 signal and background yields, as well as the selected data events, are scaled up by a factor k_L equal to the increase in integrated luminosity with respect to Run 2. The scaling of the data events is necessary for those analyses that rely on the data to properly model the backgrounds in the fit. The efficiency of the physics object reconstruction and ID is assumed to be the same as in Run 2. The same assumption is made regarding the experimental energy and momentum resolution of the physics objects. This is based on the premise that the upgraded CMS detector will ensure performance comparable to Run 2 despite the larger pileup and radiation damage to the detector components.

The exact nature and size of the systematic uncertainties in CMS during the HL–LHC are unknown. Therefore, we derive projections for three different scenarios with systematic uncertainties:

Table 5. Treatment of most important common systematic uncertainties in the S2 scenario.

Uncertainty	Scaling with respect to Run 2
Theoretical uncertainties	$1/2$
Stat. uncertainties in MC simulation	Removed
b-tagging efficiency stat. component	$1/\sqrt{k_L}$
b-tagging efficiency (nonstat. component)	Unchanged
AK4 jet absolute energy scale	$\max(0.3, 1/\sqrt{k_L})$
AK4 jet energy scale dependence on flavour	$\max(0.5, 1/\sqrt{k_L})$
AK4 jet relative energy scale	$\max(0.2, 1/\sqrt{k_L})$
AK4 jet energy scale method	$1/\sqrt{k_L}$
AK4 jet energy resolution	$\max(0.5, 1/\sqrt{k_L})$
$E_{\mathrm{T}}^{\mathrm{miss}}$	$\max(0.5, 1/\sqrt{k_L})$
Luminosity	0.6
τ_{h} ID	Unchanged
τ_{h} energy scale	Unchanged
Pileup	Unchanged
Run-2 issues	Removed

- 'S1': The systematic uncertainties are assumed to be at the same level as in Run 2.
- 'S2': The systematic uncertainties with a statistical origin, for example, statistical uncertainties in the data/MC scale factors are reduced by a factor $\sqrt{k_L}$, until 'floor' values are reached. The 'floor' values prevent uncertainties from becoming unreasonably small and are based on studies in [24]. The theoretical uncertainties in the signal and background cross-sections are halved to account for the expected progress in the theoretical calculations throughout the next years. The uncertainties originating from the limited size of the MC samples are also removed under the assumption of very large MC datasets.
- 'stat. only': No systematic uncertainties are considered in the fit.

It should be noted that the systematic uncertainties related to specific detector issues encountered in Run 2 have been removed from all three scenarios, including S1. The nominal scenario for the HL–LHC conditions is S2.

The treatment of the uncertainties common to multiple analysis channels is summarised in table 5. The analysis-specific uncertainties are treated case by case.

The projected upper limits on the HH signal strength for the statistical combination of the considered HH channels at different integrated luminosities are shown in the left panel of figure 21. We become sensitive to SM HH production at 95% CL for integrated luminosities larger than 1000 fb^{-1}, when the expected upper limit drops below one. The projections at 3000 fb^{-1} under the different systematic uncertainty scenarios are shown in the right panel of figure 21.

The projected κ_λ likelihood scans are shown in figure 22. In the S2 scenario, the expected 1 standard deviation uncertainty on κ_λ is $+80\%/-60\%$ and $+60\%/-50\%$ for an integrated luminosity of 2000 and 3000 fb^{-1}, respectively.

The expected significance of the HH signal strength assuming the SM values for all parameters is summarized in table 6. Before the end of the HL-LHC, the CMS experiment will have evidence for HH production with a significance of 3.5 standard deviations for 2000 fb^{-1} in the nominal systematic uncertainty scenario and assuming that the signal is SM-like. The left side of figure 23 shows the significance that can be achieved for the SM signal as a function of the integrated luminosity. On the right, the significance is shown to be a function of κ_λ. The sensitivity to the HH signal varies with κ_λ due to the effects of the interference between the box and triangle diagrams, discussed in section 1. The two diagrams have different kinematic properties; therefore, the interference varies not only the HH cross-section but also the HH signal acceptance rate. In particular, for $\kappa_\lambda < 1$ and $\kappa_\lambda > 5$, the destructive interference is reduced, leading to an enhancement of the cross-section relative to the SM expectation. In these regimes, evidence for the HH process can be established with smaller datasets compared to the SM case. The HH signal is suppressed for $1 < \kappa_\lambda < 5$, and the significance will be lower than expected, with minimum significance at $\kappa_\lambda = 3.4$. The projections presented here do not consider the potential improvements in triggering [120, 121], object reconstruction and selection such as b tagging or analysis techniques. Historically, advancements in software and analysis methods have allowed us to exceed expectations; therefore, the projections shown in this paper are most likely conservative. Results from Run 3 will also add valuable information regarding the potential improvements for measuring the HH

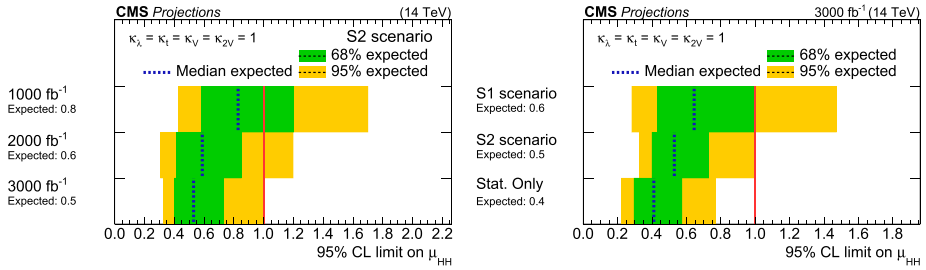


Figure 21. The expected upper limits at 95% CL on the HH signal strength from the combination of all the considered channels projected to different integrated luminosities (left), and under different assumptions on the systematic uncertainties for an integrated luminosity of 3000 fb^{-1} (right).

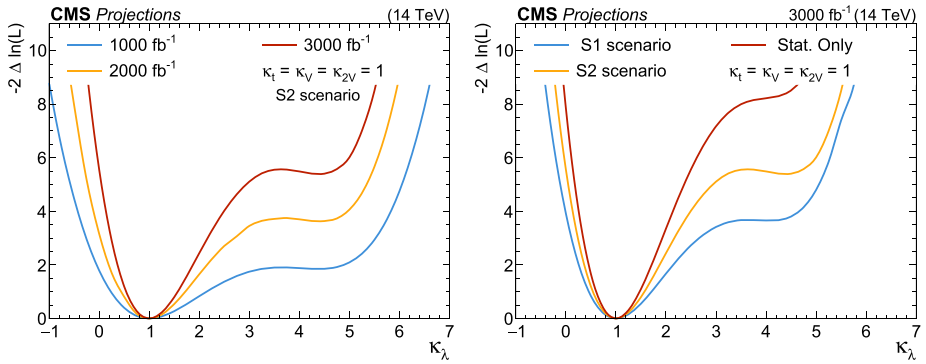


Figure 22. The expected $-2\Delta\ln(L)$ scan as a function of coupling modifier κ_λ for the combination of all contributing channels, projected to different integrated luminosities (left), and under different assumptions on the systematic uncertainties for an integrated luminosity of 3000 fb^{-1} (right). All other parameters are fixed to their SM values.

Table 6. Expected significance for the HH signal projected to 2000 or 3000 fb^{-1} under different assumptions of systematic uncertainties.

	Significance (σ) at 2000 fb^{-1}		Significance (σ) at 3000 fb^{-1}	
	S2	Stat. only	S2	Stat. only
$b\bar{b}b\bar{b}$ resolved jets	1.0	1.4	1.2	1.7
$b\bar{b}b\bar{b}$ merged jets	1.8	1.9	2.2	2.3
$b\bar{b}\tau\tau$	1.9	2.1	2.4	2.6
$b\bar{b}\gamma\gamma$	2.0	2.0	2.4	2.5
$b\bar{b}$WW	0.3	0.8	0.3	1.0
HH multilepton	0.4	0.6	0.5	0.8
Combination	3.5	3.9	4.2	4.8

process. If the trend of improvement continues, the observation of HH production by the end of the HL–LHC is within reach.

8. Summary

A combined search for nonresonant Higgs boson pair (HH) production was performed using the proton–proton collision dataset produced by the LHC at $\sqrt{s} = 13$ TeV, and collected using the CMS experiment from 2016 to 2018 (Run 2), which corresponds to an integrated luminosity of 138 fb^{-1}. Searches for HH production via gluon–gluon (ggF) and VBF production were conducted in the $b\bar{b}\gamma\gamma$, $b\bar{b}\tau\tau$, $b\bar{b}b\bar{b}$, $b\bar{b}$WW, and multilepton channels. In addition, searches for ggF HH production were conducted in the $b\bar{b}$ZZ (with both Z bosons decaying to leptons), WW$\gamma\gamma$, and $\tau\tau\gamma\gamma$ final states, which have clean signatures but relatively small branching fractions. We searched for the associated production mechanism with a vector boson in the $b\bar{b}b\bar{b}$ final state, which has the largest branching fraction. The analyses of these channels were combined to probe the Higgs boson trilinear self-coupling and the

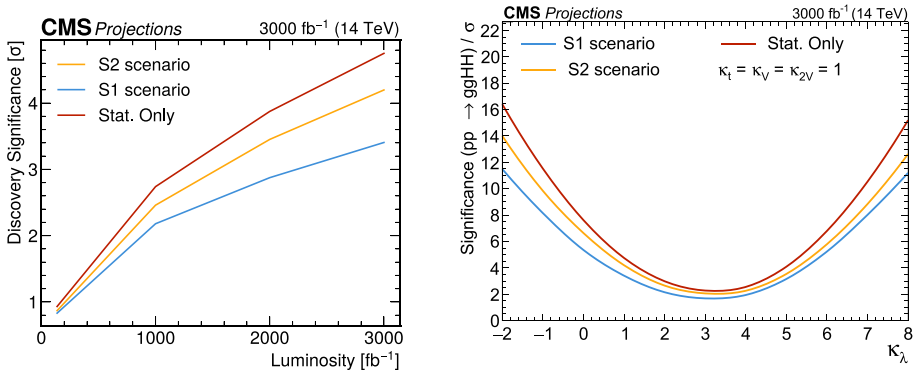


Figure 23. The expected signal significance as a function of integrated luminosity under different assumptions on the systematic uncertainties (left). The expected signal significance as a function of κ_λ under different assumptions on the systematic uncertainties for an integrated luminosity of 3000 fb^{-1} (right).

quartic coupling between two vector bosons and two Higgs bosons (VVHH) and to search for beyond the SM physics scenarios in the HEFT approach.

The observed and expected upper limits at 95% CL on the cross-section of ggF HH production were found to be 3.5 and 2.5 times the SM expectation, respectively. For the VBF production, the observed and expected 95% CL upper limits are 79 and 91 times the SM expectation, respectively. When all other parameters are set to their SM values, we constrain the Higgs boson trilinear self-coupling modifier κ_λ in the range from -1.35 to 6.37 at 95% CL (the expected 95% CL range is -2.24 to 7.89). Likewise, the VVHH coupling modifier κ_{2V} is constrained in the range from 0.64 to 1.40 (0.62 to 1.41 expected).

Two-dimensional measurements were also performed, including simultaneous measurements of κ_λ and κ_{2V}, κ_λ and the modifier of the Higgs boson coupling to the top quark (κ_t), and κ_{2V} and the modifier of the Higgs boson coupling to vector bosons (κ_V). The results are in agreement with the SM predictions.

Under the HEFT framework, the cross-section of the nonresonant ggF HH pair production is parametrized as a function of the anomalous couplings of the Higgs boson, involving the contact interactions between two Higgs and two top quarks, between two gluons and two Higgs bosons, and between two gluons and a Higgs boson. We perform searches for benchmark signals under different anomalous coupling scenarios and set upper limits on their cross-sections at 95% CL. We exclude HH production at 95% CL when the coupling modifier of the contact interaction between two Higgs bosons and two top quarks is outside the range from -0.28 to 0.59 (expected 95% CL range is -0.17 to 0.47). The HEFT parametrization is also exploited to study various UV complete models with an extended Higgs sector and set constraints on specific parameters.

These results constitute the most stringent limits and constraints obtained from the searches for nonresonant HH production using the LHC Run-2 dataset collected by the CMS experiment. Extrapolating our current results in the integrated luminosity anticipated of HL–LHC, we expect to see the first evidence for HH production with ≈2000 fb^{-1} of data.

The CMS Collaboration

A Hayrapetyan, V Makarenko, A Tumasyan[1]
Yerevan Physics Institute, Yerevan, Armenia

W Adam, J W Andrejkovic, L Benato, T Bergauer, M Dragicevic, C Giordano, P S Hussain, M Jeitler[2], N Krammer, A Li, D Liko, M Matthewman, I Mikulec, J Schieck[2], R Schöfbeck[2], D Schwarz, M Shooshtari, M Sonawane, W Waltenberger, C-E Wulz[2]
Institut für Hochenergiephysik, Vienna, Austria

T Janssen, H Kwon, D Ocampo Henao, T Van Laer, P Van Mechelen
Universiteit Antwerpen, Antwerpen, Belgium

J Bierkens, N Breugelmans, J D'Hondt, S Dansana, A De Moor, M Delcourt, F Heyen, Y Hong, P Kashko, S Lowette, I Makarenko, D Müller, J Song, S Tavernier, M Tytgat[3], G P Van Onsem, S Van Putte, D Vannerom
Vrije Universiteit Brussel, Brussel, Belgium

B Bilin, B Clerbaux, A K Das, I De Bruyn, G De Lentdecker, H Evard, L Favart, P Gianneios, A Khalilzadeh, F A Khan, A Malara, M A Shahzad, L Thomas, M Vanden Bemden, C Vander Velde, P Vanlaer, F Zhang
Université Libre de Bruxelles, Bruxelles, Belgium

M De Coen, D Dobur, G Gokbulut, J Knolle, D Marckx, K Skovpen, A M Tomaru, N Van Den Bossche, J van der Linden, J Vandenbroeck, L Wezenbeek
Ghent University, Ghent, Belgium

S Bein, A Benecke, A Bethani, G Bruno, A Cappati, J De Favereau De Jeneret, C Delaere, A Giammanco, A O Guzel, V Lemaitre, J Lidrych, P Malek, P Mastrapasqua, S Turkcapar
Université Catholique de Louvain, Louvain-la-Neuve, Belgium

G A Alves, M Barroso Ferreira Filho, E Coelho, C Hensel, T Menezes De Oliveira, C Mora Herrera, P Rebello Teles, M Soeiro, E J Tonelli Manganote[4], A Vilela Pereira[5]
Centro Brasileiro de Pesquisas Fisicas, Rio de Janeiro, Brazil

W L Aldá Júnior, H Brandao Malbouisson, W Carvalho, J Chinellato[6], M Costa Reis, E M Da Costa, G G Da Silveira[7], D De Jesus Damiao, S Fonseca De Souza, R Gomes De Souza, S S Jesus, T Laux Kuhn[7], M Macedo, K Mota Amarilo, L Mundim, H Nogima, J P Pinheiro, A Santoro, A Sznajder, M Thiel, F Torres Da Silva De Araujo[8]
Universidade do Estado do Rio de Janeiro, Rio de Janeiro, Brazil

C A Bernardes[7], F Damas, T R Fernandez Perez Tomei, E M Gregores, B Lopes Da Costa, I Maietto Silverio, P G Mercadante, S F Novaes, B Orzari, Sandra S Padula, V Scheurer
Universidade Estadual Paulista, Universidade Federal do ABC, São Paulo, Brazil

A Aleksandrov, G Antchev, P Danev, R Hadjiiska, P Iaydjiev, M Shopova, G Sultanov
Institute for Nuclear Research and Nuclear Energy, Bulgarian Academy of Sciences, Sofia, Bulgaria

A Dimitrov, L Litov, B Pavlov, P Petkov, A Petrov
University of Sofia, Sofia, Bulgaria

S Keshri, D Laroze, S Thakur
Instituto De Alta Investigación, Universidad de Tarapacá, Casilla 7 D, Arica, Chile

W Brooks
Universidad Tecnica Federico Santa Maria, Valparaiso, Chile

T Cheng, T Javaid, L Wang, L Yuan
Beihang University, Beijing, China

Z Hu, Z Liang, J Liu, X Wang, H Yang
Department of Physics, Tsinghua University, Beijing, China

G M Chen[9], H S Chen[9], M Chen[9], Y Chen, Q Hou, X Hou, F Iemmi, C H Jiang, A Kapoor[10], H Liao, G Liu, Z-A Liu[11], J N Song[11], S Song, J Tao, C Wang[9], J Wang, H Zhang, J Zhao
Institute of High Energy Physics, Beijing, China

A Agapitos, Y Ban, A Carvalho Antunes De Oliveira, S Deng, B Guo, Q Guo, C Jiang, A Levin, C Li, Q Li, Y Mao, S Qian, S J Qian, X Qin, C Quaranta, X Sun, D Wang, J Wang, M Zhang, Y Zhao, C Zhou
State Key Laboratory of Nuclear Physics and Technology, Peking University, Beijing, China

S Yang
State Key Laboratory of Nuclear Physics and Technology, Institute of Quantum Matter, South China Normal University, Guangzhou, China

Z You
Sun Yat-Sen University, Guangzhou, China

K Jaffel, N Lu, C Yu
University of Science and Technology of China, Hefei, China

G Bauer[12,13], Z Cui[13], B Li[14], H Wang, K Yi[15], J Zhang
Nanjing Normal University, Nanjing, China

Y Li
Institute of Modern Physics and Key Laboratory of Nuclear Physics and Ion-beam Application (MOE)—Fudan University, Shanghai, China

Z Lin, C Lu, M Xiao[16]
Zhejiang University, Hangzhou, Zhejiang, China

C Avila, D A Barbosa Trujillo, A Cabrera, C Florez, J Fraga, J A Reyes Vega
Universidad de Los Andes, Bogota, Colombia

C Rendón, M Rodriguez, A A Ruales Barbosa, J D Ruiz Alvarez
Universidad de Antioquia, Medellin, Colombia

N Godinovic, D Lelas, A Sculac
University of Split, Faculty of Electrical Engineering, Mechanical Engineering and Naval Architecture, Split, Croatia

M Kovac, A Petkovic, T Sculac
University of Split, Faculty of Science, Split, Croatia

P Bargassa, V Brigljevic, B K Chitroda, D Ferencek, K Jakovcic, A Starodumov, T Susa
Institute Rudjer Boskovic, Zagreb, Croatia

A Attikis, K Christoforou, C Leonidou, C Nicolaou, L Paizanos, F Ptochos, P A Razis, H Rykaczewski, H Saka, A Stepennov
University of Cyprus, Nicosia, Cyprus

M Finger[†], M Finger Jr.
Charles University, Prague, Czech Republic

E Ayala
Escuela Politecnica Nacional, Quito, Ecuador

E Carrera Jarrin
Universidad San Francisco de Quito, Quito, Ecuador

Y Assran[17,18], B El-mahdy[19]
Academy of Scientific Research and Technology of the Arab Republic of Egypt, Egyptian Network of High Energy Physics, Cairo, Egypt

A Lotfy, M A Mahmoud
Center for High Energy Physics (CHEP-FU), Fayoum University, El-Fayoum, Egypt

K Ehataht, M Kadastik, T Lange, C Nielsen, J Pata, M Raidal, N Seeba, L Tani
National Institute of Chemical Physics and Biophysics, Tallinn, Estonia

E Brücken, A Milieva, K Osterberg, M Voutilainen
Department of Physics, University of Helsinki, Helsinki, Finland

F Garcia, P Inkaew, K TS Kallonen, R Kumar Verma, T Lampén, K Lassila-Perini, B Lehtela, S Lehti, T Lindén, N R Mancilla Xinto, M Myllymäki, Mm. Rantanen, S Saariokari, N T Toikka, J Tuominiemi
Helsinki Institute of Physics, Helsinki, Finland

N Bin Norjoharuddeen, H Kirschenmann, P Luukka, H Petrow
Lappeenranta-Lahti University of Technology, Lappeenranta, Finland

M Besancon, F Couderc, M Dejardin, D Denegri, P Devouge, J L Faure, F Ferri, P Gaigne, S Ganjour, P Gras, G Hamel de Monchenault, M Kumar, V Lohezic, Y Maidannyk, J Malcles, F Orlandi, L Portales, S Ronchi, MÖ. Sahin, A Savoy-Navarro[20], P Simkina, M Titov, M Tornago
IRFU, CEA, Université Paris-Saclay, Gif-sur-Yvette, France

R Amella Ranz, F Beaudette, G Boldrini, P Busson, C Charlot, M Chiusi, T D Cuisset, O Davignon, A De Wit, T Debnath, I T Ehle, S Ghosh, A Gilbert, R Granier de Cassagnac, L Kalipoliti, M Manoni, M Nguyen, S Obraztsov, C Ochando, R Salerno, J B Sauvan, Y Sirois, G Sokmen, L Urda Gómez, A Zabi, A Zghiche
Laboratoire Leprince-Ringuet, CNRS/IN2P3, Ecole Polytechnique, Institut Polytechnique de Paris, Palaiseau, France

J-L Agram[21], J Andrea, D Bloch, J-M Brom, E C Chabert, C Collard, G Coulon, S Falke, U Goerlach, R Haeberle, A-C Le Bihan, M Meena, O Poncet, G Saha, P Vaucelle
Université de Strasbourg, CNRS, IPHC UMR 7178, Strasbourg, France

A Di Florio
Centre de Calcul de l'Institut National de Physique Nucleaire et de Physique des Particules, CNRS/IN2P3, Villeurbanne, France

D Amram, S Beauceron, B Blancon, G Boudoul, N Chanon, D Contardo, P Depasse, H El Mamouni, J Fay, S Gascon, M Gouzevitch, C Greenberg, G Grenier, B Ille, E Jourd'Huy, M Lethuillier, B Massoteau, L Mirabito, A Purohit, M Vander Donckt, J Xiao
Institut de Physique des 2 Infinis de Lyon (IP2I), Villeurbanne, France

G Adamov, I Lomidze, Z Tsamalaidze[22]
Georgian Technical University, Tbilisi, Georgia

V Botta, S Consuegra Rodríguez, L Feld, K Klein, M Lipinski, D Meuser, P Nattland, V Oppenländer, A Pauls, D Pérez Adán, N Röwert, M Teroerde
RWTH Aachen University, I Physikalisches Institut, Aachen, Germany

C Daumann, S Diekmann, A Dodonova, N Eich, D Eliseev, F Engelke, J Erdmann, M Erdmann, B Fischer, T Hebbeker, K Hoepfner, F Ivone, A Jung, N Kumar, My. Lee, F Mausolf, M Merschmeyer, A Meyer, F Nowotny, A Pozdnyakov, W Redjeb, H Reithler, U Sarkar, V Sarkisovi, A Schmidt, C Seth, A Sharma, J L Spah, V Vaulin, S Zaleski
RWTH Aachen University, III Physikalisches Institut A, Aachen, Germany

M R Beckers, C Dziwok, G Flügge, N Hoeflich, T Kress, A Nowack, O Pooth, A Stahl, A Zotz
RWTH Aachen University, III Physikalisches Institut B, Aachen, Germany

H Aarup Petersen, A Abel, M Aldaya Martin, J Alimena, S Amoroso, Y An, I Andreev, J Bach, S Baxter, M Bayatmakou, H Becerril Gonzalez, O Behnke, A Belvedere, F Blekman[23], K Borras[24], A Campbell, S Chatterjee, L X Coll Saravia, G Eckerlin, D Eckstein, E Gallo[23], A Geiser, V Guglielmi, M Guthoff, A Hinzmann, L Jeppe, M Kasemann, C Kleinwort, R Kogler, M Komm, D Krücker, W Lange, D Leyva Pernia, K-Y Lin, K Lipka[25], W Lohmann[26], J Malvaso, R Mankel, I-A Melzer-Pellmann, M Mendizabal Morentin, A B Meyer, G Milella, K Moral Figueroa, A Mussgiller, L P Nair, J Niedziela, A Nürnberg, J Park, E Ranken, A Raspereza, D Rastorguev, L Rygaard, M Scham[27,24], S Schnake[24], P Schütze, C Schwanenberger[23], D Selivanova, K Sharko, M Shchedrolosiev, D Stafford, M Torkian, F Vazzoler, A Ventura Barroso, R Walsh, D Wang, Q Wang, K Wichmann, L Wiens[24], C Wissing, Y Yang, S Zakharov, A Zimermmane Castro Santos
Deutsches Elektronen-Synchrotron, Hamburg, Germany

A R Alves Andrade, M Antonello, S Bollweg, M Bonanomi, K El Morabit, Y Fischer, M Frahm, E Garutti, A Grohsjean, A A Guvenli, J Haller, D Hundhausen, G Kasieczka, P Keicher, R Klanner, W Korcari, T Kramer, Cc. Kuo, F Labe, J Lange, A Lobanov, L Moureaux, A Nigamova, K Nikolopoulos, A Paasch, K J Pena Rodriguez, N Prouvost, B Raciti, M Rieger, D Savoiu, P Schleper, M Schröder, J Schwandt, M Sommerhalder, H Stadie, G Steinbrück, R Ward, B Wiederspan, M Wolf
University of Hamburg, Hamburg, Germany

S Brommer, E Butz, Y M Chen, T Chwalek, A Dierlamm, G G Dincer, U Elicabuk, N Faltermann, M Giffels, A Gottmann, F Hartmann[28], M Horzela, F Hummer, U Husemann, J Kieseler, M Klute, R Kunnilan Muhammed Rafeek, O Lavoryk, J M Lawhorn, A Lintuluoto, S Maier, M Mormile, Th. Müller, E Pfeffer, M Presilla, G Quast, K Rabbertz, B Regnery, R Schmieder, N Shadskiy, I Shvetsov, H J Simonis, L Sowa, L Stockmeier, K Tauqeer, M Toms, B Topko, N Trevisani, C Verstege, T Voigtländer, R F Von Cube, J Von Den Driesch, M Wassmer, R Wolf, W D Zeuner, X Zuo
Karlsruher Institut fuer Technologie, Karlsruhe, Germany

G Anagnostou, G Daskalakis, A Kyriakis
Institute of Nuclear and Particle Physics (INPP), NCSR Demokritos, Aghia Paraskevi, Greece

G Melachroinos, Z Painesis, I Paraskevas, N Saoulidou, K Theofilatos, E Tziaferi, E Tzovara, K Vellidis, I Zisopoulos
National and Kapodistrian University of Athens, Athens, Greece

T Chatzistavrou, G Karapostoli, K Kousouris, E Siamarkou, G Tsipolitis
National Technical University of Athens, Athens, Greece

I Bestintzanos, I Evangelou, C Foudas, P Katsoulis, P Kokkas, P G Kosmoglou Kioseoglou, N Manthos, I Papadopoulos, J Strologas
University of Ioánnina, Ioánnina, Greece

D Druzhkin, C Hajdu, D Horvath[29,30], K Márton, A J Rádl[31], F Sikler, V Veszpremi
HUN-REN Wigner Research Centre for Physics, Budapest, Hungary

M Csanád, K Farkas, A Fehérkuti[32], M MA Gadallah[33], Á. Kadlecsik, M León Coello, G Pásztor, G I Veres
MTA-ELTE Lendület CMS Particle and Nuclear Physics Group, Eötvös Loránd University, Budapest, Hungary

B Ujvari, G Zilizi
Faculty of Informatics, University of Debrecen, Debrecen, Hungary

G Bencze, S Czellar, J Molnar, Z Szillasi
HUN-REN ATOMKI - Institute of Nuclear Research, Debrecen, Hungary

T Csorgo[32], F Nemes[32], T Novak, I Szanyi[34]
Karoly Robert Campus, MATE Institute of Technology, Gyongyos, Hungary

S Bansal, S B Beri, V Bhatnagar, G Chaudhary, S Chauhan, N Dhingra[35], A Kaur, A Kaur, H Kaur, M Kaur, S Kumar, T Sheokand, J B Singh, A Singla
Panjab University, Chandigarh, India

A Bhardwaj, A Chhetri, B C Choudhary, A Kumar, A Kumar, M Naimuddin, S Phor, K Ranjan, M K Saini
University of Delhi, Delhi, India

S Acharya[36], B Gomber, B Sahu[36]
University of Hyderabad, Hyderabad, India

S Mukherjee
Indian Institute of Technology Kanpur, Kanpur, India

S Baradia, S Bhattacharya, S Das Gupta, S Dutta, S Dutta, S Sarkar
Saha Institute of Nuclear Physics, HBNI, Kolkata, India

M M Ameen, P K Behera, S Chatterjee, G Dash, A Dattamunsi, P Jana, P Kalbhor, S Kamble, J R Komaragiri[37], T Mishra, P R Pujahari, A K Sikdar, R K Singh, P Verma, S Verma, A Vijay
Indian Institute of Technology Madras, Madras, India

B K Sirasva
IISER Mohali, India, Mohali, India

L Bhatt, S Dugad, G B Mohanty, M Shelake, P Suryadevara
Tata Institute of Fundamental Research-A, Mumbai, India

A Bala, S Banerjee, S Barman[38], R M Chatterjee, M Guchait, Sh. Jain, A Jaiswal, B M Joshi, S Kumar, M Maity[38], G Majumder, K Mazumdar, S Parolia, R Saxena, A Thachayath
Tata Institute of Fundamental Research-B, Mumbai, India

S Bahinipati[39], D Maity[40], P Mal, K Naskar[40], A Nayak[40], S Nayak, K Pal, R Raturi, P Sadangi, S K Swain, S Varghese[40], D Vats[40]
National Institute of Science Education and Research, An OCC of Homi Bhabha National Institute, Bhubaneswar, Odisha, India

A Alpana, S Dube, P Hazarika, B Kansal, A Laha, R Sharma, S Sharma, K Y Vaish
Indian Institute of Science Education and Research (IISER), Pune, India

S Ghosh
Indian Institute of Technology Hyderabad, Telangana, India

H Bakhshiansohi[41], A Jafari[42], V Sedighzadeh Dalavi, M Zeinali[43]
Isfahan University of Technology, Isfahan, Iran

S Bashiri, S Chenarani[44], S M Etesami, Y Hosseini, M Khakzad, E Khazaie, M Mohammadi Najafabadi, S Tizchang[45]
Institute for Research in Fundamental Sciences (IPM), Tehran, Iran

M Felcini, M Grunewald
University College Dublin, Dublin, Ireland

M Abbrescia[a,b], M Barbieri[a,b], M Buonsante[a,b], A Colaleo[a,b], D Creanza[a,c], N De Filippis[a,c], M De Palma[a,b], W Elmetenawee[a,b,46], N Ferrara[a,c], L Fiore[a], L Longo[a], M Louka[a,b], G Maggi[a,c], M Maggi[a], I Margjeka[a], V Mastrapasqua[a,b], S My[a,b], F Nenna[a,b], S Nuzzo[a,b], A Pellecchia[a,b], A Pompili[a,b], G Pugliese[a,c], R Radogna[a,b], D Ramos[a], A Ranieri[a], L Silvestris[a], F M Simone[a,c], Ü. Sözbilir[a], A Stamerra[a,b], D Troiano[a,b], R Venditti[a,b], P Verwilligen[a], A Zaza[a,b]
INFN Sezione di Bari[a], Università di Bari[b], Politecnico di Bari[c], Bari, Italy

G Abbiendi[a], D Bonacorsi[a,b], P Capiluppi[a,b], F R Cavallo[a], M Cuffiani[a,b], G M Dallavalle[a], T Diotalevi[a,b], F Fabbri[a], A Fanfani[a,b], R Farinelli[a], D Fasanella[a], P Giacomelli[a], L Guiducci[a,b], S Lo Meo[a,47], M Lorusso[a,b], L Lunerti[a], S Marcellini[a], G Masetti[a], F L Navarria[a,b], G Paggi[a,b], A Perrotta[a], F Primavera[a,b], A M Rossi[a,b], S Rossi Tisbeni[a,b], T Rovelli[a,b], G P Siroli[a,b]
INFN Sezione di Bologna[a], Università di Bologna[b], Bologna, Italy

S Costa[a,b,48], A Di Mattia[a], A Lapertosa[a], R Potenza[a,b], A Tricomi[a,b,48]
INFN Sezione di Catania[a], Università di Catania[b], Catania, Italy

J Altork[a,b], P Assiouras[a], G Barbagli[a], G Bardelli[a], M Bartolini[a,b], A Calandri[a,b], B Camaiani[a,b], A Cassese[a], R Ceccarelli[a], V Ciulli[a,b], C Civinini[a], R D'Alessandro[a,b], L Damenti[a,b], E Focardi[a,b], T Kello[a], G Latino[a,b], P Lenzi[a,b], M Lizzo[a], M Meschini[a], S Paoletti[a], A Papanastassiou[a,b], G Sguazzoni[a], L Viliani[a]
INFN Sezione di Firenze[a], Università di Firenze[b], Firenze, Italy

L Benussi, S Bianco, S Meola[49], D Piccolo
INFN Laboratori Nazionali di Frascati, Frascati, Italy

M Alves Gallo Pereira[a], F Ferro[a], E Robutti[a], S Tosi[a,b]
INFN Sezione di Genova[a], Università di Genova[b], Genova, Italy

A Benaglia[a], F Brivio[a], V Camagni[a,b], F Cetorelli[a,b], F De Guio[a,b], M E Dinardo[a,b], P Dini[a], S Gennai[a], R Gerosa[a,b], A Ghezzi[a,b], P Govoni[a,b], L Guzzi[a], M R Kim[a], G Lavizzari[a,b], M T Lucchini[a,b], M Malberti[a], S Malvezzi[a], A Massironi[a], D Menasce[a], L Moroni[a], M Paganoni[a,b], S Palluotto[a,b], D Pedrini[a], A Perego[a,b], G Pizzati[a,b], S Ragazzi[a,b], T Tabarelli de Fatis[a,b]
INFN Sezione di Milano-Bicocca[a], Università di Milano-Bicocca[b], Milano, Italy

S Buontempo[a], C Di Fraia[a,b], F Fabozzi[a,c], L Favilla[a,d], A OM Iorio[a,b], L Lista[a,b,50], P Paolucci[a,28], B Rossi[a]
INFN Sezione di Napoli[a], Università di Napoli'Federico II'[b], Napoli, Italy; Università della Basilicata[c], Potenza, Italy; Scuola Superiore Meridionale (SSM)[d], Napoli, Italy

P Azzi[a], N Bacchetta[a,51], D Bisello[a,b], P Bortignon[a,c], G Bortolato[a,b], A CM Bulla[a,c], R Carlin[a,b], P Checchia[a], T Dorigo[a,52], U Gasparini[a,b], S Giorgetti[a], E Lusiani[a], M Margoni[a,b], A T Meneguzzo[a,b], F Montecassiano[a], J Pazzini[a,b], P Ronchese[a,b], R Rossin[a,b], F Simonetto[a,b], M Tosi[a,b], A Triossi[a,b], M Zanetti[a,b], P Zotto[a,b], A Zucchetta[a,b], G Zumerle[a,b]
INFN Sezione di Padova[a], Università di Padova[b], Padova, Italy; Universita degli Studi di Cagliari[c], Cagliari, Italy

S Abu Zeid[a,53], A Braghieri[a], S Calzaferri[a], P Montagna[a,b], M Pelliccioni[a], V Re[a], P Salvini[a], I Vai[a,b], P Vitulo[a,b]
INFN Sezione di Pavia[a], Università di Pavia[b], Pavia, Italy

S Ajmal[a,b], M E Ascioti[a,b], G M Bilei[a], C Carrivale[a,b], D Ciangottini[a,b], L Della Penna[a,b], L Fanò[a,b], V Mariani[a,b], M Menichelli[a], F Moscatelli[a,54], A Rossi[a,b], A Santocchia[a,b], D Spiga[a], T Tedeschi[a,b]
INFN Sezione di Perugia[a], Università di Perugia[b], Perugia, Italy

C Aimè[a,b], C A Alexe[a,c], P Asenov[a,b], P Azzurri[a], G Bagliesi[a], L Bianchini[a,b], T Boccali[a], E Bossini[a], D Bruschini[a,c], L Calligaris[a,b], R Castaldi[a], F Cattafesta[a,c], M A Ciocci[a,d], M Cipriani[a,b], R Dell'Orso[a], S Donato[a,b], R Forti[a,b], A Giassi[a], F Ligabue[a,c], A C Marini[a,b], D Matos Figueiredo[a], A Messineo[a,b], S Mishra[a], V K Muraleedharan Nair Bindhu[a,b], S Nandan[a], F Palla[a], M Riggirello[a,c], A Rizzi[a,b], G Rolandi[a,c], S Roy Chowdhury[a,55], T Sarkar[a], A Scribano[a], P Solanki[a,b], P Spagnolo[a], F Tenchini[a,b], R Tenchini[a], G Tonelli[a,b], N Turini[a,d], F Vaselli[a,c], A Venturi[a], P G Verdini[a]
INFN Sezione di Pisa[a], Università di Pisa[b], Scuola Normale Superiore di Pisa[c], Pisa, Italy; Università di Siena[d], Siena, Italy

P Akrap[a,b], C Basile[a,b], S C Behera[a], F Cavallari[a], L Cunqueiro Mendez[a,b], F De Riggi[a,b], D Del Re[a,b], E Di Marco[a], M Diemoz[a], F Errico[a], L Frosina[a,b], R Gargiulo[a,b], B Harikrishnan[a,b], F Lombardi[a,b], E Longo[a,b], L Martikainen[a,b], J Mijuskovic[a,b], G Organtini[a,b], N Palmeri[a,b], R Paramatti[a,b], S Rahatlou[a,b], C Rovelli[a], F Santanastasio[a,b], L Soffi[a], V Vladimirov[a,b]
INFN Sezione di Roma[a], Sapienza Università di Roma[b], Roma, Italy

N Amapane[a,b], R Arcidiacono[a,c], S Argiro[a,b], M Arneodo[a,c], N Bartosik[a,c], R Bellan[a,b], A Bellora[a,b], C Biino[a], C Borca[a,b], N Cartiglia[a], M Costa[a,b], R Covarelli[a,b], N Demaria[a], L Finco[a], M Grippo[a,b], B Kiani[a,b], L Lanteri[a,b], F Legger[a], F Luongo[a,b], C Mariotti[a], S Maselli[a], A Mecca[a,b], L Menzio[a,b], P Meridiani[a], E Migliore[a,b], M Monteno[a], M M Obertino[a,b], G Ortona[a], L Pacher[a,b], N Pastrone[a], M Ruspa[a,c], F Siviero[a,b], V Sola[a,b], A Solano[a,b], A Staiano[a], C Tarricone[a,b], D Trocino[a], G Umoret[a,b], E Vlasov[a,b], R White[a,b]
INFN Sezione di Torino[a], Università di Torino[b], Torino, Italy; Università del Piemonte Orientale[c], Novara, Italy

J Babbar[a,b], S Belforte[a], V Candelise[a,b], M Casarsa[a], F Cossutti[a], K De Leo[a], G Della Ricca[a,b], R Delli Gatti[a,b]
INFN Sezione di Trieste[a], Università di Trieste[b], Trieste, Italy

S Dogra, J Hong, J Kim, T Kim, D Lee, H Lee, J Lee, S W Lee, C S Moon, Y D Oh, S Sekmen, B Tae, Y C Yang
Kyungpook National University, Daegu, Korea

M S Kim
Department of Mathematics and Physics - GWNU, Gangneung, Korea

G Bak, P Gwak, H Kim, D H Moon, J Seo
Chonnam National University, Institute for Universe and Elementary Particles, Kwangju, Korea

E Asilar, F Carnevali, J Choi[56], T J Kim, Y Ryou
Hanyang University, Seoul, Korea

S Ha, S Han, B Hong, J Kim, K Lee, K S Lee, S Lee, J Yoo
Korea University, Seoul, Korea

J Goh, J Shin, S Yang
Kyung Hee University, Department of Physics, Seoul, Korea

Y Kang, H S Kim, Y Kim, S Lee
Sejong University, Seoul, Korea

J Almond, J H Bhyun, J Choi, J Choi, W Jun, H Kim, J Kim, T Kim, Y Kim, Y W Kim, S Ko, H Lee, J Lee, J Lee, B H Oh, S B Oh, J Shin, U K Yang, I Yoon
Seoul National University, Seoul, Korea

W Jang, D Y Kang, D Kim, S Kim, B Ko, J SH Lee, Y Lee, I C Park, Y Roh, I J Watson
University of Seoul, Seoul, Korea

G Cho, K Hwang, B Kim, S Kim, K Lee, H D Yoo
Yonsei University, Department of Physics, Seoul, Korea

Y Lee, I Yu
Sungkyunkwan University, Suwon, Korea

T Beyrouthy, Y Gharbia
College of Engineering and Technology, American University of the Middle East (AUM), Dasman, Kuwait

F Alazemi
Kuwait University - College of Science - Department of Physics, Safat, Kuwait

K Dreimanis, O M Eberlins, A Gaile, C Munoz Diaz, D Osite, G Pikurs, R Plese, A Potrebko, M Seidel, D Sidiropoulos Kontos
Riga Technical University, Riga, Latvia

N R Strautnieks
University of Latvia (LU), Riga, Latvia

M Ambrozas, A Juodagalvis, S Nargelas, A Rinkevicius, G Tamulaitis
Vilnius University, Vilnius, Lithuania

I Yusuff[57], Z Zolkapli
National Centre for Particle Physics, Universiti Malaya, Kuala Lumpur, Malaysia

J F Benitez, A Castaneda Hernandez, A Cota Rodriguez, L E Cuevas Picos, H A Encinas Acosta, L G Gallegos Marí nez, J A Murillo Quijada, L Valencia Palomo
Universidad de Sonora (UNISON), Hermosillo, Mexico

G Ayala, H Castilla-Valdez, H Crotte Ledesma, R Lopez-Fernandez, J Mejia Guisao, R Reyes-Almanza, A Sánchez Hernández
Centro de Investigacion y de Estudios Avanzados del IPN, Mexico City, Mexico

C Oropeza Barrera, D L Ramirez Guadarrama, M Ramírez García
Universidad Iberoamericana, Mexico City, Mexico

I Bautista, F E Neri Huerta, I Pedraza, H A Salazar Ibarguen, C Uribe Estrada
Benemerita Universidad Autonoma de Puebla, Puebla, Mexico

I Bubanja, N Raicevic
University of Montenegro, Podgorica, Montenegro

P H Butler
University of Canterbury, Christchurch, New Zealand

A Ahmad, M I Asghar, A Awais, M IM Awan, W A Khan
National Centre for Physics, Quaid-I-Azam University, Islamabad, Pakistan

V Avati, L Forthomme, L Grzanka, M Malawski, K Piotrzkowski
AGH University of Krakow, Krakow, Poland

M Bluj, M Górski, M Kazana, M Szleper, P Zalewski
National Centre for Nuclear Research, Swierk, Poland

K Bunkowski, K Doroba, A Kalinowski, M Konecki, J Krolikowski, A Muhammad
Institute of Experimental Physics, Faculty of Physics, University of Warsaw, Warsaw, Poland

P Fokow, K Pozniak, W Zabolotny
Warsaw University of Technology, Warsaw, Poland

M Araujo, D Bastos, C Beir ao Da Cruz E Silva, A Boletti, M Bozzo, T Camporesi, G Da Molin, M Gallinaro, J Hollar, N Leonardo, G B Marozzo, A Petrilli, M Pisano, J Seixas, J Varela, J W Wulff
Laboratório de Instrumentação e Física Experimental de Partículas, Lisboa, Portugal

P Adzic, L Markovic, P Milenovic, V Milosevic
Faculty of Physics, University of Belgrade, Belgrade, Serbia

D Devetak, M Dordevic, J Milosevic, L Nadderd, V Rekovic, M Stojanovic
VINCA Institute of Nuclear Sciences, University of Belgrade, Belgrade, Serbia

M Alcalde Martinez, J Alcaraz Maestre, Cristina F Bedoya, J A Brochero Cifuentes, Oliver M Carretero, M Cepeda, M Cerrada, N Colino, B De La Cruz, A Delgado Peris, A Escalante Del Valle, D Fernández Del Val, J P Fernández Ramos, J Flix, M C Fouz, M Gonzalez Hernandez, O Gonzalez Lopez, S Goy Lopez, J M Hernandez, M I Josa, J Llorente Merino, C Martin Perez, E Martin Viscasillas, D Moran, C M Morcillo Perez, Á. Navarro Tobar, R Paz Herrera, C Perez Dengra, A Pérez-Calero Yzquierdo, J Puerta Pelayo, I Redondo, J Vazquez Escobar
Centro de Investigaciones Energéticas Medioambientales y Tecnológicas (CIEMAT), Madrid, Spain

J F de Trocóniz
Universidad Autónoma de Madrid, Madrid, Spain

B Alvarez Gonzalez, J Ayllon Torresano, A Cardini, J Cuevas, J Del Riego Badas, D Estrada Acevedo, J Fernandez Menendez, S Folgueras, I Gonzalez Caballero, P Leguina, M Obeso Menendez, E Palencia Cortezon, J Prado Pico, A Soto Rodríguez, C Vico Villalba, P Vischia
Universidad de Oviedo, Instituto Universitario de Ciencias y Tecnologías Espaciales de Asturias (ICTEA), Oviedo, Spain

S Blanco Fernández, I J Cabrillo, A Calderon, J Duarte Campderros, M Fernandez, G Gomez, C Lasaosa García, R Lopez Ruiz, C Martinez Rivero, P Martinez Ruiz del Arbol, F Matorras, P Matorras Cuevas, E Navarrete Ramos, J Piedra Gomez, C Quintana San Emeterio, L Scodellaro, I Vila, R Vilar Cortabitarte, J M Vizan Garcia
Instituto de Física de Cantabria (IFCA), CSIC-Universidad de Cantabria, Santander, Spain

B Kailasapathy[58], D DC Wickramarathna
University of Colombo, Colombo, Sri Lanka

W GD Dharmaratna[59], K Liyanage, N Perera
University of Ruhuna, Department of Physics, Matara, Sri Lanka

D Abbaneo, C Amendola, R Ardino, E Auffray, J Baechler, D Barney, J Bendavid, M Bianco, A Bocci, L Borgonovi, C Botta, A Bragagnolo, C E Brown, C Caillol, G Cerminara, P Connor, D d'Enterria, A Dabrowski, A David, A De Roeck, M M Defranchis, M Deile, M Dobson, P J Fernández Manteca, B A Fontana Santos Alves, W Funk, A Gaddi, S Giani, D Gigi, K Gill, F Glege, M Glowacki, A Gruber, J Hegeman, J K Heikkilä, R Hofsaess, B Huber, T James, P Janot, O Kaluzinska, O Karacheban[26], G Karathanasis, S Laurila, P Lecoq, E Leutgeb, C Lourenço, A-M Lyon, M Magherini, L Malgeri, M Mannelli, A Mehta, F Meijers, J A Merlin, S Mersi, E Meschi, M Migliorini, F Monti, F Moortgat, M Mulders, M Musich, I Neutelings, S Orfanelli, F Pantaleo, M Pari, G Petrucciani, A Pfeiffer, M Pierini, M Pitt, H Qu, D Rabady, A Reimers, B Ribeiro Lopes, F Riti, P Rosado, M Rovere, H Sakulin, R Salvatico, S Sanchez Cruz, S Scarfi, M Selvaggi, A Sharma, K Shchelina, P Silva, P Sphicas[60], A G Stahl Leiton, A Steen, S Summers, D Treille, P Tropea, E Vernazza, J Wanczyk[61], J Wang, S Wuchterl, M Zarucki, P Zehetner, P Zejdl, G Zevi Della Porta
CERN, European Organization for Nuclear Research, Geneva, Switzerland

T Bevilacqua[62], L Caminada[62], W Erdmann, R Horisberger, Q Ingram, H C Kaestli, D Kotlinski, C Lange, U Langenegger, L Noehte[62], T Rohe, A Samalan
PSI Center for Neutron and Muon Sciences, Villigen, Switzerland

T K Aarrestad, M Backhaus, G Bonomelli, C Cazzaniga, K Datta, P De Bryas Dexmiers D'Archiacchiac[61], A De Cosa, G Dissertori, M Dittmar, M Donegà, F Eble, K Gedia, F Glessgen, C Grab, N Härringer, T G Harte, W Lustermann, M Malucchi, R A Manzoni, M Marchegiani, L Marchese, A Mascellani[61], F Nessi-Tedaldi, F Pauss, V Perovic, B Ristic, R Seidita, J Steggemann[61], A Tarabini, D Valsecchi, R Wallny
ETH Zurich - Institute for Particle Physics and Astrophysics (IPA), Zurich, Switzerland

C Amsler[63], P Bärtschi, F Bilandzija, M F Canelli, G Celotto, K Cormier, M Huwiler, W Jin, A Jofrehei, B Kilminster, T H Kwok, S Leontsinis, V Lukashenko, A Macchiolo, F Meng, M Missiroli, J Motta, P Robmann, M Senger, E Shokr, F Stäger, R Tramontano, P Viscone
Universität Zürich, Zurich, Switzerland

D Bhowmik, C M Kuo, P K Rout, S Taj, P C Tiwari[37]
National Central University, Chung-Li, Taiwan

L Ceard, K F Chen, Zg. Chen, A De Iorio, W-S Hou, Th. Hsu, Yw. Kao, S Karmakar, G Kole, Yy. Li, R-S Lu, E Paganis, Xf. Su, J Thomas-Wilsker, Ls. Tsai, D Tsionou, Hy. Wu, E Yazgan
National Taiwan University (NTU), Taipei, Taiwan

C Asawatangtrakuldee, N Srimanobhas
High Energy Physics Research Unit, Department of Physics, Faculty of Science, Chulalongkorn University, Bangkok, Thailand

Y Maghrbi
Tunis El Manar University, Tunis, Tunisia

D Agyel, F Dolek, I Dumanoglu[64], Y Guler[65], E Gurpinar Guler[65], C Isik, O Kara, A Kayis Topaksu, Y Komurcu, G Onengut, K Ozdemir[66], B Tali[67], U G Tok, E Uslan, I S Zorbakir
Çukurova University, Physics Department, Science and Art Faculty, Adana, Turkey

S Sen
Hacettepe University, Ankara, Turkey

M Yalvac[68]
Middle East Technical University, Physics Department, Ankara, Turkey

B Akgun, I O Atakisi[69]**, E Gülmez, M Kaya**[70]**, O Kaya**[71]**, M A Sarkisla**[72]**, S Tekten**[73]
Bogazici University, Istanbul, Turkey

A Cakir, K Cankocak[64,74]
Istanbul Technical University, Istanbul, Turkey

B Hacisahinoglu, I Hos[75]**, B Kaynak, S Ozkorucuklu, O Potok, H Sert, C Simsek, C Zorbilmez**
Istanbul University, Istanbul, Turkey

S Cerci, C Dozen[76]**, B Isildak**[77]**, E Simsek, D Sunar Cerci, T Yetkin**[76]
Yildiz Technical University, Istanbul, Turkey

A Boyaryntsev, O Dadazhanova, B Grynyov
Institute for Scintillation Materials of National Academy of Science of Ukraine, Kharkiv, Ukraine

L Levchuk
National Science Centre, Kharkiv Institute of Physics and Technology, Kharkiv, Ukraine

J J Brooke, A Bundock, F Bury, E Clement, D Cussans, D Dharmender, H Flacher, J Goldstein, H F Heath, M-L Holmberg, L Kreczko, S Paramesvaran, L Robertshaw, M S Sanjrani[41]**, J Segal, V J Smith**
University of Bristol, Bristol, United Kingdom

A H Ball, K W Bell, A Belyaev[78]**, C Brew, R M Brown, D JA Cockerill, A Elliot, K V Ellis, J Gajownik, K Harder, S Harper, J Linacre, K Manolopoulos, M Moallemi, D M Newbold, E Olaiya, D Petyt, T Reis, A R Sahasransu, G Salvi, T Schuh, C H Shepherd-Themistocleous, I R Tomalin, K C Whalen, T Williams**
Rutherford Appleton Laboratory, Didcot, United Kingdom

I Andreou, R Bainbridge, P Bloch, O Buchmuller, C A Carrillo Montoya, D Colling, I Das, P Dauncey, G Davies, M Della Negra, S Fayer, G Fedi, G Hall, H R Hoorani, A Howard, G Iles, C R Knight, P Krueper, J Langford, K H Law, J León Holgado, L Lyons, A-M Magnan, B Maier, S Mallios, A Mastronikolis, M Mieskolainen, J Nash[79]**, M Pesaresi, P B Pradeep, B C Radburn-Smith, A Richards, A Rose, L Russell, K Savva, C Seez, R Shukla, A Tapper, K Uchida, G P Uttley, T Virdee**[28]**, M Vojinovic, N Wardle, D Winterbottom**
Imperial College, London, United Kingdom

J E Cole, A Khan, P Kyberd, I D Reid
Brunel University, Uxbridge, United Kingdom

S Abdullin, A Brinkerhoff, E Collins, M R Darwish, J Dittmann, K Hatakeyama, V Hegde, J Hiltbrand, B McMaster, J Samudio, S Sawant, C Sutantawibul, J Wilson
Baylor University, Waco, Texas, USA

J M Hogan[80]
Bethel University, St. Paul, Minnesota, USA

R Bartek, A Dominguez, S Raj, A E Simsek, S S Yu
Catholic University of America, Washington, DC, USA

B Bam, A Buchot Perraguin, S Campbell, R Chudasama, S I Cooper, C Crovella, G Fidalgo, S V Gleyzer, A Khukhunaishvili, K Matchev, E Pearson, C U Perez, P Rumerio[81], E Usai, R Yi
The University of Alabama, Tuscaloosa, Alabama, USA

S Cholak, G De Castro, Z Demiragli, C Erice, C Fangmeier, C Fernandez Madrazo, E Fontanesi, J Fulcher, F Golf, S Jeon, J O'Cain, I Reed, J Rohlf, K Salyer, D Sperka, D Spitzbart, I Suarez, A Tsatsos, E Wurtz, A G Zecchinelli
Boston University, Boston, Massachusetts, USA

G Barone, G Benelli, D Cutts, S Ellis, L Gouskos, M Hadley, U Heintz, K W Ho, T Kwon, L Lambrecht, G Landsberg, K T Lau, J Luo, S Mondal, J Roloff, T Russell, S Sagir[82], X Shen, M Stamenkovic, N Venkatasubramanian
Brown University, Providence, Rhode Island, USA

S Abbott, B Barton, R Breedon, H Cai, M Calderon De La Barca Sanchez, E Cannaert, M Chertok, M Citron, J Conway, P T Cox, R Erbacher, O Kukral, G Mocellin, S Ostrom, I Salazar Segovia, J S Tafoya Vargas, W Wei, S Yoo
University of California, Davis, Davis, California, USA

K Adamidis, M Bachtis, D Campos, R Cousins, A Datta, G Flores Avila, J Hauser, M Ignatenko, M A Iqbal, T Lam, Yf. Lo, E Manca, A Nunez Del Prado, D Saltzberg, V Valuev
University of California, Los Angeles, California, USA

R Clare, J W Gary, G Hanson
University of California, Riverside, Riverside, California, USA

A Aportela, A Arora, J G Branson, S Cittolin, S Cooperstein, B D'Anzi, D Diaz, J Duarte, L Giannini, Y Gu, J Guiang, V Krutelyov, R Lee, J Letts, H Li, M Masciovecchio, F Mokhtar, S Mukherjee, M Pieri, D Primosch, M Quinnan, V Sharma, M Tadel, E Vourliotis, F Würthwein, A Yagil, Z Zhao
University of California, San Diego, La Jolla, California, USA

A Barzdukas, L Brennan, C Campagnari, S Carron Montero[83], K Downham, C Grieco, M M Hussain, J Incandela, M WK Lai, A J Li, P Masterson, J Richman, S N Santpur, U Sarica, R Schmitz, F Setti, J Sheplock, D Stuart, TÁ. Vámi, X Yan, D Zhang
University of California, Santa Barbara - Department of Physics, Santa Barbara, California, USA

A Albert, S Bhattacharya, A Bornheim, O Cerri, R Kansal, J Mao, H B Newman, G Reales Gutiérrez, T Sievert, M Spiropulu, J R Vlimant, R A Wynne, S Xie
California Institute of Technology, Pasadena, California, USA

J Alison, S An, M Cremonesi, V Dutta, E Y Ertorer, T Ferguson, T A Gómez Espinosa, A Harilal, A Kallil Tharayil, M Kanemura, C Liu, P Meiring, T Mudholkar, S Murthy, P Palit, K Park, M Paulini, A Roberts, A Sanchez, W Terrill
Carnegie Mellon University, Pittsburgh, Pennsylvania, USA

J P Cumalat, W T Ford, A Hart, S Kwan, J Pearkes, C Savard, N Schonbeck, K Stenson, K A Ulmer, S R Wagner, N Zipper, D Zuolo
University of Colorado Boulder, Boulder, Colorado, USA

J Alexander, X Chen, J Dickinson, A Duquette, J Fan, X Fan, J Grassi, S Hogan, P Kotamnives, J Monroy, G Niendorf, M Oshiro, J R Patterson, A Ryd, J Thom, P Wittich, R Zou, L Zygala
Cornell University, Ithaca, New York, USA

M Albrow, M Alyari, O Amram, G Apollinari, A Apresyan, L AT Bauerdick, D Berry, J Berryhill, P C Bhat, K Burkett, J N Butler, A Canepa, G B Cerati, H WK Cheung, F Chlebana, C Cosby, G Cummings, I Dutta, V D Elvira, J Freeman, A Gandrakota, Z Gecse, L Gray, D Green, A Grummer, S Grünendahl, D Guerrero, O Gutsche, R M Harris, T C Herwig, J Hirschauer, V Innocente, B Jayatilaka, S Jindariani, M Johnson, U Joshi, B Klima, K HM Kwok, S Lammel, C Lee, D Lincoln, R Lipton, T Liu, K Maeshima, D Mason, P McBride, P Merkel, S Mrenna, S Nahn, J Ngadiuba, D Noonan, S Norberg, V Papadimitriou, N Pastika, K Pedro, C Pena[84], C E Perez Lara, F Ravera, A Reinsvold Hall[85], L Ristori, M Safdari, E Sexton-Kennedy, N Smith, A Soha, L Spiegel, S Stoynev, J Strait, L Taylor, S Tkaczyk, N V Tran, L Uplegger, E W Vaandering, C Wang, I Zoi
Fermi National Accelerator Laboratory, Batavia, Illinois, USA

C Aruta, P Avery, D Bourilkov, P Chang, V Cherepanov, R D Field, C Huh, E Koenig, M Kolosova, J Konigsberg, A Korytov, G Mitselmakher, K Mohrman, A Muthirakalayil Madhu, N Rawal, S Rosenzweig, V Sulimov, Y Takahashi, J Wang
University of Florida, Gainesville, Florida, USA

T Adams, A Al Kadhim, A Askew, S Bower, R Goff, R Hashmi, A Hassani, R S Kim, T Kolberg, G Martinez, M Mazza, H Prosper, P R Prova, R Yohay
Florida State University, Tallahassee, Florida, USA

B Alsufyani, S Butalla, S Das, M Hohlmann, M Lavinsky, E Yanes
Florida Institute of Technology, Melbourne, Florida, USA

M R Adams, N Barnett, A Baty, C Bennett, R Cavanaugh, R Escobar Franco, O Evdokimov, C E Gerber, H Gupta, M Hawksworth, A Hingrajiya, D J Hofman, Jh. Lee, C Mills, S Nanda, G Nigmatkulov, B Ozek, T Phan, D Pilipovic, R Pradhan, E Prifti, P Roy, T Roy, N Singh, M B Tonjes, N Varelas, M A Wadud, J Yoo
University of Illinois Chicago, Chicago, Illinois, USA

M Alhusseini, D Blend, K Dilsiz[86], O K Köseyan, A Mestvirishvili[87], O Neogi, H Ogul[88], Y Onel, A Penzo, C Snyder, E Tiras[89]
The University of Iowa, Iowa City, Iowa, USA

B Blumenfeld, J Davis, A V Gritsan, L Kang, S Kyriacou, P Maksimovic, M Roguljic, S Sekhar, M V Srivastav, M Swartz
Johns Hopkins University, Baltimore, Maryland, USA

A Abreu, L F Alcerro Alcerro, J Anguiano, S Arteaga Escatel, P Baringer, A Bean, R Bhattacharya, Z Flowers, D Grove, J King, G Krintiras, M Lazarovits, C Le Mahieu, J Marquez, M Murray, M Nickel, S Popescu[90], C Rogan, C Royon, S Rudrabhatla, S Sanders, C Smith, G Wilson
The University of Kansas, Lawrence, Kansas, USA

B Allmond, N Islam, A Ivanov, K Kaadze, Y Maravin, J Natoli, G G Reddy, D Roy, G Sorrentino
Kansas State University, Manhattan, Kansas, USA

A Baden, A Belloni, J Bistany-riebman, S C Eno, N J Hadley, S Jabeen, R G Kellogg, T Koeth, B Kronheim, S Lascio, P Major, A C Mignerey, C Palmer, C Papageorgakis, M M Paranjpe, E Popova[91], A Shevelev, L Zhang
University of Maryland, College Park, Maryland, USA

C Baldenegro Barrera, H Bossi, S Bright-Thonney, I A Cali, Yc. Chen, Pc. Chou, M D'Alfonso, J Eysermans, C Freer, G Gomez-Ceballos, M Goncharov, G Grosso, P Harris, D Hoang, G M Innocenti, K Ivanov, D Kovalskyi, J Krupa, L Lavezzo, Y-J Lee, K Long, C Mcginn, A Novak, M I Park, C Paus, C Reissel, C Roland, G Roland, S Rothman, Ta. Sheng, G SF Stephans, D Walter, Z Wang, B Wyslouch, T J Yang
Massachusetts Institute of Technology, Cambridge, Massachusetts, USA

B Crossman, W J Jackson, C Kapsiak, M Krohn, D Mahon, J Mans, B Marzocchi, R Rusack, O Sancar, R Saradhy, N Strobbe
University of Minnesota, Minneapolis, Minnesota, USA

K Bloom, D R Claes, G Haza, J Hossain, C Joo, I Kravchenko, A Rohilla, J E Siado, W Tabb, A Vagnerini, A Wightman, F Yan
University of Nebraska-Lincoln, Lincoln, Nebraska, USA

H Bandyopadhyay, L Hay, Hw. Hsia, I Iashvili, A Kalogeropoulos, A Kharchilava, A Mandal, M Morris, D Nguyen, S Rappoccio, H Rejeb Sfar, A Williams, P Young, D Yu
State University of New York at Buffalo, Buffalo, New York, USA

G Alverson, E Barberis, J Bonilla, B Bylsma, M Campana, J Dervan, Y Haddad, Y Han, I Israr, A Krishna, M Lu, N Manganelli, R Mccarthy, D M Morse, T Orimoto, L Skinnari, C S Thoreson, E Tsai, D Wood
Northeastern University, Boston, Massachusetts, USA

S Dittmer, K A Hahn, M Mcginnis, Y Miao, D G Monk, M H Schmitt, A Taliercio, M Velasco, J Wang
Northwestern University, Evanston, Illinois, USA

G Agarwal, R Band, R Bucci, S Castells, A Das, A Ehnis, R Goldouzian, M Hildreth, K Hurtado Anampa, T Ivanov, C Jessop, A Karneyeu, K Lannon, J Lawrence, N Loukas, L Lutton, J Mariano, N Marinelli, I Mcalister, T McCauley, C Mcgrady, C Moore, Y Musienko[22], H Nelson, M Osherson, A Piccinelli, R Ruchti, A Townsend, Y Wan, M Wayne, H Yockey
University of Notre Dame, Notre Dame, Indiana, USA

A Basnet, M Carrigan, R De Los Santos, L S Durkin, C Hill, M Joyce, M Nunez Ornelas, D A Wenzl, B L Winer, B R Yates
The Ohio State University, Columbus, Ohio, USA

H Bouchamaoui, G Dezoort, P Elmer, A Frankenthal, M Galli, B Greenberg, N Haubrich, K Kennedy, G Kopp, Y Lai, D Lange, A Loeliger, D Marlow, I Ojalvo, J Olsen, F Simpson, D Stickland, C Tully
Princeton University, Princeton, New Jersey, USA

S Malik, R Sharma
University of Puerto Rico, Mayaguez, Puerto Rico, USA

S Chandra, R Chawla, A Gu, L Gutay, M Jones, A W Jung, D Kondratyev, M Liu, G Negro, N Neumeister, G Paspalaki, S Piperov, N R Saha, J F Schulte, F Wang, A Wildridge, W Xie, Y Yao, Y Zhong
Purdue University, West Lafayette, Indiana, USA

N Parashar, A Pathak, E Shumka
Purdue University Northwest, Hammond, Indiana, USA

D Acosta, A Agrawal, C Arbour, T Carnahan, P Das, K M Ecklund, S Freed, F JM Geurts, T Huang, I Krommydas, N Lewis, W Li, J Lin, O Miguel Colin, B P Padley, R Redjimi, J Rotter, M Wulansatiti, E Yigitbasi, Y Zhang
Rice University, Houston, Texas, USA

O Bessidskaia Bylund, A Bodek, P de Barbaro†, R Demina, A Garcia-Bellido, H S Hare, O Hindrichs, N Parmar, P Parygin[91], H Seo, R Taus
University of Rochester, Rochester, New York, USA

B Chiarito, J P Chou, S V Clark, S Donnelly, D Gadkari, Y Gershtein, E Halkiadakis, C Houghton, D Jaroslawski, A Kobert, S Konstantinou, I Laflotte, A Lath, J Martins, M Perez Prada, B Rand, J Reichert, P Saha, S Salur, S Schnetzer, S Somalwar, R Stone, S A Thayil, S Thomas, J Vora
Rutgers, The State University of New Jersey, Piscataway, New Jersey, USA

D Ally, A G Delannoy, S Fiorendi, J Harris, T Holmes, A R Kanuganti, N Karunarathna, J Lawless, L Lee, E Nibigira, B Skipworth, S Spanier
University of Tennessee, Knoxville, Tennessee, USA

D Aebi, M Ahmad, T Akhter, K Androsov, A Bolshov, O Bouhali[92], A Cagnotta, V D'Amante, R Eusebi, P Flanagan, J Gilmore, Y Guo, T Kamon, S Luo, R Mueller, A Safonov
Texas A&M University, College Station, Texas, USA

N Akchurin, J Damgov, Y Feng, N Gogate, Y Kazhykarim, K Lamichhane, S W Lee, C Madrid, A Mankel, T Peltola, I Volobouev
Texas Tech University, Lubbock, Texas, USA

E Appelt, Y Chen, S Greene, A Gurrola, W Johns, R Kunnawalkam Elayavalli, A Melo, D Rathjens, F Romeo, P Sheldon, S Tuo, J Velkovska, J Viinikainen, J Zhang
Vanderbilt University, Nashville, Tennessee, USA

B Cardwell, H Chung, B Cox, J Hakala, G Hamilton Ilha Machado, R Hirosky, M Jose, A Ledovskoy, C Mantilla, C Neu, C Ramón Álvarez, Z Wu
University of Virginia, Charlottesville, Virginia, USA

S Bhattacharya, P E Karchin
Wayne State University, Detroit, Michigan, USA

A Aravind, S Banerjee, K Black, T Bose, E Chavez, S Dasu, P Everaerts, C Galloni, H He, M Herndon, A Herve, C K Koraka, S Lomte, R Loveless, A Mallampalli, A Mohammadi, S Mondal, T Nelson, G Parida, L Pétré, D Pinna, A Savin, V Shang, V Sharma, W H Smith, D Teague, H F Tsoi, W Vetens, A Warden
University of Wisconsin - Madison, Madison, Wisconsin, USA

S Afanasiev, V Alexakhin, Yu. Andreev, T Aushev, D Budkouski, R Chistov, M Danilov, T Dimova, A Ershov, S Gninenko, I Gorbunov, A Gribushin, A Kamenev, V Karjavine, M Kirsanov, V Klyukhin, O Kodolova[93], V Korenkov, I Korsakov, A Kozyrev, N Krasnikov, A Lanev, A Malakhov, V Matveev, A Nikitenko[94,93], V Palichik, V Perelygin, S Petrushanko, S Polikarpov, O Radchenko, M Savina, V Shalaev, S Shmatov, S Shulha, Y Skovpen, K Slizhevskiy, V Smirnov, O Teryaev, I Tlisova, A Toropin, N Voytishin, A Zarubin, I Zhizhin
Authors affiliated with an international laboratory covered by a cooperation agreement with CERN

E Boos, V Bunichev, M Dubinin[84], V Savrin, A Snigirev, L Dudko, V Kim[22], V Murzin, V Oreshkin, D Sosnov
Authors affiliated with an institute formerly covered by a cooperation agreement with CERN

†: Deceased
[1]Also at Yerevan State University, Yerevan, Armenia
[2]Also at TU Wien, Vienna, Austria
[3]Also at Ghent University, Ghent, Belgium
[4]Also at FACAMP – Faculdades de Campinas, Sao Paulo, Brazil
[5]Also at Universidade do Estado do Rio de Janeiro, Rio de Janeiro, Brazil
[6]Also at Universidade Estadual de Campinas, Campinas, Brazil
[7]Also at the Federal University of Rio Grande do Sul, Porto Alegre, Brazil
[8]Also at The University of the State of Amazonas, Manaus, Brazil
[9]Also at the University of Chinese Academy of Sciences, Beijing, China
[10]Also at the China Center of Advanced Science and Technology, Beijing, China
[11]Also at the University of Chinese Academy of Sciences, Beijing, China
[12]Also at School of Physics, Zhengzhou University, Zhengzhou, China
[13]Now at Henan Normal University, Xinxiang, China
[14]Also at University of Shanghai for Science and Technology, Shanghai, China
[15]Now at The University of Iowa, Iowa City, Iowa, USA
[16]Also at the Center for High Energy Physics, Peking University, Beijing, China
[17]Also at Suez University, Suez, Egypt
[18]Now at British University in Egypt, Cairo, Egypt
[19]Also at Cairo University, Cairo, Egypt
[20]Also at Purdue University, West Lafayette, Indiana, USA
[21]Also at Université de Haute Alsace, Mulhouse, France
[22]Also at an institute formerly covered by a cooperation agreement with CERN
[23]Also at University of Hamburg, Hamburg, Germany
[24]Also at RWTH Aachen University, III. Physikalisches Institut A, Aachen, Germany
[25]Also at Bergische University Wuppertal (BUW), Wuppertal, Germany
[26]Also at Brandenburg University of Technology, Cottbus, Germany
[27]Also at Forschungszentrum Jülich, Juelich, Germany
[28]Also at CERN, European Organization for Nuclear Research, Geneva, Switzerland
[29]Also at HUN-REN ATOMKI - Institute of Nuclear Research, Debrecen, Hungary
[30]Now at Universitatea Babes-Bolyai - Facultatea de Fizica, Cluj-Napoca, Romania
[31]Also at MTA-ELTE Lendület CMS Particle and Nuclear Physics Group, Eötvös Loránd University, Budapest, Hungary
[32]Also at HUN-REN Wigner Research Centre for Physics, Budapest, Hungary
[33]Also at Physics Department, Faculty of Science, Assiut University, Assiut, Egypt
[34]Also at The University of Kansas, Lawrence, Kansas, USA
[35]Also at Punjab Agricultural University, Ludhiana, India
[36]Also at University of Hyderabad, Hyderabad, India
[37]Also at Indian Institute of Science (IISc), Bangalore, India
[38]Also at University of Visva-Bharati, Santiniketan, India
[39]Also at IIT Bhubaneswar, Bhubaneswar, India
[40]Also at Institute of Physics, Bhubaneswar, India
[41]Also at Deutsches Elektronen-Synchrotron, Hamburg, Germany
[42]Also at Isfahan University of Technology, Isfahan, Iran
[43]Also at Sharif University of Technology, Tehran, Iran
[44]Also in the Department of Physics, University of Science and Technology of Mazandaran, Behshahr, Iran
[45]Also at the Department of Physics, Faculty of Science, Arak University, ARAK, Iran
[46]Also at Helwan University, Cairo, Egypt
[47]Also at Italian National Agency for New Technologies, Energy and Sustainable Economic Development, Bologna, Italy
[48]Also at Centro Siciliano di Fisica Nucleare e di Struttura Della Materia, Catania, Italy
[49]Also at Università degli Studi Guglielmo Marconi, Roma, Italy
[50]Also at Scuola Superiore Meridionale, Università di Napoli'Federico II', Napoli, Italy
[51]Also at Fermi National Accelerator Laboratory, Batavia, Illinois, USA
[52]Also at Lulea University of Technology, Lulea, Sweden
[53]Also at Ain Shams University, Cairo, Egypt
[54]Also at Consiglio Nazionale delle Ricerche - Istituto Officina dei Materiali, Perugia, Italy
[55]Also at UPES - University of Petroleum and Energy Studies, Dehradun, India

[56]Also at Institut de Physique des 2 Infinis de Lyon (IP2I), Villeurbanne, France
[57]Also at Department of Applied Physics, Faculty of Science and Technology, Universiti Kebangsaan Malaysia, Bangi, Malaysia
[58]Also at Trincomalee Campus, Eastern University, Sri Lanka, Nilaveli, Sri Lanka
[59]Also at Saegis Campus, Nugegoda, Sri Lanka
[60]Also at National and Kapodistrian University of Athens, Athens, Greece
[61]Also at Ecole Polytechnique Fédérale Lausanne, Lausanne, Switzerland
[62]Also at Universität Zürich, Zurich, Switzerland
[63]Also at Stefan Meyer Institute for Subatomic Physics, Vienna, Austria
[64]Also at Near East University, Research Center of Experimental Health Science, Mersin, Turkey
[65]Also at Konya Technical University, Konya, Turkey
[66]Also at Izmir Bakircay University, Izmir, Turkey
[67]Also at Adiyaman University, Adiyaman, Turkey
[68]Also at Bozok Universitetesi Rektörlügü, Yozgat, Turkey
[69]Also at Istanbul Sabahattin Zaim University, Istanbul, Turkey
[70]Also at Marmara University, Istanbul, Turkey
[71]Also at Milli Savunma University, Istanbul, Turkey
[72]Also at Informatics and Information Security Research Center, Gebze/Kocaeli, Turkey
[73]Also at Kafkas University, Kars, Turkey
[74]Now at Istanbul Okan University, Istanbul, Turkey
[75]Also at Istanbul University - Cerrahpasa, Faculty of Engineering, Istanbul, Turkey
[76]Also at Istinye University, Istanbul, Turkey
[77]Also at Yildiz Technical University, Istanbul, Turkey
[78]Also at School of Physics and Astronomy, University of Southampton, Southampton, United Kingdom
[79]Also at Monash University, Faculty of Science, Clayton, Australia
[80]Also at Bethel University, St. Paul, Minnesota, USA
[81]Also at Università di Torino, Torino, Italy
[82]Also at Karamanoğlu Mehmetbey University, Karaman, Turkey
[83]Also at California Lutheran University;, Thousand Oaks, California, USA
[84]Also at California Institute of Technology, Pasadena, California, USA
[85]Also at United States Naval Academy, Annapolis, Maryland, USA
[86]Also at Bingol University, Bingol, Turkey
[87]Also at Georgian Technical University, Tbilisi, Georgia
[88]Also at Sinop University, Sinop, Turkey
[89]Also at Erciyes University, Kayseri, Turkey
[90]Also at Horia Hulubei National Institute of Physics and Nuclear Engineering (IFIN-HH), Bucharest, Romania
[91]Now at another institute formerly covered by a cooperation agreement with CERN
[92]Also at Hamad Bin Khalifa University (HBKU), Doha, Qatar
[93]Also at Yerevan Physics Institute, Yerevan, Armenia
[94]Also at Imperial College, London, United Kingdom

Acknowledgements

We congratulate our colleagues in the CERN accelerator departments for the excellent performance of the LHC and thank the technical and administrative staffs at CERN and at other CMS institutes for their contributions to the success of the CMS effort. In addition, we gratefully acknowledge the computing centres and personnel of the Worldwide LHC Computing Grid and other centres for delivering so effectively the computing infrastructure essential to our analyses. Finally, we acknowledge the enduring support for the construction and operation of the LHC, the CMS detector, and the supporting computing infrastructure provided by the following funding agencies: SC (Armenia), BMBWF and FWF (Austria); FNRS and FWO (Belgium); CNPq, CAPES, FAPERJ, FAPERGS, and FAPESP (Brazil); MES and BNSF (Bulgaria); CERN; CAS, MoST, and NSFC (China); MINCIENCIAS (Colombia); MSES and CSF (Croatia); RIF (Cyprus); SENESCYT (Ecuador); ERC PRG, TARISTU24-TK10 and MoER TK202 (Estonia); Academy of Finland, MEC, and HIP (Finland); CEA and CNRS/IN2P3 (France); SRNSF (Georgia); BMFTR, DFG, and HGF (Germany); GSRI (Greece); NKFIH (Hungary); DAE and DST (India); IPM (Iran); SFI (Ireland); INFN (Italy); MSIT and NRF (Republic of Korea); MES (Latvia);

LMTLT (Lithuania); MOE and UM (Malaysia); BUAP, CINVESTAV, CONACYT, LNS, SEP, and UASLP-FAI (Mexico); MOS (Montenegro); MBIE (New Zealand); PAEC (Pakistan); MES, NSC, and NAWA (Poland); FCT (Portugal); MESTD (Serbia); MICIU/AEI and PCTI (Spain); MOSTR (Sri Lanka); Swiss Funding Agencies (Switzerland); MST (Taipei); MHESI (Thailand); TUBITAK and TENMAK (Türkiye); NASU (Ukraine); STFC (United Kingdom); DOE and NSF (USA).

Individuals have received support from the Marie-Curie programme and the European Research Council and Horizon 2020 Grant, contract Nos. 675440, 724704, 752730, 758316, 765710, 824093, 101115353, 101002207, 101001205, and COST Action CA16108 (European Union); the Leventis Foundation; the Alfred P. Sloan Foundation; the Alexander von Humboldt Foundation; the Science Committee, Project No. 22rl-037 (Armenia); the Fonds pour la Formation à la Recherche dans l'Industrie et dans l'Agriculture (FRIA) and Fonds voor Wetenschappelijk Onderzoek Contract No. 1228724N (Belgium); the Beijing Municipal Science & Technology Commission, No. Z191100007219010, the Fundamental Research Funds for the Central Universities, the Ministry of Science and Technology of China under Grant No. 2023YFA1605804, the Natural Science Foundation of China under Grant No. 12061141002 and USTC Research Funds of the Double First-Class Initiative No. YD2030002017 (China); the Ministry of Education, Youth and Sports (MEYS) of the Czech Republic; the Shota Rustaveli National Science Foundation, grant FR-22-985 (Georgia); the Deutsche Forschungsgemeinschaft (DFG), among others, under Germany's Excellence Strategy—EXC 2121 'Quantum Universe' – 390833306, and under project number 400140256 - GRK2497; the Hellenic Foundation for Research and Innovation (HFRI), Project Number 2288 (Greece); the Hungarian Academy of Sciences, the New National Excellence Program - ÚNKP, the NKFIH research grants K 131991, K 133046, K 138136, K 143460, K 143477, K 146913, K 146914, K 147048, 2020-2.2.1-ED-2021-00181, TKP2021-NKTA-64, and 2021-4.1.2-NEMZ_KI-2024-00036 (Hungary); the Council of Science and Industrial Research, India; ICSC—National Research Centre for High Performance Computing, Big Data and Quantum Computing, FAIR—Future Artificial Intelligence Research, and CUP I53D23001070006 (Mission 4 Component 1), funded by the NextGenerationEU program (Italy); the Latvian Council of Science; the Ministry of Education and Science, project no. 2022/WK/14, and the National Science Center, contracts Opus 2021/41/B/ST2/01369, 2021/43/B/ST2/01552, 2023/49/B/ST2/03273, and the NAWA contract BPN/PPO/2021/1/00011 (Poland); the Fundação para a Ciência e a Tecnologia, grant CEECIND/01334/2018 (Portugal); the National Priorities Research Program by Qatar National Research Fund; MICIU/AEI/10.13039/501100011033, ERDF/EU, 'European Union NextGenerationEU/PRTR', and Programa Severo Ochoa del Principado de Asturias (Spain); the Chulalongkorn Academic into Its 2nd Century Project Advancement Project, the National Science, Research and Innovation Fund program IND_FF_68_369_2300_097, and the Program Management Unit for Human Resources & Institutional Development, Research and Innovation, grant B39G680009 (Thailand); the Kavli Foundation; the Nvidia Corporation; the SuperMicro Corporation; the Welch Foundation, contract C-1845; and the Weston Havens Foundation (USA).

Data availability statement

Release and preservation of data used by the CMS Collaboration as the basis for publications is guided by the CMS data preservation, re-use and open access policy.

Supplemental Material available at: https://doi.org/10.1088/1361-6471/ae8ff1/data1.

ORCID iD

The CMS Collaboration 0000-0001-6651-1178

References

[1] CMS Collaboration 2012 Observation of a new boson at a mass of 125 GeV with the CMS experiment at the LHC *Phys. Lett. B* **716** 30

[2] CMS Collaboration 2013 Observation of a new boson with mass near 125 GeV in pppp collisions at $\sqrt{s} = 7$ and 8 TeV *J. High Energy Phys.* **06** JHEP06(2013)081

[3] ATLAS Collaboration 2012 Observation of a new particle in the search for the standard model Higgs boson with the ATLAS detector at the lhc *Phys. Lett. B* **716** 1

[4] CMS Collaboration 2022 A portrait of the Higgs boson by the CMS experiment ten years after the discovery *Nature* **607** 60–68

[5] ATLAS Collaboration 2022 A detailed map of Higgs boson interactions by the ATLAS experiment ten years after the discovery *Nature* **607** 52–59
[6] Dawson S and Murphy C W 2017 Standard model EFT and extended scalar sectors *Phys. Rev. D* **96** 015041
[7] de Blas J, Chala M, Perez-Victoria M and Santiago J 2015 Observable effects of general new scalar particles *J. High Energy Phys.* JHEP04(2015)078
[8] Lee T D 1973 A theory of spontaneous *T* violation *Phys. Rev. D* **8** 1226
[9] Branco G C *et al* 2012 Theory and phenomenology of two-Higgs-doublet models *Phys. Rep.* **516** 1
[10] Haber H E and Stål O 2015 New LHC benchmarks for the *CP*-conserving two-Higgs-doublet model *Eur. Phys. J. C* **75** 491
[11] Kling F, No J M and Su S 2016 Anatomy of exotic Higgs decays in 2HDM *J. High Energy Phys.* JHEP09(2016)093
[12] Giudice G F, Grojean C, Pomarol A and Rattazzi R 2007 The strongly-interacting light Higgs *J. High Energy Phys.* **06** JHEP06(2007)045
[13] Gröber R and Mühlleitner M 2011 Composite Higgs boson pair production at the LHC *J. High Energy Phys.* JHEP06(2011)020
[14] Contino R, Ghezzi M, Grojean C, Mühlleitner M and Spira M 2013 Effective Lagrangian for a light Higgs-like scalar *J. High Energy Phys.* JHEP07(2013)035
[15] Contino R 2011 The Higgs as a composite Nambu–Goldstone boson *Theor. Adv. Study Inst. Elem. Part. Phys.: Phys. Large Small* 235
[16] Huang P, Long A J and Wang L-T 2016 Probing the electroweak phase transition with Higgs factories and gravitational waves *Phys. Rev. D* **94** 075008
[17] Ramsey-Musolf M J, Tenkanen T V I. and Tran V Q 2024 Refining gravitational wave and collider physics dialogue via singlet scalar extension (arXiv:2409.17554)
[18] Mazumdar A and White G 2019 Review of cosmic phase transitions: Their significance and experimental signatures *Rep. Prog. Phys.* **82** 076901
[19] Zhang W *et al* 2023 Probing electroweak phase transition in the singlet standard model via $bb\gamma\gamma$ and 4ℓ channels *J. High Energy Phys.* JHEP12(2023)018
[20] Bednyakov A V, Pikelner A F and Velizhanin V N 2015 Stability of the electroweak vacuum: Gauge independence and radiative corrections *Phys. Rev. Lett.* **115** 201802
[21] Basler P, Biermann L and Mühlleitner M *et al* 2023 Electroweak baryogenesis in the CP-violating two-Higgs doublet model *Eur. Phys. J. C* **83** 57
[22] Morrissey D E and Ramsey-Musolf M J 2012 Electroweak baryogenesis: a review *New J. Phys.* **14** 125003
[23] Plehn T and Rauch M 2005 The quartic Higgs coupling at hadron colliders *Phys. Rev. D* **72** 053008
[24] Dainese A *et al* 2019 Report from Working Group 2: Higgs physics at the HL-LHC and HE-LHC *CERN Yellow Rep. Monogr.* **7** 221
[25] Chiesa M, Maltoni F, Mantani L, Mele B, Piccinini F and Zhao X 2020 Measuring the quartic Higgs self-coupling at a multi-TeVns muon collider *J. High Energy Phys.* JHEP09(2020)098
[26] Abouabid H *et al* 2024 HHH whitepaper *Eur. Phys. J. C* **84** 1183
[27] Borowka S, Greiner N, Heinrich G, Jones S, Kerner M, Schlenk J, Schubert U and Zirke T 2016 Higgs boson pair production in gluon fusion at next-to-leading order with full top-quark mass dependence *Phys. Rev. Lett.* **117** 012001
[28] Baglio J , Campanario F, Glaus S, Mühlleitner M, Spira M and Streicher J 2019 Gluon fusion into Higgs pairs at NLO QCD and the top mass scheme *Eur. Phys. J. C* **79** 459
[29] Dreyer F A and Karlberg A 2018 Vector-boson fusion Higgs pair production at N^3LO *Phys. Rev. D* **98** 114016
[30] Baglio J *et al* 2013 The measurement of the Higgs self-coupling at the LHC: theoretical status *J. High Energy Phys.* JHEP04(2013)151
[31] Grazzini M , Heinrich G, Jones S, Kallweit S, Kerner M, Lindert J M and Mazzitelli J 2018 Higgs boson pair production at NNLO with top quark mass effects *J. High Energy Phys.* JHEP05(2018)059
[32] Alasfar L *et al* 2024 Effective field theory descriptions of Higgs boson pair production *SciPost Phys. Comm. Rep.* 2
[33] ATLAS Collaboration 2024 Combination of searches for Higgs boson pair production in pppp collisions at $\sqrt{s} = 13$ TeV with the ATLAS detector *Phys. Rev. Lett.* **133** 101801
[34] HEPData record for this analysis 2025 (available at: https://doi.org/10.17182/hepdata.16528210.17182/hepdata.165282)
[35] CMS Collaboration 2008 The CMS experiment at the CERN LHC *J. Instrum.* **3** S08004
[36] CMS Collaboration 2024 Development of the CMS detector for the CERN LHC Run 3 *J. Instrum.* **19** 05064
[37] CMS Collaboration 2020 Performance of the CMS Level-1 trigger in proton-proton collisions at $\sqrt{s} = 13$ TeV *J. Instrum.* **15** 10017
[38] CMS Collaboration 2017 The CMS trigger system *J. Instrum.* **12** 01020
[39] CMS Collaboration 2024 Performance of the CMS high-level trigger during LHC Run 2 *J. Instrum.* **19** 11021
[40] CMS Collaboration 2021 Electron and photon reconstruction and identification with the CMS experiment at the CERN LHC *J. Instrum.* **16** 05014
[41] CMS Collaboration 2018 Performance of the CMS muon detector and muon reconstruction with proton-proton collisions at $\sqrt{s} = 13$ TeV *J. Instrum.* **13** 06015
[42] CMS Collaboration 2014 Description and performance of track and primary-vertex reconstruction with the CMS tracker *J. Instrum.* **9** 10009
[43] CMS Collaboration 2017 Particle-flow reconstruction and global event description with the CMS detector *J. Instrum.* **12** 10003
[44] CMS Collaboration 2015 Technical proposal for the Phase-II upgrade of the Compact Muon Solenoid CMS Technical Proposal CERN-LHCC-2015-010 CMS-TDR-15-02 (available at: http://cds.cern.ch/record/2020886)
[45] Cacciari M, Salam G P and Soyez G 2008 The anti-k_T jet clustering algorithm *J. High Energy Phys.* **04** JHEP04(2008)063
[46] Cacciari M, Salam G P and Soyez G 2012 FastJet user manual *Eur. Phys. J. C* **72** 1896
[47] CMS Collaboration 2019 Performance of missing transverse momentum reconstruction in proton-proton collisions at $\sqrt{s} = 13$ TeV using the CMS detector *J. Instrum.* **14** 07004
[48] Heinrich G, Jones S P, Kerner M, Luisoni G and Scyboz L 2019 Probing the trilinear Higgs boson coupling in di-Higgs production at NLO QCD including parton shower effects *J. High Energy Phys.* JHEP06(2019)066
[49] de Florian D , Fabre I, Heinrich G, Mazzitelli J and Scyboz L 2021 Anomalous couplings in Higgs-boson pair production at approximate NNLO QCD *J. High Energy Phys.* JHEP09(2021)161
[50] Carvalho A , Goertz F, Mimasu K, Gouzevitch M and Aggarwal A 2021 On the reinterpretation of non-resonant searches for Higgs boson pairs *J. High Energy Phys.* JHEP02(2021)049

[51] Carvalho A *et al* 2016 Higgs pair production: choosing benchmarks with cluster analysis *J. High Energy Phys.* JHEP04(2016)126
[52] Capozi M and Heinrich G 2020 Exploring anomalous couplings in Higgs boson pair production through shape analysis *J. High Energy Phys.* JHEP03(2020)091
[53] CMS Collaboration 2025 Constraints on the Higgs boson self-coupling from the combination of single and double Higgs boson production in proton-proton collisions at $\sqrt{s} = 13$ TeV *Phys. Lett. B* **861** 139210
[54] Nason P 2004 A new method for combining NLO QCD with shower Monte Carlo algorithms *J. High Energy Phys.* **11** JHEP11(2004)040
[55] Frixione S, Nason P and Oleari C 2007 Matching NLO QCD computations with parton shower simulations: The POWHEG method *J. High Energy Phys.* **11** JHEP11(2007)070
[56] Alioli S, Nason P, Oleari C and Re E 2010 A general framework for implementing NLO calculations in shower Monte Carlo programs: the POWHEG BOX *J. High Energy Phys.* JHEP06(2010)043
[57] Amoroso S *et al* 2020 Les Houches 2019: physics at TeVns colliders: standard model working group report *Proc. 11th Les Houches Workshop on Physics at TeVns Colliders: PhysTeV Les Houches* (arXiv:2003.01700)
[58] Alwall J *et al* 2014 The automated computation of tree-level and next-to-leading order differential cross sections and their matching to parton shower simulations *J. High Energy Phys.* JHEP07(2014)079
[59] Alwall J *et al* 2007 Comparative study of various algorithms for the merging of parton showers and matrix elements in hadronic collisions *Eur. Phys. J. C* **53** 473
[60] Frederix R and Frixione S 2012 Merging meets matching in MC@NLO *J. High Energy Phys.* JHEP12(2012)061
[61] Dreyer F A and Karlberg A 2019 Fully differential vector-boson fusion Higgs pair production at next-to-next-to-leading order *Phys. Rev. D* **99** 074028
[62] Sjöstrand T, Mrenna S and Skands P Z 2008 A brief introduction to PYTHIA 8.1 *Comput. Phys. Commun.* **178** 852
[63] Sirunyan A M *et al* 2020 Extraction and validation of a new set of CMS PYTHIA8 tunes from underlying-event measurements *Eur. Phys. J. C* **80** 4
[64] Tumasyan A *et al* 2023 CMS PYTHIA8 colour reconnection tunes based on underlying-event data *Eur. Phys. J. C* **83** 587
[65] NNPDF Collaboration 2013 Parton distributions with QED corrections *Nucl. Phys. B* **877** 290
[66] NNPDF Collaboration 2015 Parton distributions for the LHC Run II *J. High Energy Phys.* JHEP04(2015)040
[67] NNPDF Collaboration 2017 Parton distributions from high-precision collider data *Eur. Phys. J. C* **77** 663
[68] GEANT4 Collaboration 2003 GEANTfour—a simulation toolkit *Nucl. Instrum. Meth. A* **506** 250
[69] CMS Collaboration 2022 Search for Higgs Boson Pair production in the four *b* Quark Final State in Proton-Proton Collisions at $\sqrt{s} = 13$ TeV *Phys. Rev. Lett.* **129** 081802
[70] CMS Collaboration 2023 Search for nonresonant pair production of highly energetic Higgs bosons decaying to bottom quarks *Phys. Rev. Lett.* **131** 041803
[71] CMS Collaboration 2024 Search for Higgs boson pair production with one associated vector boson in proton-proton collisions at $\sqrt{s} = 13$ TeV *J. High Energy Phys.* JHEP10(2024)061
[72] CMS Collaboration 2023 Search for nonresonant Higgs boson pair production in final state with two bottom quarks and two tau leptons in proton-proton collisions at $\sqrt{s} = 13$ TeV *Phys. Lett. B* **842** 137531
[73] CMS Collaboration 2021 Search for nonresonant Higgs boson pair production in final states with two bottom quarks and two photons in proton-proton collisions at $\sqrt{s} = 13$ TeV *J. High Energy Phys.* JHEP03(2021)257
[74] CMS Collaboration 2024 Search for Higgs boson pair production in the $\mathrm{b\bar{b}W^{+}W^{-}}$ decay mode in proton-proton collisions at $\sqrt{s} = 13$ TeV *J. High Energy Phys.* **07** 293
[75] CMS Collaboration 2023 Search for Higgs boson pairs decaying to $\mathrm{WW^{*}WW^{*}}$, $\mathrm{WW^{*}}\tau\tau$ and $\tau\tau\tau\tau$ in proton-proton collisions at $\sqrt{s} = 13$ TeV *J. High Energy Phys.* JHEP07(2023)095
[76] CMS Collaboration 2025 Search for the nonresonant and resonant production of a Higgs boson in association with an additional scalar boson in the $\gamma\gamma\tau\tau$ final state in proton-proton collisions at $\sqrt{s} = 13$ TeV Submitted to JHEP (arXiv:2506.23012)
[77] CMS Collaboration 2023 Search for nonresonant Higgs boson pair production in the four leptons plus twob jets final state in proton-proton collisions at $\sqrt{s} = 13$ TeV *J. High Energy Phys.* JHEP06(2023)130
[78] Bols E *et al* 2020 Jet flavour classification using DeepJet *J. Instrum.* **15** 12012
[79] CMS Collaboration 2020 A deep neural network for simultaneous estimation of b jet energy and resolution *Comput. Softw. Big Sci.* **4** 10
[80] Larkoski A J, Marzani S, Soyez G and Thaler J 2014 Soft drop *J. High Energy Phys.* JHEP05(2014)146
[81] Henrion I *et al* 2017 Neural message passing for jet physics *Deep Learning for Physical Sciences Workshop at 31st Conf. on Neural Information Processing Systems* (*07em Long Beach, CA, USA*)
[82] Qu H and Gouskos L 2020 Jet tagging via particle clouds *Phys. Rev. D* **101** 056019
[83] Moreno E A, Cerri O, Duarte J M, Newman H B, Nguyen T Q, Periwal A, Pierini M, Serikova A, Spiropulu M and Vlimant J-R 2020 JEDI-net: a jet identification algorithm based on interaction networks *Eur. Phys. J. C* **80** 58
[84] Moreno E A *et al* 2020 Interaction networks for the identification of boosted $\mathrm{H} \to \mathrm{b\bar{b}}$ decays *Phys. Rev. D* **102** 012010
[85] CMS Collaboration 2023 Performance of heavy-flavour jet identification in boosted topologies in proton-proton collisions at $\sqrt{s} = 13$ TeV, CMS Physics Analysis Summary CMS-PAS-BTV-22-001 (available at: http://cds.cern.ch/record/2866276)
[86] CMS Collaboration 2021 Mass regression of highly-boosted jets using graph neural networks, CMS Detector Performance Note CMS-DP-2021-017 (available at: https://cds.cern.ch/record/2777006)
[87] CMS Collaboration 2018 Search for a massive resonance decaying to a pair of Higgs bosons in the four b quark final state in proton-proton collisions at $\sqrt{s} = 13$ TeV *Phys. Lett. B* **781** 244
[88] CMS Collaboration 2019 Search for production of Higgs boson pairs in the four b quark final state using large-area jets in proton-proton collisions at $\sqrt{s} = 13$ TeV *J. High Energy Phys.* JHEP01(2019)040
[89] CMS Collaboration 2020 Inclusive search for highly boosted Higgs bosons decaying to bottom quark-antiquark pairs in proton-proton collisions at $\sqrt{s} = 13$ TeV *J. High Energy Phys.* JHEP12(2020)085
[90] CMS Collaboration 2020 Identification of heavy, energetic, hadronically decaying particles using machine-learning techniques *J. Instrum.* **15** 06005
[91] CMS Collaboration 2022 Identification of hadronic tau lepton decays using a deep neural network *J. Instrum.* **17** 07023
[92] Bianchini L, Calpas B, Conway J, Fowlie A, Marzola L, Perrini L and Veelken C 2017 Reconstruction of the Higgs mass in events with Higgs bosons decaying into a pair of τ leptons using matrix element techniques *Nucl. Instrum. Meth. A* **862** 54
[93] CMS Collaboration 2018 Evidence for associated production of a Higgs boson with a top quark pair in final states with electrons, muons and hadronically decaying τ leptons at $\sqrt{s} = 13$ TeV *J. High Energy Phys.* JHEP08(2018)066

[94] Qu H, *et al* 2022 Particle transformer for jet tagging *Proc. 39th Int. Conf. on Machine Learning* vol 162, ed K Chaudhuri p 18281 (available at: https://proceedings.mlr.press/v162/qu22b.html)
[95] CMS Collaboration 2025 Particle transformers for identifying Lorentz-boosted Higgs bosons decaying to a pair of W bosons CMS Physics Analysis Summary CMS-PAS-JME-25-001 (available at: https://cds.cern.ch/record/2939451)
[96] CMS Collaboration 2025 A new method for correcting the substructure of multi-prong jets using Lund jet plane reweighting in the CMS experiment CMS Physics Analysis Summary CMS-PAS-JME-23-001 (available at: https://cds.cern.ch/record/2924412)
[97] Dreyer F A, Salam G P and Soyez G 2018 The Lund jet plane *J. High Energy Phys.* JHEP12(2018)064
[98] CMS Collaboration 2021 Measurement of the Higgs boson production rate in association with top quarks in final states with electrons, muons and hadronically decaying tau leptons at $\sqrt{s} = 13\,\text{TeV}$ *Eur. Phys. J. C* **81** 378
[99] LHC Higgs Cross section Working Group 2017 Handbook of LHC Higgs cross sections: 4. deciphering the nature of the Higgs sector *CERN Yellow Rep. Monogr.* **2**
[100] Manzoni S *et al* 2023 Taming a leading theoretical uncertainty in HH measurements via accurate simulations for $b\bar{b}H$ production *J. High Energy Phys.* JHEP09(2023)179
[101] Baglio J *et al* 2021 gg $\rightarrow$ HH: combined uncertainties *Phys. Rev. D* **103** 056002
[102] Ling L-S, Zhang R-Y, Ma W-G, Guo L, Li W-H and Li X-Z 2014 NNLO QCD corrections to Higgs pair production via vector boson fusion at hadron colliders *Phys. Rev. D* **89** 073001
[103] Czakon M , Heymes D, Mitov A, Pagani D, Tsinikos I and Zaro M 2017 Top-pair production at the LHC through NNLO QCD and NLO EW *J. High Energy Phys.* JHEP10(2017)186
[104] CMS Collaboration 2021 Precision luminosity measurement in proton-proton collisions at $\sqrt{s} = 13\,\text{TeV}$ in 2015 and 2016 at CMS *Eur. Phys. J. C* **81** 800
[105] CMS Collaboration 2018 CMS luminosity measurement for the 2017 data-taking period at $\sqrt{s} = 13\,\text{TeV}$ CMS Physics Analysis Summary CMS-PAS-LUM-17-004 (available at: https://cds.cern.ch/record/2621960)
[106] CMS Collaboration 2019 CMS luminosity measurement for the 2018 data-taking period at $\sqrt{s} = 13\,\text{TeV}$ CMS Physics Analysis Summary CMS-PAS-LUM-18-002 (available at: https://cds.cern.ch/record/2676164)
[107] CMS Collaboration 2018 Measurement of the inelastic proton-proton cross section at $\sqrt{s} = 13\,\text{TeV}$ *J. High Energy Phys.* JHEP07(2018)161
[108] Barlow R and Beeston C 1993 Fitting using finite Monte Carlo samples *Comput. Phys. Commun.* **77** 219
[109] ATLAS and CMS Collaborations 2011 and LHC Higgs Combination Group, Procedure for the LHC Higgs boson search combination in Summer *Technical Report* CMS-NOTE-2011-005, ATL-PHYS-PUB-2011-11, 2011 (available at: https://cds.cern.ch/record/1379837)
[110] Cowan G, Cranmer K, Gross E and Vitells O 2011 Asymptotic formulae for likelihood-based tests of new physics *Eur. Phys. J. C* **71** 1554
[111] Junk T 1999 Confidence level computation for combining searches with small statistics *Nucl. Instrum. Methods A* **434** 435
[112] Read A L 2002 Presentation of search results: the CLs technique *J. Phys. G* **28** 2693
[113] Wilks S S 1938 The large-sample distribution of the likelihood ratio for testing composite hypotheses *Ann. Math. Stat.* **9** 60
[114] Bernlochner F U, Fry D C, Menary S B and Persson E 2023 Cover your bases: asymptotic distributions of the profile likelihood ratio when constraining effective field theories in high-energy physics *SciPost Phys. Core* **6** 013
[115] CMS Collaboration 2025 Combined effective field theory interpretation of Higgs boson, electroweak vector boson, top quark, and multi-jet measurements Submitted to Eur. Phys. J. C. (arXiv:2504.02958)
[116] CMS Collaboration 2024 The CMS statistical analysis and combination tool: COMBINE *Comput. Softw. Big Sci.* **8** 19
[117] Verkerke W and Kirkby D P 2003 The RooFit toolkit for data modeling *eConf* (arXiv:physics/0306116)
[118] Moneta L *et al* 2010 The RooStats project *PoS ACA* **T2010** 057
[119] Fernandez I Z *et al* 2020 High-Luminosity Large Hadron Collider (HL-LHC): Technical design report CERN Yellow Rep. Monogr. **10** (available at: http://dx.doi.org/10.23731/CYRM-2020-001010.23731/CYRM-2020-0010)
[120] CMS Collaboration 2020 The Phase-2 upgrade of the CMS level-1 trigger CMS Technical Design Report CERN-LHCC-2020-004, CMS-TDR-021 (available at: https://cds.cern.ch/record/2714892)
[121] CMS Collaboration 2021 The Phase-2 upgrade of the CMS data acquisition and high level trigger CMS Technical Design Report CERN-LHCC-2021-007, CMS-TDR-022 (available at: https://cds.cern.ch/record/2759072)